Materials Science and Technology - Nuclear Materials, Advanced Course

Kon-67.5100 Postgraduate Seminar on Engineering Materials - Seminar papers 8 October, 2015

Editors: Hannu Hänninen & Timo Kiesi

Materials Science and Technology - Nuclear Materials, Advanced Course

Kon-67.5100 Postgraduate Seminar on Engineering Materials - Seminar papers 8 October, 2015

Editors: Hannu Hänninen & Timo Kiesi

441   697
Printed matter

Preface

Material science and technology is the key engineering field in enhancing the safety, economy, operation and maintenance of the nuclear industry. In the existing reactors the material science and engineering issues are related to the plant life extension and the material aging mechanisms have the dominating role. In new build reactors most of the old materials problems have been tried to be solved by the materials selection and development of manufacturing techniques. Intensive work is underway to develop the next generation reactor systems (Gen IV), which are based on the closed fuel cycle. These new concepts represent unprecedented materials problems related to irradiation damage, corrosion and high temperature properties of the materials.

The Engineering materials research group of Department of Engineering Design and Production of Aalto University arranged a postgraduate course on nuclear materials. The course consisted of three day long lecture session given in April 20-22, 2015. Lectures were given by professionals from nuclear power related research institutes (Aalto and VTT), nuclear industry and authority. The course also included a seminar session held October 8, 2015. The seminar session was targeted to postgraduate students, who prepared articles from their field of expertise. This proceeding is the collection of these seminar articles.

Table of Contents

Comparison of Steam Generator Tube Materials Using CES-software

Timo Kiesi
Aalto ENG Department of Engineering Design and Production
Email: timo.kiesi@aalto.fi

Abstract

Steam generators (SG) are key components in pressurized water reactors (PWR). Their task is to convert heat generated in nuclear reaction into steam for turbines. This is done in a heat exchanger where the primary pressurized water (radioactive) heats and boils secondary water (non-radioactive). The heat exchanger part of SG is a tubular structure consisting of thousands of tubes manufactured from stainless steels or nickel based alloys.

For materials selection point of view SG tubes have several aspects that have to be taken into account. They must withstand both chemical and mechanical load but at the same time must have good physical properties in order to conduct heat between water cycles. SGs in PWRs are at the boundary of primary and secondary water cycle loops. Therefore their structural integrity is important for safe NPP operation. This paper reviews and compares alternative materials used in SG-tubes based on their physical and mechanical properties using Cambridge Engineering Selector –software (CES).

Keywords: Nuclear Power Plant, Steam Generator Tubes, CES, Alloy 600, Alloy 690, Alloy 800, AISI 321 Austenitic Stainless Steel.

1. Introduction

Steam generators are heat exchanger assemblies on pressurized water reactors (PWR). Their task is to transfer heat from primary coolant flow (radioactive) to secondary coolant flow (non-radioactive). Steam generators are essential component on PWR water systems and are situated inside reactor building. Typical PWR coolant system can have several steam generators. The total number varies by manufacturer but typically nuclear power reactor unit has two to four steam generators (Fyfitch, 2012). Typical Westinghouse-type reactor coolant system is presented in Figure 1.

The steam generator generates steam for turbines by remove the heat from primary water flow and thus cools the core. While producing steam the steam generator is also a barrier against radioactive environment. It is estimated that around 75 % of total area against environment is in steam generators. (MacDonald et al., 1996)
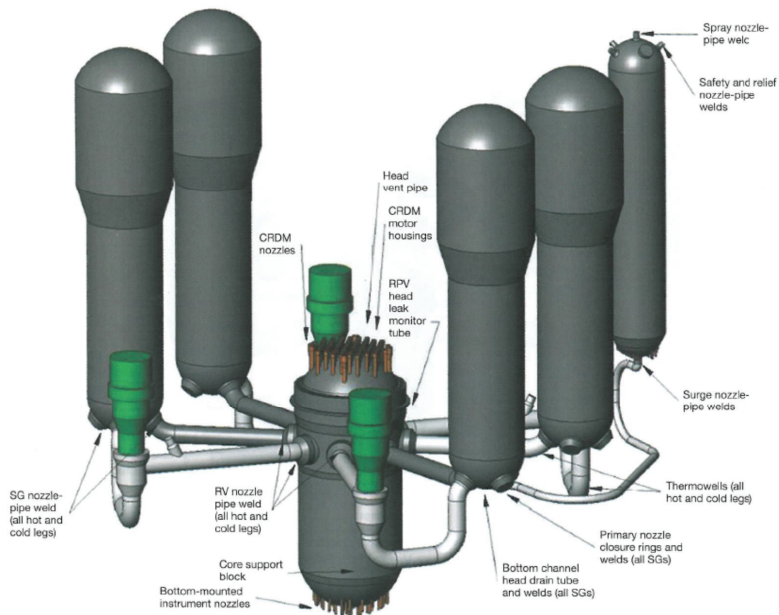
Figure 1. Westinghouse-type reactor coolant system with four steam generators. Steam generators transfer heat from primary water coolant flow to secondary coolant flow. (Fyfitch 2012)

All heat exchangers consist of a series of tubes inside a shell structure. Tubes are supported against vibrations from coolant flow. The exact layout of the heat exchanger varies by manufacturer but two basic steam generator layouts exist in NPPs: vertical design and horizontal design. Vertical design is used in western reactors and horizontal layout is used in VVER-type reactors. Horizontal steam generators are also common in smaller reactor units, such as nuclear powered naval vessels. In Figure 2 vertical and horizontal steam generators are compared.
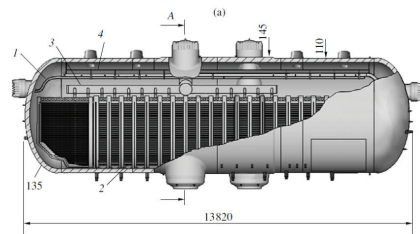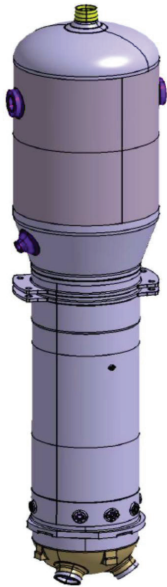
EPR
Vertical structure
Thermal power 1125 MW
Tube material Inconel 690
5980 tubes
Wall thickness 1.09 mm
Heat-exchange surface 7960 m^2
Mean length of tube 21.7 m

PGV-1000MK Russian (VVER)
Horizontal structure
Thermal power 750 MW
Tube material 08Kh18N10T
10 978 tubes
Wall thickness 1.5 mm
Heat-exchange surface 6105 m^2
Mean length of tube 11.10 m

Figure 2. Comparison of two basic types of steam generators, vertical and horizontal.
(Teller, 2010; Trunov et al., 2008)

The operating principle of a modern vertical steam generator (European Pressurized Reactor, EPR for example) is quite simple. Primary hot water enters the steam generator from the bottom of the assembly. Water then flows into tube system, which is submerged into secondary water. Tube structure is typically bended as U-form. Primary water heats the secondary water and then flows back into bottom of the assembly and further to reactor vessel. The secondary water is heated and boiled by the heat, and the produced steam is dried and guided via pipe system into turbine at top of the vessel. In Figure 3 the general layout of vertical steam generator is presented.

However, the assembly itself is anything but simple. Main components of a modern steam generator (EPR-type) are (Teller, 2010):

- Pressure shell
- Channel head with primary coolant inlet and outlet nozzles, partition plate and manhole
- Tube sheet

3

- Lower internals including:
  - Tube bundle
  - Bundle wrapper (separating heated upward water flow from downward feedwater)
  - Tube bundle supporting system (support structure and anti-vibration system)
- Upper internals including
  - Main feedwater system
  - Emergency feedwater system
  - Primary separators
  - Secondary separators
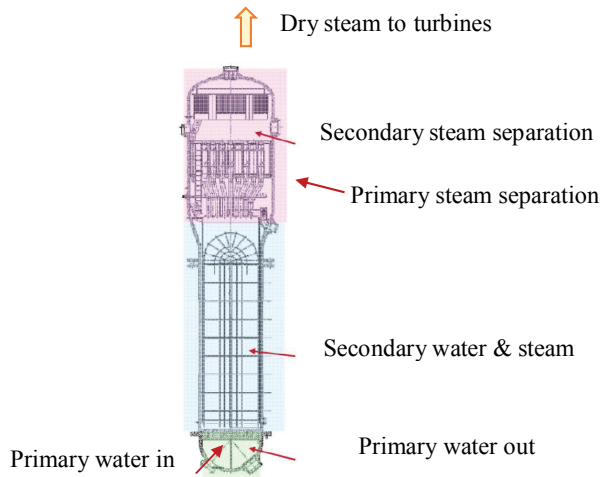
Figure 3. General layout of EPR-type (vertical) steam generator. (Teller, 2010)

2. Requirements for steam generator tube materials

Steam generators operate at highly demanding, corrosive environment. Nearly all problems related to steam generators are a consequence of corrosion. Due to this fact steam generators have been consistently troublesome for PWR plants. Figure 4 presents the main reasons for tube plugging. At the beginning the tube wastage and denting were the most relevant issues. These were, however, mostly solved by better water chemistry and redesign of SGs (Green and Hetsroni, 1995; Grimmel, 2005; IAEA, 2011, Roberts, 1981). The most imminent problem in steam generators nowadays is the stress corrosion cracking (SCC). Therefore the material selection is generally based on corrosion behavior of materials.

Materials that are currently used in NPP steam generator tubes fall into three categories: austenitic stainless steels (08Kh18N10T (Type 321), nickel-base corrosion resistant alloys (Alloy 600 and 690) and ferrous-based corrosion resistant alloys (Alloy 800). The chemical composition of these alloys is given in Table 1. The stress corrosion cracking behavior of these alloys in given in Figure 5.

Figure 4. Primary cause for SG tube plugging in US by year. (Diercks et al. 1999)

3.   Properties of alternative materials for steam generator tubes

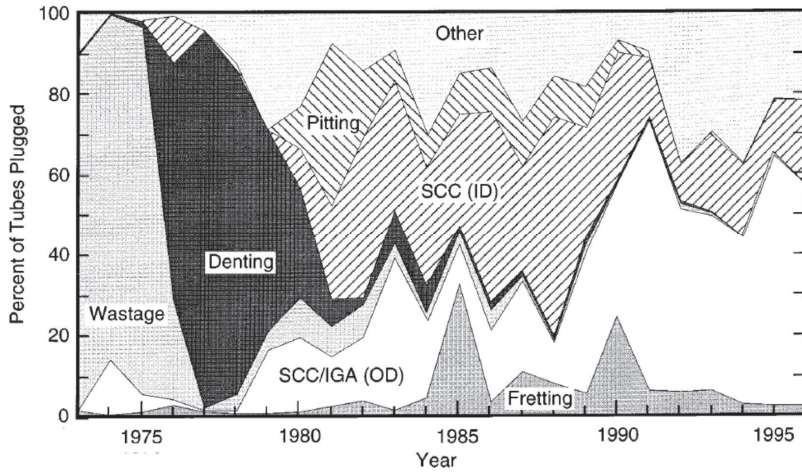Alloy 600 (UNS N06600, EN 2.4816) is widely used corrosion resistant and high temperature alloy in chemical, petrochemical, food processing and nuclear industries. It was developed originally as a high temperature alloy. The addition of approximately 15 % of chromium into nickel matrix provided a good thermal properties and particularly good corrosion resistance in dry chlorine in high temperatures. The microstructure of Alloy 600 is stable austenitic structure produced by solution treatment followed cooling. The microstructure is stable and resistant to long-term ageing and degradation of toughness and ductility. (Farrar, 2004)

Alloy 600 in SG-tubes are typically in mill-annealed (MA) condition. The purpose of mill-annealing (annealing at 980 ºC or above for several hours) is to dissolve all carbides to solution and obtain a relatively large grain size. A slow cooling follows the solution treatment. The purpose of slow cooling is to obtain uniform chromium-carbide structure at grain boundaries. The mill-annealing temperature controls the mechanical and corrosion properties of the alloy. Later an additional thermal treatment (TT) was included following the mill-annealing. (MacDonald et al., 1996) The purpose of TT is to further improve the microstructure and lower the residual stress level in material. The thermal treatment incudes annealing the material in the temperature range 650-750 ºC in order to enhance the chromium carbide precipitation to grain boundaries and thus lowering the risk of PWSCC. (Fyfitch 2012)

Alloy 690 (UNS N06690, EN 2.4642) was developed as an improved Ni-alloy to replace Alloy 600 in chemical and nuclear industries. It has one of the highest chromium contents (around 30 %) of any Ni-alloys, and therefore has exceptional resistance to oxidation at high temperatures. It also has improved resistance against SCC at high temperatures in water-based cooling systems. The microstructure of Alloy 690 is austenitic produced by solution treatment and rapid quenching. Alloy 690 in

SG-tubes is usually in MA+TT state. The heat treatment process is quite similar to Alloy 600. (MacDonald et al., 1996)

Table 1. Chemical composition of alternative steam generator tube materials. (MacDonal et al., 1996; Anon, 2015)

| Element	Alloy 600 (EPRI Guidelines)	Alloy 690 (EPRI Guidelines)	Alloy 800 (Nuclear grade)	08Kh18N10T
C (%)	0.025-0.05	0.015-0.025	0.03	<0.08 (max)
Mn (%)	1.00 (max)	0.50	0.4-1.0	2.0 (max)
P (%)	0.015	0.015	0.020	<0.035 (max)
S (%)	0.010 (max)	0.003	0.015	<0.02 (max)
Si (%)	0.50 (max)	0.50	0.3-0.7	0.8 (max)
Cr (%)	15.0-17.0	28.5-31.0	20.0-23.0	17-19
Ni (%)	> 72.0	Bal (> 58.0)	32.0-35.0	9-11
Mo (%)	-	0.2	-	
Fe (%)	6.0-10.0	9.0-11.0	Bal	
Cu (%)	0.50 (max)	0.10	0.75	
Co (%)	0.015	0.014	0.10	
Al (%)	-	0.40	0.15-0.45	
Ti (%)	-	0.40	0.60	5 x C-0.7
Other (%)	-	N: 0.050 B: 0.005 Nb: 0.1	Ti/C ≥ 12 Ti/(C+N) ≥ 8 N ≥ 0.03	Cu: 0.3 (max)
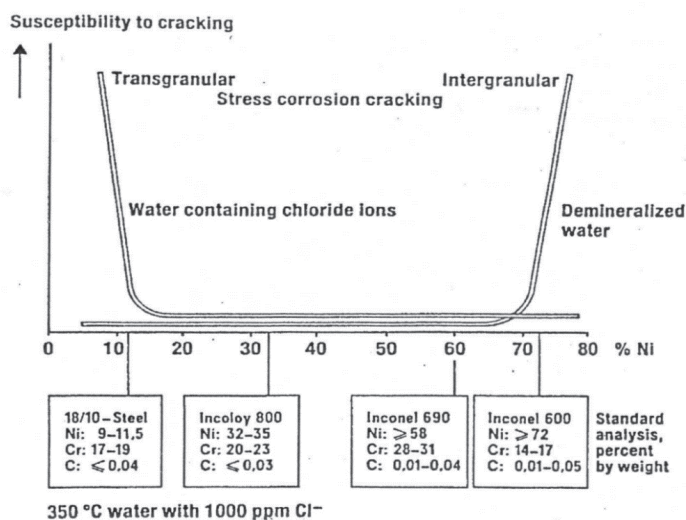
Figure 5. Generalized summary of SCC properties of alternative SG tube materials. (Staehle & Gorman, 2003)

Alloy 800 is an iron-nickel-chromium alloy. It was originally developed in 1950's as a relatively "cheap", low nickel content alloy for corrosion and heat exchanger use. The low nickel content introduced some corrosion problems, and the carbon content levels were controlled more closely. Also some adjustment was made to maximum allowed grain size, and aluminum and titanium content. These variations are usually designated as Alloy 800H and 800HT. Alloy 800 is a common material in furnaces and heat exchangers. However, in some environments the risk of pitting is quite high and therefore restricts the use of Alloy 800. (Farrar, 2004)

Alloy 800 is used in German NPPs built by Siemens/KWU. The alloy was chosen over Alloy 600 for the poor performance of Alloy 600 and SCC issues in German NPPs. The version used in SG is Alloy 800M. Its nickel content is about half of the nickel level in Alloy 600. Also the carbon content is restricted to lower level and stabilization ratio (Ti/C) is high, over 12. Also chromium and nickel contents are slightly higher than "normal" Alloy 800 for better pitting and stress corrosion cracking resistance. (MacDonald et al., 1996)

AISI 321 type austenitic stainless steel is stabilized version of the common 18-8 stainless steel. The original steam generators in early NPPs were made out of AISI 304 and 316. However, the sensitization of these alloys led to development of stabilized version of the alloy. The sensitization is generally solved by either: lowering the carbon content, or by adding carbide-forming ("stabilizing") elements to the alloy, such as titanium or niobium. The VVER-440 and 1000 plants use Russian 08Kh18N10T (08X10N10T) steel in steam generators (Trunov et al, 2006). The alloy is generally identical to AISI 321 and is Ti-stabilized.

4.   Materials indexes for heat exchanger materials using CES

Heat exchangers transfer heat from one medium to another. Typically this is done in liquids usually water under pressure. Heat moves from one liquid into membrane wall and then to other liquid. The essential materials selection problem is thus converted into problem of conduction and convection, and damage tolerance of a pressurized components (Ashby, 2011). Schematic presentation of heat exchanger operating principle is given in Figure 6.
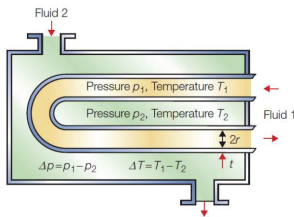

Figure 6. Schematic structure of heat exchanger. (Ashby, 2011)

Material indices for materials selection

In order for the heat exchanger to be as small as possible the total volume of tubes must be as small as possible. If operating pressure inside tube is considered as constant

and the length of the U-bend tube is also fixed the smallest volume of material is achieved by making the tube from the materials which has the highest yield strength:

$$M_1 = \sigma_y,\qquad(1)$$

where σ_y is the yield strength of the material.

The safety of a pressure vessel is usually achieved by designing the vessel according to "leak-before-brake" or "yield-before-brake" methology. The general idea is that before catastrophical failure occurs in the vessel the operating pressure can be released. In heat exchangers it is impossible to utilize constant visual evaluation and thus the leak-before-brake methology is chosen. In the case of crack growth based failure mechanism (SCC or fatigue, for example) the leak-before-break conditions ensure that the crack can grow through the tube wall before reaching unstable stress intensity levels. The highest safe operating pressure in leak-before-brake conditions is ensured by

$$M_2 = \frac{K_{IC}^2}{\sigma_y},\qquad(2)$$

where K_{IC} is the fracture toughness of material.

The heat flow in heat exchangers depends on convection of heat from heating medium into membrane wall, conduction of heat through membrane, and yet again convection into cooling medium. In liquid based systems the dominating section in total thermal resistance of system is the conduction through membrane wall $\left(\lambda/t\right)$ and the effect of convection into membrane wall is negligible. The tube wall must also support the pressure difference between mediums. Therefore the highest heat flow per unit area in tube wall is achieved by

$$M_3 = \lambda\sigma_y,\qquad(3)$$

where λ is the thermal conductivity of material.

The temperature difference in water systems creates temperature gradients into tube materials. This creates thermal stresses and distortions to tube materials. Thermal strains in material in given heat flux can be expressed as $\frac{d\varepsilon}{dx} = \alpha\frac{dT}{dx} = \frac{\alpha}{\lambda}q$. Therefore the minimum thermal distortion is in material with highest value of:

$$M_4 = \frac{\lambda}{\alpha},\qquad(4)$$

where α is the thermal expansion coefficient of material.

The cost of material can be evaluated by price. However in material selection studies it is usually more convenient to compare the price by performance values, i.e. analyzing the possible gain in performance rather than just cost on material. The cheapest heat exchanger is the one with highest value of:

$$M_5 = \frac{\lambda(\sigma_y)^2}{C_m\rho},\qquad(5)$$

where ρ is the density and C_m cost per kg of material.

5. Results and discussion

The graphical solutions utilizing CES Selector Aero Package are given in Figures 7-11.

Figure 7. Material selection map of index M1: Wall thickness. (Map created with CES Selector 2014 Aerospace Edition by the author)
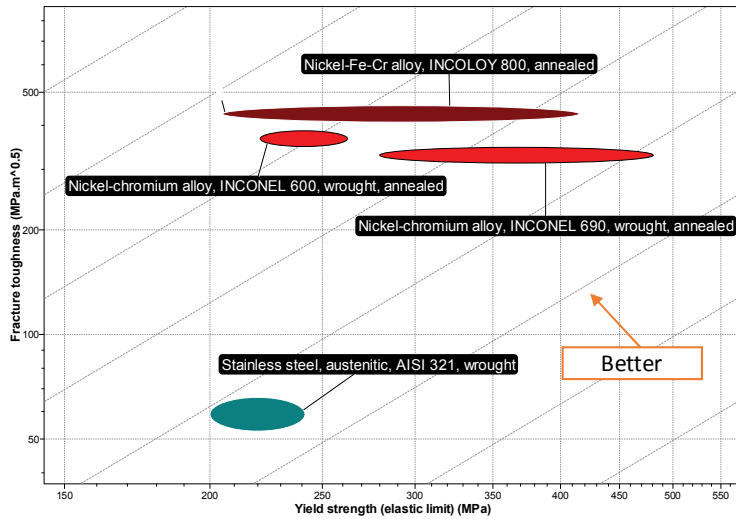
Figure 8. Material selection map of index M2: Most safe max pressure. (Map created with CES Selector 2014 Aerospace Edition by the author)
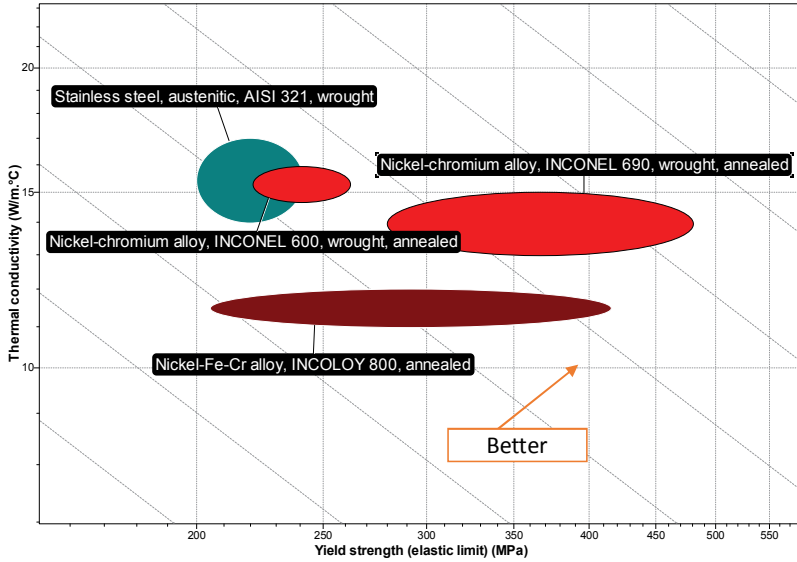
Figure 9. Material selection map of index M3: Heat flow per unit area. (Map created with CES Selector 2014 Aerospace Edition by the author)
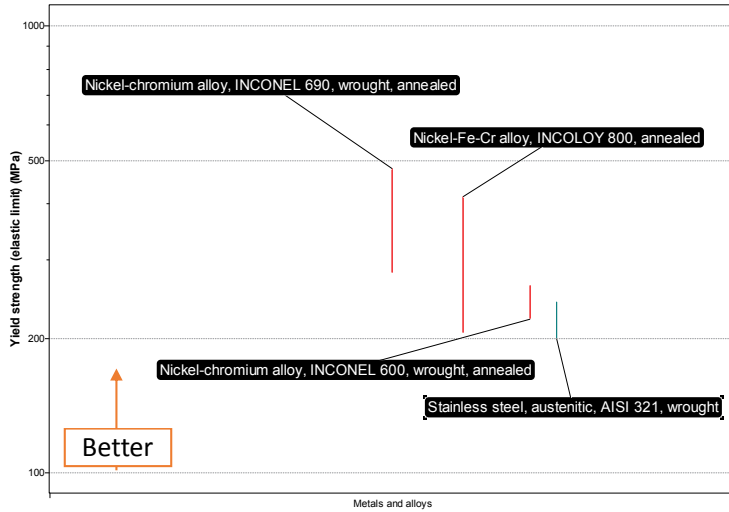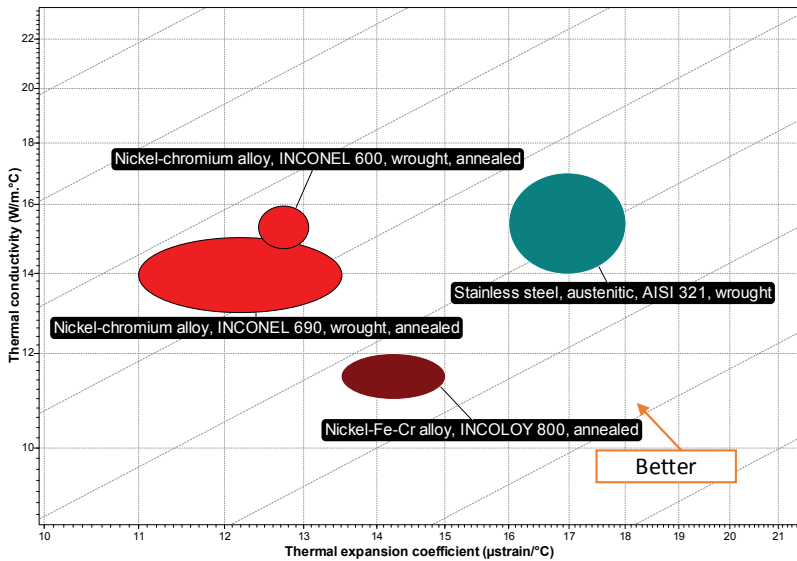

Figure 10. Material selection map of index M4: Thermal distortion. (Map created with CES Selector 2014 Aerospace Edition by the author)
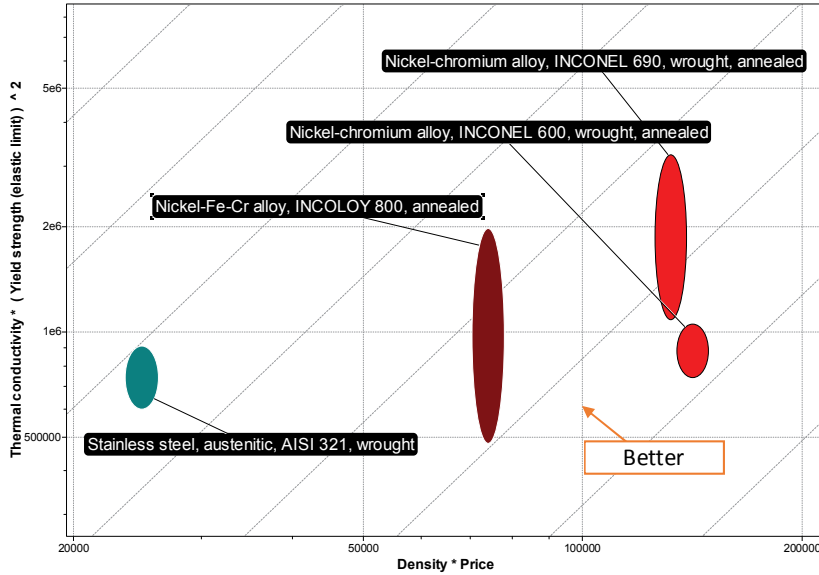
Figure 11. Material selection map of index M5: Price by performance. (Map created with CES Selector 2014 Aerospace Edition by the author)

Numerical solutions were obtained by calculating numerical values for each material indices using physical and mechanical properties given in Table 2 and 3. The results are collected to Table 5. Material properties are from CES Selector database. They have been compared to values found in literature sources and databases (Cverna, 2002; Anon, 2015).

Table 2. Mechanical properties for studied alloys (values for 08Kh18N10T are for pipe product, AISI 321 type alloy values are given in brackets). (CES Edupack 2015).

	Inconel 600 (annealed)	Inconel 690 (annealed)	Inconel 800 (annealed)	08Kh18N10T (AISI 321)
Yield strength [MPa]	221-262	280-480	205-415	216 (200-241)
Tensile strength [MPa]	517-586	630-845	515-725	530 (510-660)
Elongation [%]	25-35	30-55	30-60	37 (30-60)
Fracture toughness [MPam½]	349-386	314-347	412-456	- (53-66) [*]

*) The fracture toughness value for AISI 321 is quite low in CES database. For example Little 1985 gives much higher fracture toughness values. See discussion for more details.

11

Table 3. Physical properties for studied alloys (values for 08Kh18N10T are for pipe product, AISI 321 type alloy values are given in brackets). (CES Edupack 2015).

	Inconel 600	Inconel 690	Inconel 800	08Kh18N10T (AISI 321)
Coefficient of linear thermal expansion [10-6 / K]	11.6 (RT) 14.4 (21-316)	14.04 (24-93) 14.5 (RT-300)	14.2 (RT) 16.2 (21-316)	16.7 (RT) 17.2 (0-315)
Specific heat capacity [J/kg]	475 (RT)	450 (RT)	502 (20)	565.2 (RT)
Thermal conductivity [W/m*K]	15 (RT) 18.4 (300)	13.5 (RT) 18 (300)	13 (RT) 18.3 (21-427)	15 (RT) 25.4 (RT-150)

Table 4. Calculated material index values for Equations 1-5 using material data from Table 2 and 3. Calculated values are based on average values unless stated otherwise. Higher value means better performance.

	Inconel 600 (annealed)	Inconel 690 (annealed)	Inconel 800 (annealed)	08Kh18N10T (AISI 321)
Wall thickness: $M_1 = \sigma_y$	242	**380**	310	221
Most safe max pressure: $M_2 = \frac{K_{Ic}^2}{\sigma_y}$	559	287	**607**	16 / 404
Heat flow per unit A: $M_3 = \lambda \sigma_y$	4 033	**5 985**	3 565	3 418
Thermal distorsion: $M_4 = \frac{\lambda}{\alpha}$	**1.31**	1.29	0.81	0.93
Price by performance: $M_5 = \frac{\lambda(\sigma_y)^2}{c_m \rho}$	6.89	17.25	14.91	**30.38**

The thinnest wall material is Inconel 690 due its high yield strength. Also Inconel 800 has quite high index value. AISI 321 type austenitic stainless steel has the lowest index value for wall thickness because of its low yield strength.

The most safe maximum pressure material (in leak-before-brake conditions) is Inconel 800 due to its high fracture toughness and yield strength combination. The index for Inconel 690 is lower due to its high yield strength. The poor performance of AISI 321 can be explained by its low fracture toughness value in CES database. Calculating material index by using fracture toughness value $J_{ID} = 421 \frac{kJ}{m^2}$ (Little, 1985) ($K_{mat} = 299 \, MPa\sqrt{m}$ converted value for 23 ºC with E = 193 GPa and $\nu = 0.3$) gives much higher index value, about two thirds of Inconel 800.

The best material for heat exchanger based on heat flux per unit area is Inconel 690. It performs nearly twice as well as Inconel 800 or AISI 321. Inconel 600 has also very high index value for heat exchanger use.

Lowest thermal distortions are in Inconel 600. Inconel 690 performs nearly as well. For Inconel 800 and AISI 321 the thermal distortion index is much lower.

The lowest price by performance index has AISI 321 with clear difference. The price of AISI 321 tubes is half of those of high performance alloys Inconel 690 and 800. The highest price is for Inconel 600 due to its exceptionally high nickel content.

6.   Conclusion

CES Selector does not have tools for detailed material selection based on corrosion properties of the materials. Therefore the analysis was done based on performance of studied alloys.

The best material for steam generator use is Inconel 690. It has the best heat transfer per unit area properties and the higher strength of the alloy allows to make thin wall tubes. Also the material safety index is high. Thermal distortion is low. The only drawback is the high price of the alloy.

Inconel 800 performs well based on indices and is thus good material choice. It has lower index values in heat exchanger use, but its exceptional safe maximum pressure index value together with good real-life performance evidence make it an interesting material choice.

Inconel 600 performed quite well based on pure physical and mechanical properties thus making it an interesting heat exchanger material. However, poor real-life SCC performance in pure water environments makes it impossible choice for nuclear power heat exchangers.

AISI 321 type stainless steel performance based on pure mechanical and physical properties makes it average choice at the best. However, the alloy has exceptional price by performance index and thus makes it the cheapest material alternative for steam generator tubes. The use of AISI 321 leads to high wall thickness, which together with high thermal distortion behavior may lead to restrictions in tube length in vertical steam generator applications.

References

Anon, 2015. 08KH18N10T (08X18H10T). Database of Steel and Alloy (Marochnik), University of Kharkov. URL: < http://www.splav-kharkov.com/en>. Visited 10.11.2015.

Ashby, M. F. 2011. Materials Selection in Mechanical Design, 4th edition. Elsevier. 646 pages. ISBN 978-2-85617-663-7.

Cverna, F. (ed). 2002. Thermal Properties of Metals. ASM Materials Data Series. ASM International. 560 pages. ISBN 0-87170-768-3.

Diercks, D. R., Shack, W. J. & Muscara, J. 1999. Overview of Steam Generator Tube Degredation and Intergrity Issues. Nuclear Engineering and Design. Vol 192. Pp 19-30.

Farrar, J. C. M. 2004. The Alloy Tree. CRC-press. 192 pages. ISBN 1-85573-766-3.

Fyfitch, S. 2012. Corrosion and Stress Corrosion Cracking of Ni-Base Alloys. In: Konings, R. J. M. et al (eds). Comprehensive Nuclear Materials. Volume 5: Material Performance and Corrosion/Waste Materials. Elsevier. Pp. 69-92. ISBN 978-0-08-056027-4.

Granta Design. 2014. CES Selector 2014 Aerospace edition. (Computer database)

Granta Design. 2015. CES EduPack 2015 Aerospace database. (Computer database)

Green, S. J. & Hetsroni, G. 1995. PWR Steam Generators. International Journal of Multiphase Flow. Vol 21. Pp. 1-97.

Grimmel, B. 2005. U.S. Plant Experience with Alloy 600 Cracking and Boric Acid Corrosion of Light Water Reactors. NUREG-1823. U.S. Nuclear Regulatory Commision. 38 pages + 25 appendixes.

IAEA. 2011. Stress Corrosion Cracking in Light Water Reactors: Good Practices and Lessons. IAEA Nuclear Energy Series No NP-T-3.13. 100 pages. ISBN 978-92-0-117210-5.

Little, E. A. 1985. Dynamic J-Intergral Toughness and Fractographic Studies of Fast Reactor Irradiated Type 321 Stainless Steel. In: Garner, F. A. & Perrin, J. S. (eds). Effect of Radiation on Materials: Twelfth International Symposium. ASTM STP 870. ASTM. Pp. 563-579.

MacDonald, P. E., Shah, V. N., Ward, L. W. & Ellison, P. G. 1996. Steam Generator Tube Failures. NUREG/CR-6365. Idaho National Engineering Laboratory. 307 pages.

Robets, J. T. A. 1981. Structural Materials in Nuclear Power Systems. Plenum Press. 485 pages. ISBN 0-306-40669-1.

Staehle, R. W. & Gorman, J. A. 2003. Quantitative Assessment of Submodes of Stress Corrosion Cracking on the Secondary Side of Steam Generator Tubing in Pressurized Water Reactors: Part 1. Corrosion, Vol. 59, Nro. 11. Pp. 931-994.

Teller, A. 2010. EPR by AREVA. Main EPR Componts. Areva, Paris, France. Presentation in Slovak University of Technology in Bratislava. September 2010. 37 pages. Available in URL:
<http://www.iaea.org/inis/collection/NCLCollectionStore/_Public/44/078/44078372.pdf>

Trunov, N. B., Denisov, V. V., Kharchemko, S. A. & Lukasevich, B. I. 2006. Consideration of Field Experience in Developing New Projects of Steam Generators for Nuclear Power Stations Equipped with VVER Reactors. Thermal Engineering. Vol 53 No 1. Pp. 37-42.

Trunov, N. B., Lukasevich, B. I., Veselov, D. O. & Dragunov, Yu. G. 2008. Steam Generators – Horizontal or Vertical (Which Type Should Be Used in Nuclear Power Plants with VVER). Atomic Energy. Vol. 105. No. 3. Pp. 165-174.

Stress Corrosion Cracking in Piping Welds of BWRs

Elina Salenius
Email: elina.salenius@stuk.fi

Abstract

Aging Nuclear Power Plants are facing several degradation mechanisms. One of the major concerns last decades has been stress corrosion cracking (SCC) in its different forms. It has especially been problem in piping welds of boiler water reactors (BWR). Intergranular Stress Corrosion Cracking (IGSCC) has been dominating degradation mechanism in austenitic stainless steel piping. It makes a ductile austenitic stainless steel to fracture in brittle manner.

Stress corrosion cracking mechanism requires three factors; high applied or residual stress, susceptible microstructure (austenitic stainless steel), and aggressive environment at elevated temperatures. If any of these is eliminated, the stress corrosion doesn't occur.

The first stress corrosion cracking findings in 1960's showed problems with reliable detection of cracks with ultrasonic examination procedures. This started research and development processes of ultrasonic techniques and extensive qualification actions have been performed since.

Stress corrosion cracks have been and still are the main detection focus of boiling water reactor austenitic piping when implementing yearly is-service inspections. In Finland the inspections are done according to risk significance, according to so called risk informed in-service inspections. If the piping weld is prone to stress corrosion cracking and the consequence of possible pipe rupture or leakage is significant in terms of core damage frequency or early release frequency, the risk significance of the weld is considered high and 10-25% of welds of that piping segment belong to the inspection program.

1   History/Operating experience

Stress corrosion cracking (SCC) has been a major degradation problem of aging nuclear power plant components [1]. The first stress corrosion cracking (SCC) incidents were reported in 1965 in the USA and a decade later the SCC phenomenon was recognized as a generic issue for type 304 and 316 stainless steel in boiling water reactor (BWR) type nuclear power plants [2].

IGSCC, intergranular stress corrosion cracking in austenitic stainless steels has been the most significant single degradation mechanism in boiling water reactor (BWR) piping. Intergranular stress corrosion cracking (IGSCC) occurred first in the small diameter piping where higher residual stresses were present, but afterwards IGSCC started to occur also in the large diameter piping [3].

IGSCC has been the dominating damage mechanism in straight boiling water reactor (BWR) pipes as is shown in the Figure 1. The example is from Swedish BWR study

[1]. The picture shows that the main percentage of damages on straight pipes were caused by SCC during the research years from 1972 to 1998.
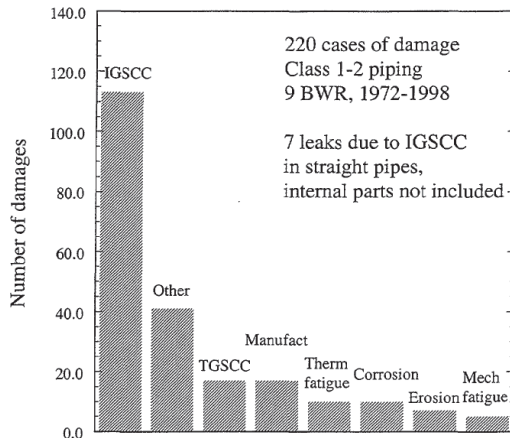
Figure 1. Number of damages occurred in Swedish BWR straight pipes from 1972 to 1998. [1]

One of the main reasons for SCC degradation phenomenon is that SCC had not been taken into account in the original design of BWRs. IGSCC findings made clear that piping materials which had been thought to be excellent in quality, such as alloy 600, had degradation issues [2]. Finnish boiling water reactors, Olkiluoto 1 and 2, were built in late 1970's when there was already knowledge of SCC and its prevention. Therefore SCC has been able to take into account in material selection of Olkiluoto 1 and 2.

2   SCC in theory

Stress corrosion cracking (SCC) has different forms of appearance. It can be intergranular IGSCC, transgranular TGSCC, primary water based PWSCC or irradiation assisted IASCC. Sometimes the growth modes are mixed to each other or the mode can change to another during the growth process of a crack [4].

Inter granular stress corrosion cracking (IGSCC) is known to attack the heat-affected zone (HAZ) of a weld [5]. The IGSCC crack in the heat-affected zone is presented in Figure 2. IGSCC can occur and propagate in stainless steels (type 304, type 316) and nickel based alloys (Alloy 600, Alloy 182) if the environment is favorable for SCC. In order to occur, IGSCC needs oxidizing environment, susceptible material and static tensile stress on the pipe surface. The static tensile stresses on the piping surface are normally due to either residual stresses of the welding process, uneven cold deformation, fast cooling or volume changing phase transformations [2].
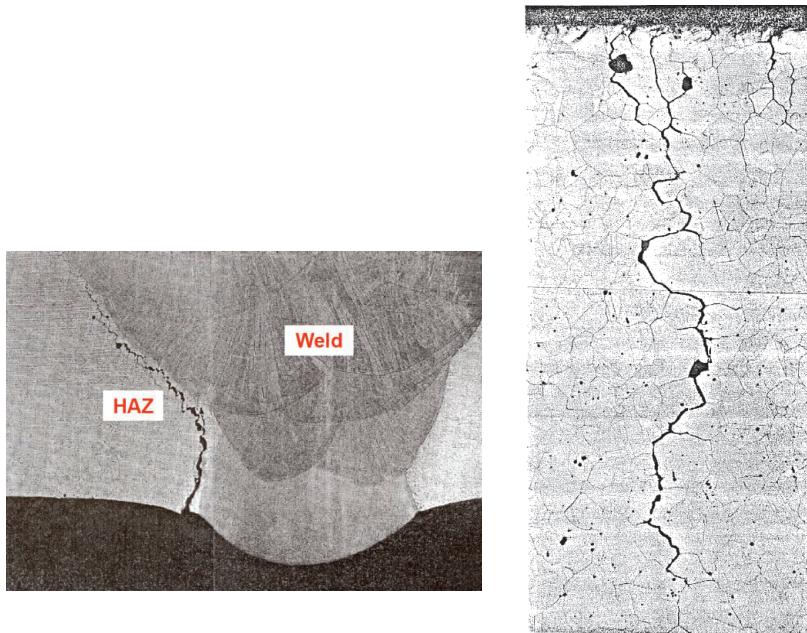
Figure 2. IGSCC [6, 5]

Boiling water reactor water chemistry is oxidizing so the electrochemical corrosion potential, which indicates the oxidation power of the environment, is high. BWR conditions are therefore suitable for SCC. Other environmental factors that have influence on SCC are impurities and high temperature [2].

The pipes of nuclear power plants are usually made of austenitic stainless steel or a combination of austenitic stainless steels and ferritic steel. Non-stabilized austenitic stainless steels with a high carbon content (~0.06%) were used in the original designs of BWR. These steels assured good mechanical properties, but a high carbon content increased the risk of sensitization [2].

Stress corrosion cracking is complex phenomenon but the elimination or reduction of any one of these three factors below some threshold level can in principle prevent SCC [2]. These three components influencing SCC are shown in Figure 3.

Figure 3. Critical factors for stress corrosion cracking. [2]

2.1 Thermal sensitization

Austenitic stainless steels are sensitized when subjected to temperatures between approximately 500°C–800°C. Thermal sensitization occurs in the heat affected zones of welds in austenitic alloys both during welding and also during stress relief heat treatments. Critical heat treatment time may vary between tens of seconds and many hours depending on the carbon content. During welding, chromium carbides form on the grain boundaries where the diffusion rate is higher than that in the matrix [2]. Figure 4 describes this carbide formation on the grain boundary.
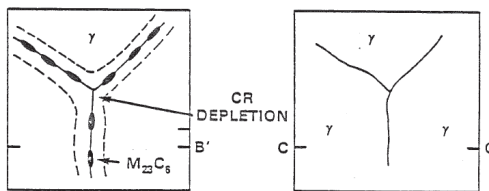
Figure 4. Diagram of sensitized and unsensitized 304 SS microstructure [5]

When the carbides grow, surrounding areas get poorer from chromium at the same time. Small carbides can grow at low temperatures such as BWR operation temperature which causes low temperature sensitization [2]. Chromium depleted area acts like anode, which has small area in comparison to large high chromium cathode. Electrochemical conditions enable crack-like propagation of the corrosion [7].

2.2 Cold and warm deformation

Thermal sensitization of materials was the first reason to cause IGSCC of austenitic stainless steels and nickel-based alloys. Thermally sensitized materials were then replaced with low carbon or stabilized steels. However, cold deformation manufacturing processes have lately caused IGSCC also of these materials without clear evidence of sensitization. This type of susceptibility to IGSCC is due to cold work during fabrication process [2].

Plastic deformation due to cold work induces formation of brittle martensite. The cold work methods are grinding or other severe surface machining techniques. IGSCC has happened also in cold bend piping. In many cases, the cracking initiated as transgranular mode and then changed to intergranular mode [8].

In Japan SCC was detected both from base material and the weld metal of low carbon 316L stainless steel in primary loop recirculation pipes of BWR's. No sensitization had occurred. TGSCC was initiated in machined surface which had been cold worked. SCC was also detected in weld areas which had been heavily strained by thermal deformation [9].

3 Crack properties

Stress corrosion cracking propagates usually perpendicular to the principal tensile stress. The break can happen with lower stresses than what is the yield strength. All SCC types have a brittle-like appearance, since cracks propagate with little or no macroscopic plastic deformation [2].

IGSCC crack growth happens along grain boundaries because grain boundary is an active corrosion path [9]. In the chapter 2.2 mentioned Japan case the cracks initiated at fist as TGSCC and after propagation of hundreds of micrometers they changed to IGSCC [9].This type of mixed-mode crack growth is typical for SCC.

The initiation time of a crack can vary from a short time up to several decades. The propagation happens in phases, which are slow propagation and fast propagation phase. The crack growth is dependent of the different acting stresses. The acting stresses are weld residual stresses and operational stresses [2].

4 Prevention of SCC

The main way to reduce the occurrence of SCC has been the replacement of piping material [3]. Nuclear power plants have widely used alloy 600 and austenitic stainless steel. This means that the replacement activities have been enormous. Thermal sensitization can be mitigated by using low carbon grades in which the carbon content is limited to ≤0.03%. These L-grades are, for example, type 304L or 316L. Stabilized stainless steels on the other hand use strong carbide formers such as niobium or titanium. Alloy 347 and alloy 321 are stabilized grades [2].

The fabrication has a lot of influence on the static tensile stresses on the piping surface. Optimizing welding process as well as performing pressure test of fabricated piping, is possible to reduce weld residual stresses. If possible, post-weld heat treatment should be done.

If material replacement is not possible and piping welds are prone to SCC, comprehensive inspections should be performed.

5 Risk informed in-service inspections

Components made of SCC sensitive materials and which are not replaced by non-sensitive materials should be in the scope of in-service inspections in order to detect possible cracks and to avoid leaks [4]. There are several inspection procedures for different piping inspections. There are manual UT inspections, manual UT phased array inspections and mechanized UT phased array inspections.

FAILURE CATEGORY	CONSEQUECE CATEGORY			
	No significance	Low	Medium	High
High	Low risk	Medium risk	High risk	High risk
Medium	Low risk	Low risk	Medium risk	High risk
Low	Low risk	Low risk	Low risk	Medium risk

Figure 5. Example of risk matrix [10]

The in-service inspections of pipes have to be based on the nuclear risk significance of the piping. The selection is done by dividing the systems selected into piping segments with the same failure potential and similar consequences of failure. The combination of the failure potential and consequences of failure defines the risk and the different combinations are illustrated in matrix form as in Figure 5. Risk categories help to identify the piping segments with the highest importance to safety [10].

If the risk is high, the required inspection percentage is 25 % of the welds of the segment. If the risk is medium the inspection percentage is 10% of the welds [11]. If anything alarming is found during inspection, ASME XI requires, that the inspections have to be expanded to cover 10% of welds of the same kind.

5.1 ASEA-atom BWRs

In Finnish BWR's the sensitized piping materials have been mostly changed. Still in in-service inspection of BWR austenitic piping, the IGSCC is postulated to be most probable degradation mechanism [12]. At Olkiluoto 1 and 2 some piping systems have high IGSCC degradation potential. One of the system of interest is the shut-down cooling system 321. (The system numbering is similar to all ASEA-atom BWR) [11]. The IGSCC potential of system 321 has been noticed also in the similar BWRs in Sweden [1].

During outage the shut-down cooling system (system 321) cools the fuel and reactor pools together with the pool water system. The system 321 includes 400 m pipes and there are approximately 500 welds. The system is divided into 20 piping segments according to risk significance. For some segments, the consequence of piping failure is considered high because it can cause leakage to the containment building or loss of decay heat removal during outage (LOCA, Loss of Coolant Accident). If the

degradation mechanism due to IGSCC is high and the consequence of failure is significant, then 25 % of the weld of the piping segment are included into the in-service inspection program [11].

Especially the carbon content of the weld material (≥0.035%) with high operating temperature (150 - 286 °C) are important factors considering the degradation potential. Also if the material hasn't been Niobium stabilized, the material is considered susceptible to SCC. Even though almost all Inconel 600 material have been replaces, there are still some Inconel 600 welds which have SCC potential. At the moment straight pipes of the system 321 are usually austenitic stainless steel 376 TP 303 and piping bends are usually austenitic stainless steel 403 WP 304 W [12].

5.2 NDT

The first findings of SCC in the 1960's showed the deficiency of the detection and sizing capability of the used NDT methods. The inspections were done at that time according to ASME Code Section V. Research programs such as PISC were utilized in 1970's in order to determine the capability of NDT inspections done according to ASME V. The results showed that crack-like defects were more difficult to detect than other types of defects [13].

Today, for example in Finland, the inspections have to be qualified according to ENIQ (European Network for Inspection Qualification) qualification procedure [14]. The first and important thing in the qualification procedure is to determine the defects that are most likely to appear. This means that aging and degradation mechanisms of the power plant need to be well known.
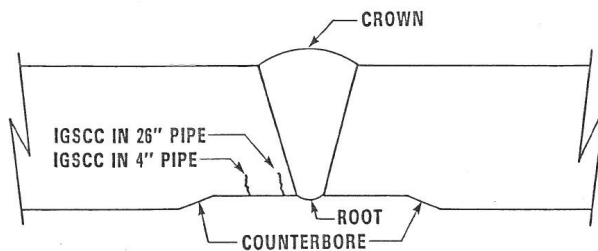
Figure 6. Relative locations of IGSCC for different pipe diameters 100 mm and 660 mm [5]

The stress corrosion crack is assumed to be found from the HAZ of the weld as illustrated in Figure 6. HAZ has hardness variations and residual stresses and it is favorable location for SCC initiation and growth. This is why only the welds are inspected and the base material is normally not of interest.

The crack is assumed to initiate from the inner surface of the pipe, at the root of the weld. This is why only 1/3 of the thickness of the pipe is inspected. The inspection volume is illustrated in Figure 7. The volume of inspection is C-D-E-F.
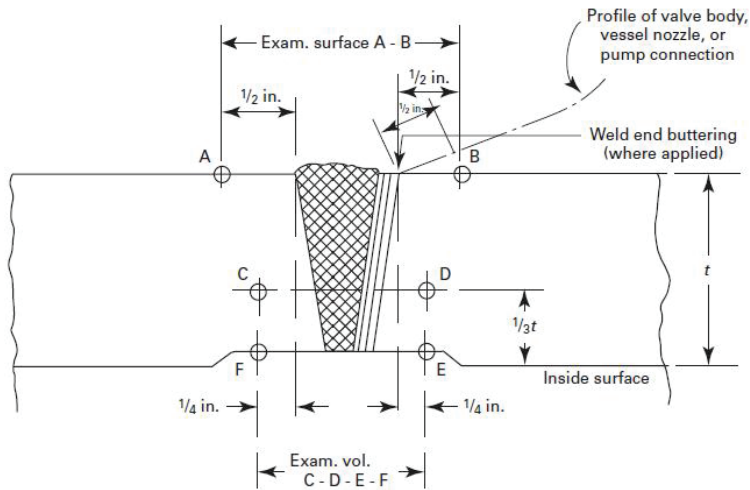
Figure 7. Inspection areas of similar and dissimilar piping welds according to ASME Section XI [15]

The typical locations of the SCC are challenging to NDT inspection because the weld can reflect echoes that disturb the analysis. Orientation can also be challenging. SCC cracks are not actually perfectly perpendicular to the weld but can be branched, bended or transverse to the weld. Different possible orientations are described with tilt and skew angles [16].

Branched crack may not give strong enough echo from its crack tip which makes it difficult to size the crack height. There can also be pressure induced stress in the crack tip which hinders the detection of the crack by letting the ultrasound trough it. Cracks that have initiated from the surface may also be filled with water [16]. In some cases the SCC crack doesn't appear alone but in a group of cracks [17]. All these variations in the crack morphology have to be considered in order to detect and size SCC cracks properly.

6   Conclusions

SCC has been mitigated in Finnish BWRs by material selection and water chemistry. Still SCC is estimated as potential degradation mechanism in Finnish BWRs piping. During periodic in-service inspections of pressure vessels and piping SCC degradation is searched. Qualification process confirms that inspections are reliable and the found indications can be measured accurately. Periodic inspections are important because it is priority to constantly know in what state the nuclear power plant is. If degradation is found, needed actions can be taken such as replacement activities or repair. Good quality of the inspections is essential in order evaluate the inspection results right. Unnecessary repair can make harm to the structure. Grindings and surface welds can be potential locations for crack initiation.

Nuclear power plants need to be ready to face new degradation mechanisms. Aging of the older power plant materials is of interest because the failure probability increases

by time, but also new materials can show unexpected features. For example, it was thought that Alloy 600 was excellent material, but turned up that it was also susceptible to SCC.

In the regulation guide for Finnish nuclear power plant in-service inspections is a requirement to prepare for postulated defects when the initiation of defects of particular type is postulated in a particular structure but there is also a requirement to prepare for unspecified defects even when no specific degradation mechanism exists of a structure and the nature of potential defects is thus unknown [10]. Observing constantly operating experiences from nuclear power plants around the world gives information of new aging and degradation mechanisms.

7   References

1 Brickstad B., The Use of Risk Based Methods for Establishing ISI-Priorities for Piping Components at Oskarshamn 1 Nuclear Power Station, 2000, SKI

2 Stress Corrosion Cracking in Light Water Reactors: Good Practices and Lessons Learned. IAEA Nuclear Energy Series, No. NP-T-3.13. 2011

3 Technical Report on Material Selection and Processing Guidelines for BWR Coolant Pressure Boundary Piping. NUREG-0313 rev. 2. NRC, 1988

4 Sanda R., Renev A., Peinador Veira M., Events related to Leaks and Cracks of the Reactor Coolant Pressure Boundary, NRSA/CLEAR/14 01 003 Rev. 00, European Commission Joint Research Centre, Petten, 2014

5 UT Operator Training for the Detection of Intergranular stress Corrosion Cracking (IGSCC), EPRI NDE Center, Charlotte, 1983

6 IGSCC in BWRs, Corrosion and Corrosion Control in LWRs, Structural Integrity Associates, 2010. Available [www]: http://pbadupws.nrc.gov/docs/ML1122/ML11229A052.pdf

7 Safety Aspects of Nuclear Power Plant Ageing. IAEA-TECDOC-540, IAEA, Vienna, 1990.

8 Hänninen H., Aho-Mantila I., Effect of Sensitization and Cold Work on Stress Corrosion
Susceptibility of Austenitic Stainless Steel in BWR and PWR Conditions. 1981. VTT

9 Tetsuo S., Progress in the Mechanistic Understanding of BWR SCC and Its Implication to the Prediction of SCC Growth Behavior in Plants Fracture, Research Institute, Tohoku University, Japan, 2003

10 Guide YVL E.5 In-service Inspection of Nuclear Facility Pressure Equipment with Non-destructive Testing Methods, STUK, 2014

11 Cronvall O., Männistö I., Alhainen J., Development of Risk Informed In-Service Inspection Analysis Procedures and Application to Finnish BWR Unit Piping Components, 2009, VTT.

12 Simola, K., Holmberg, J., Cronvall, O., 2005, RI-ISI Pilot Study of the Shut Down Cooling System of the Olkiluoto 1/2 NPP units, VTT

13 Forstén J., Kauppinen P., Teräskappaleiden ultraäänitestauksen luotettavuus. Espoo. VTT. 1987

14 European Methodology for Qualification of Non-Destructive Testing- Third Issue, ENIQ report Nr 31 EUR 22906 EN, 2007

15 Boiler and Pressure Vessel Code, Section XI, Rules for In-service Inspection of Nuclear Power Plant Components, ASME, 2010

16 Simola K., Pulkkinen U. Statistical Models for Reliability and Management of Ultrasonic Inspection Data. Espoo. VTT1996.

17 Särkiniemi P., Kauppinen P., Jeskanen H., Jännityskorroosiosäröjen ultraäänitutkimus, VTT, 1987

The Safe-end Dissimilar Metal Weld Designs in Light Water Reactors

Teemu Sarikka

Aalto University School of Engineering
Department of Engineering Design and Production
teemu.sarikka@aalto.fi

Abstract

Dissimilar metal welds (DMW) are extensively used in nuclear power plants (NPP) to join the ferritic steel nozzles of reactor pressure vessels (RPV), steam generators, and pressurizers to the austenitic stainless steel piping using different types of safe-end designs. A conventional NPP safe-end weld design is a V-grooved DMW with a separate buttering layer, whereas in the modern pressurized water reactor (PWR) designs, the safe-end DMWs are manufactured using a new weld design which takes advantage of narrow-gap (NG) welding technique. In addition to the new weld design, the filler metals have been changed from Alloys 82 and 182 to higher Cr containing Alloys 52 and 152. To ensure the structural integrity of the modern DMWs, the changes in the weld design and filler metal require extensive knowledge of the correlations and relationships between the dilution of the base metal and the compositional gradients of alloying elements, the resulting microstructures, and the resulting mechanical and fracture mechanical properties as well as the damage and failure mechanisms of the DMWs.

1 Introduction

The operational concept of a nuclear power plant (NPP) is to produce energy by using the heat generated by the fission reaction of the fissile elements occurring in the core of a nuclear power plant. The fission heat is used to heat up coolant, which is then vaporized and further lead to a turbine. The steam will spin the turbine bound to a generator, which will transform the turbine's kinetic energy into electricity. As of 2015, there are a total of 438 nuclear power reactors in operation producing about $380\,000$ MW$_e$, 2 reactors in long-term shutdown, and 68 reactors under construction (IAEA 2015). Nuclear reactors are divided into either fast reactors or thermal reactors depending on the energies of the fission neutrons used to maintain the controlled fission chain reaction. In the thermal reactors, the fission neutrons are slowed down from MeV energies into eV energies before causing a new fission reaction whilst in the fast reactors the fission reaction is maintained by the MeV energy-state fission neutrons.

All nuclear reactors in commercial use are thermal reactors and a majority of the nuclear reactors in commercial use are so called light water reactors (LWR), which means that they use normal water both as a coolant and as a moderator. Two of the most commonly used LWR types are the boiling water reactor (BWR) and the pressurized water reactor (PWR). As of 2015, there are a total of 279 PWRs and

78 BWRs in operation worldwide (IAEA 2015). The other types of reactors in commercial usage include pressurized heavy-water reactor (PHWR, 49 in operation), light-water-cooled and graphite-moderated reactor (LWGR, also known as RBMK, 15 in operation), gas-cooled and graphite-moderated reactor (GCR, 15 in operation), and fast breeder reactor (FBR, 2 in operation) (IAEA 2015). Figure 1 shows the basic components of a thermal nuclear reactor.
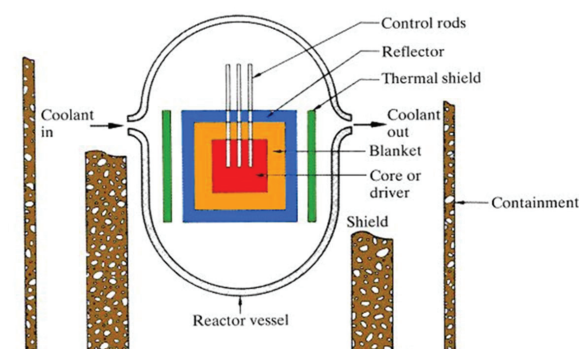
Figure 1. Basic components of a thermal nuclear reactor.

Basically all thermal nuclear reactors contain the following basic components: a core, a moderator, a reflector, a control rod system, a thermal shield, a reactor pressure vessel (RPV), and a biological shield. The purpose of the core is to maintain the nuclear reaction itself and, thus, to produce the heat required to heat up the coolant. In thermal reactors, the core consists of fuel, moderator, and coolant. In PWRs and BWRs, the fuel is around $2-3$ wt. % U^{235} enriched uranium oxide and water acts as a coolant and, also, as a moderator, whose purpose in thermal reactors is to slow down fast fission neutrons into thermal energies for better fission triggering. Reactor pressure vessel also contains reflector, whose purpose is to reflect a part of escaping neutrons back into the core, and control rods, which are constructed from strongly neutron-absorbing material, such as silver or cadmium. The purpose of the control rods is to absorb the fission neutrons in a nuclear power plant shut down situation. Reactor pressure vessel contains all of the components mentioned above and shields them from the environment and vice versa. In addition to the reactor pressure vessel, thermal nuclear reactor also contains a biological shield to protect the personnel from radiation and a containment to prevent radiation leaks to the environment in case of an accident.

2 Nuclear power plant safe-end dissimilar metal weld designs

Dissimilar metal welds (DMW) are extensively used in NPPs to join the ferritic steel nozzles of RPVs, steam generators, and pressurizers to the austenitic stainless steel piping using a different type safe-end designs (Hänninen et al. 2007). The ferritic steels are used as the

structural material of the RPVs because of their relatively good mechanical properties and low cost whereas the stainless steels are used in components in which a good corrosion resistance is mandatory. The simultaneous usage of these two types of crystallographically different materials makes the presence of DMWs in NPPs obligatory. One of the most critical DMWs in an NPP is the one joining the RPV through its nozzle to the main coolant piping. For a number of reasons, the assembly is facilitated using a transition piece called safe-end in between the ferritic RPV nozzle and the austenitic stainless steel piping. The safe-ends are made of either austenitic stainless steel or Ni-base alloy, depending on the plant design. Figure 2 shows location of the DMW joining the RPV nozzle to the safe-end. The main purpose of the safe-end is to enable the manufacturer to weld the difficult dissimilar metal joint at the RPV manufacturing site and, thus, leave the easier similar metal joint between the austenitic materials to be welded at the plant construction site.
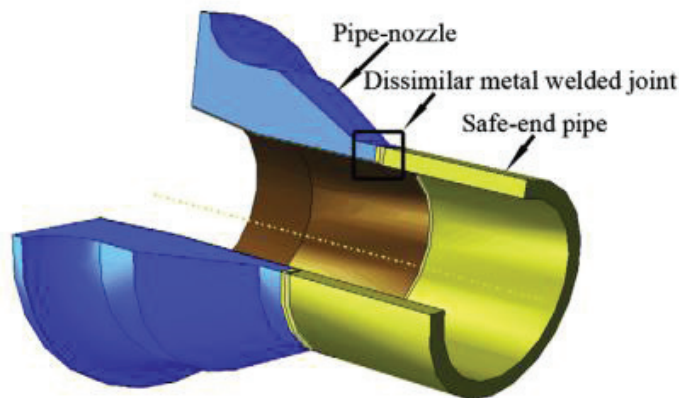
Figure 2. DMW joining the ferritic RPV nozzle to the austenitic safe-end (Wang et al. 2011).

A conventional NPP safe-end weld design is a V-grooved DMW consisting of the heat-affected zones (HAZs) of the base metals, the fusion boundary area/near interface zone (NIZ), the interface between the weld metal/buttering and the base metals, the buttering layer, and the weld metal (Lippold and Kotecki 2005). The welds are manufactured by welding the buttering layer to the ferritic steel nozzle and then manufacturing the weld itself by starting at the root of the V-groove and gradually building up the weld pass by pass. The total amount of the filler metal required in manufacturing a V-grooved DMW is quite high since the cross-sectional area of the V-groove is large resulting in a large weld volume. The larger weld volumes result in higher manufacturing costs due to longer welding times (Biswas et al. 2010) as well as higher distortions due to weld shrinkage and higher residual stresses in the weld (Nelson and Lewis 1967, Biswas et al. 2010). A cross-section image showing a traditional V-grooved DMW safe-end design is shown in Figure 3.
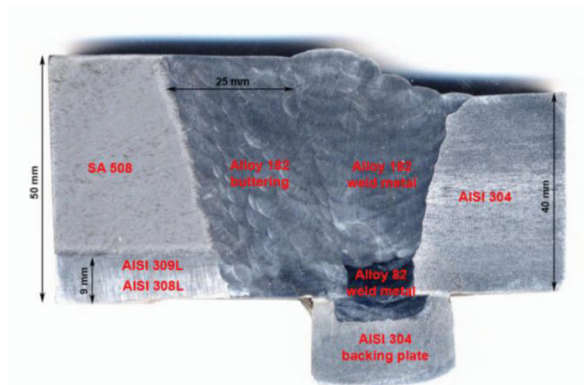
Figure 3. A traditional V-grooved DMW safe-end design.

In traditional BWR designs, Alloy 600 based filler metal Alloy 82/182 is used as filler metal of the safe-end DMWs. Alloy 82/182 has a face-centered cubic (FCC) solid solution structure and the thermal expansion coefficient of Alloy 82/182 is between the thermal expansion coefficients of the ferritic RPV steel and austenitic stainless steel. In addition, Alloy 82/182 retards the carbon diffusion from the ferritic RPV steel to the weld metal significantly. The main problem with the Alloy 82/182 is that there has been concerns about the integrity of the Alloy 82/182 containing DMWs due to the Alloy 82/182's high susceptibility to stress corrosion cracking (SCC) in different LWR environments (Hänninen et al. 2007, Andresen et al. 2008, Hänninen et al. 2008, Seifert et al. 2008, Karlsen and Pakarinen 2009, Hänninen et al. 2009, Hou et al. 2010B, Hänninen et al. 2011). DMWs have been found susceptible to environmentally assisted cracking (EAC) in BWR conditions where their microstructures and prevailing residual stresses and residual strains affect the EAC susceptibility (Hänninen et al. 2007). DMWs are also used in primary water systems of PWRs (Wang et al. 2013) where Ni-base filler metal DMWs have been found to suffer from the stress corrosion cracking susceptibility in primary water conditions (PWSCC) (Hänninen et al. 2007, Andresen et al. 2008, Hänninen et al. 2008, Seifert et al. 2008, Karlsen and Pakarinen 2009, Hänninen et al. 2009, Hänninen et al. 2011). The operating experience of major NPP pressure boundary components has shown (Hänninen et al. 2007, Hänninen et al. 2008, Hänninen et al. 2011) that DMW joints can markedly affect the plant availability and safety because of increased incidences of EAC and PWSCC of Alloy 600 and corresponding nickel-base weld metals, such as Alloys 182/82. All-weld metals of Alloy 182 and 82 had been found clearly more susceptible to EAC than all-weld metals of Alloy 152 and 52 which hardly show any crack initiation susceptibility in e.g. doped steam conditions (Karlsen and Pakarinen 2009, Hänninen et al. 2009, Hänninen et al. 2011).

In modern PWR designs, the safe-end DMWs are manufactured using a narrow-gap (NG) welding technique without a separate buttering layer and with Alloy 690 based filler metal, Alloy 52 (Joly et al. 2014). The transition from Alloy 600 based filler metals to Alloy 690 based filler metals with higher Cr contents and the new weld design using NG welding technique are made to ensure the structural integrity of the welds as well as to decrease the joining costs due to the higher productivity of the narrow gap welding technique (Engelhard et al. 2000, Joly et al. 2014). NG weld is more economical than the conventional V-grooved weld as it requires less welding consumable, shorter welding times, and reduces the volume of inspection. In addition, the reduced amount of weld metal and lower heat input used in NG welding leads to less shrinkage, distortion and smaller residual stresses/strains. A cross-section image showing a modern NG DMW safe-end design is shown in Figure 4 and the difference in the weld design and the reduction of the total weld volume due to the difference in the weld designs are further demonstrated in Figure 5.

Figure 4. A modern NG DMW safe-end design.

Narrow Gap Welding
material: stainless steel thickness: 90mm

Conventional Weld
material: carbon steel thickness: 90mm

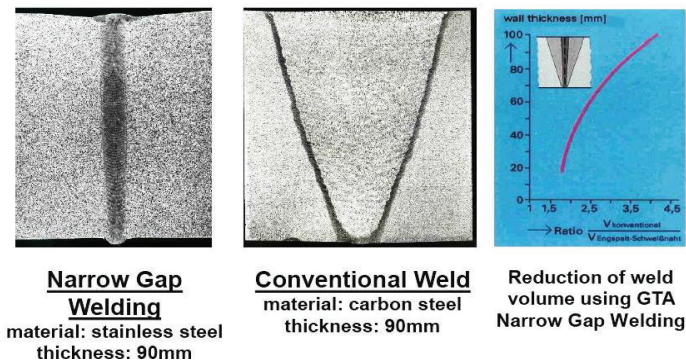**Reduction of weld volume using GTA Narrow Gap Welding**

Figure 5. Reduction of the weld volume using NG-GTAW technique compared to a conventional V-grooved weld. The reduction of weld volume e.g. for 90 mm wall thickness is a factor of 4 (Engelhard et al. 2000).

Similarly to the Alloy 82/182, Alloy 52 has an FCC solid solution structure, which is designed to take Ni, Cu, Cr, and Fe into solution upon dilution from the base metals whilst keeping a normal single-phase dendritic structure. Typically, a planar growth zone without precipitates appears at the weld interface followed by a cellular dendritic zone with precipitates in the interdendritic regions. Further in the weld metal, a columnar dendritic zone results from solidification along preferential growth directions and temperature gradients (Alexandrov et al. 2012). Compared to the Alloy 82/182, the Alloy 52 contains less Nb and more Ti and it has a smaller solidification temperature range (Naffakh et al. 2009). The main consequence is a coarser dendritic structure with less Nb-rich precipitates. The precipitates are mostly TiN and TiC, distributed in the interdendritic regions and at the grain boundaries (GB). Their number is lower than in Alloy 82/182 weld metal, although the precipitation is increased with post-weld heat treatment (PWHT) (Soares et al. 2007). Alloy 52 hardness is therefore in average lower than that of the Alloy 82/182 welds (Kuo and Lee 2002). In addition, it has a lower tensile strength (Lee and Jeng 2001). Due to its higher Cr content, Alloy 52 exhibits superior corrosion resistance compared to the Alloy 82/182. However, it can contain dynamically recrystallized zones which may decrease SCC resistance (Morra et al. 2011).

3 Structural integrity of dissimilar metal welds

Cracking associated with DMWs has been a constant problem and may typically occur near the fusion boundary either along the martensitic boundary adjacent to the fusion boundary or along the Type II boundary in the weld metal side of the fusion boundary (Nelson et al. 1999). A characteristic feature of a DMW is the metallurgical and mechanical mismatch resulting from a steep gradient of changing narrow compositional and microstructural zones with significantly different strength and toughness properties across the weld between two physically different materials. This results in metallurgical mismatch which affects the entire failure behavior of a DMW under external operational loads, not only from the crack initiation standpoint, but especially regarding the development of the crack driving force, subsequent crack growth behavior and development of local plastic constraint that can result in crack path deviation (Nevasmaa et al. 2000, Faidy et al. 2004, Laukkanen et al. 2007).

One of the driving forces of the current mismatch research has been the insight that the fracture toughness and the strength properties of the different zones interact with each other during the progress of the final failure in the case of external loading. This means that measuring the toughness properties alone is not enough to describe the entire failure behavior of a heterogeneous system, e.g., DMW, if the mechanical properties of the different zones are not known. The traditional concept of mismatch in welds focuses on the different strength levels of the weld metal and the base metal in a form of strength mismatch factor M, defined in the

Brite Euram structural integrity assessment procedure for European industry (SINTAP) as the ratio of the yield strength of the weld metal σ_{WM} to that of the base material σ_{BM} (Kim et al. 2000). If the mismatched situation is considered from the fracture mechanical point of view, traditionally, overmatching the weld metal has been used as a way to secure the weld metal against plastic strains and existing flaws (Moran and Shih 1998).

In bimetal welds, however, crack growth mechanisms and directions have been found to depend on the mechanical mismatch, the position of the different zones in relation to each other, the dimensions of the zones, and the local strength and toughness properties of the adjacent weld zones (Hutchinson et al. 1987, Homma et al. 1995, Jiang et al. 2003, Neves and Loureiro 2004, Laukkanen et al. 2007). The strength mismatch between different materials or microstructural regions produces different local plastic constraints which further affect the distribution and magnitude of local stress triaxiality and plastic strain ahead of the crack tip locating at the interface (Wang et al. 2013). Irrespective of the existence of the original flaw or defect in a weld, the actual damage formation can therefore occur and escalate in a neighboring microstructure (Nevasmaa et al. 2000, Laukkanen et al. 2007). This, together with the dendritic microstructure, tends to appear as irregular crack front shape of a propagating crack, which is another characteristic feature of DMWs.

Unstable crack growth can occur after initially ductile initiation in the fusion boundary and NIZ of a DMW (Nevasmaa et al. 2000, Laukkanen et al. 2001, Faidy et al. 2004, Laukkanen et al. 2007). Rather than the presence of a single weaker region, a combination of several adjacent microstructures, i.e., a carbon-depleted zone (CDZ) in the ferritic coarse-grained HAZ, a weld interface with discontinuous martensitic regions, and a fully austenitic region in the first buttering layer, all with mismatching mechanical properties, has been found responsible for unstable crack growth. The combination of stress triaxiality and asymmetric plastic strain is considered as the principal driving force for damage formation and ductile fracture in DMWs. Thus, the significance of mismatch can be related to the failure behavior of 'brittle' constituents as an increase in constraint (if linear mismatch is concerned), and the localized deformation experienced by the softer regions and the resulting compatibility requirements set to the harder microstructures (in the case of elastic-plastic mismatch). A notch or a crack-like defect at the interface of two materials of which one exhibits plastic behavior that affects the crack tip plasticity development while the other still behaves practically linear-elastically has hence been concluded to represent the worst mismatch scenario in terms of structural integrity (Nevasmaa et al. 2000, Laukkanen et al. 2007).

Currently there are no standards available to assess the structural integrity of DMW components or to test materials of DMWs. Therefore, ensuring safe service of a DMW

component requires complete strength and fracture toughness based information from all microstructural zones of a DMW. Their stress-strain behavior, local fracture resistance, and crack growth behavior should be experimentally investigated and underlying characteristics understood. To ensure the structural integrity of the modern DMWs, the changes in the weld design require extensive knowledge of the correlations and relationships between the dilution of the base metal and the compositional gradients of alloying elements, the resulting microstructures, and the resulting mechanical and fracture mechanical properties as well as the damage and failure mechanisms of the DMWs.

References

Alexandrov, B.T., Lippold, J.C., Sowards, J.W., Hope, A.T., and Saltzmann, D.R. (2012) Fusion Boundary Microstructure Evolution Associated with Embrittlement of Ni-base Alloy Overlays Applied to Carbon Steel. Welding in the World. Vol. 57. pp. 39-53.

Andresen, P.L., and Morra, M.M. (2008) Stress Corrosion Cracking of Stainless Steels and Nickel Alloys in High-Temperature Water. Corrosion the Journal of Science and Engineering. Vol. 64. No. 1. pp. 15-29.

Biswas, P., Mandal, N.R., Vasu, P., and Padasalag, S.B. (2010) Analysis of Welding Distortion due to Narrow-Gap Welding of Upper Port Plug. Fusion Engineering and Design. Vol. 85. pp. 780-788.

Engelhard, G., Habip, L.M., Pellkofer, D., Schmidt, J., and Weber, J. (2000) Optimization of Residual Welding Stresses in Austenitic Steel Piping: Proof-Testing and Numerical Simulation of Welding and Post-Welding Processes. Nuclear Engineering and Design. Vol 198. pp. 141-151.

Faidy, C., Martin, G., Taylor, N., Youtsos, A., Katsareas, D., Keinänen, H., Laukkanen, A., Wintle, J., Sherry, A., Lidbury, D., Safa, N., Cipiere, M. F., Gilles, P., Chapuliot, S., Kaiser, Y., and Lenkey, G. (2004) Assessment of Aged Piping Dissimilar Metal Weld Integrity. ADIMEW Synthesis report. Contract FIKS-CT-2000-00047. European Commission. 45 p.

Homma, H., Kanto, Y., Kubo, T., and Tanaka, Y. (1995) Crack Growth Resistance in Bi-Metallic Weldment. International Journal of Pressure Vessels and Piping. Vol. 63. pp. 225-236.

Hutchinson, J.W., Mear, M.E., and Rice, J.R. (1987) Crack Paralleling an Interface between Dissimilar Materials. Journal of Applied Mechanics. Vol. 54. pp. 828-832.

Hänninen, H., Toivonen, A., Brederholm, A., Saukkonen, T., Ehrnstén, U., and Aaltonen, P. (2007) Environment-Assisted Cracking and Hot Cracking of Ni-Base Alloy Dissimilar Metal Welds. Proceedings of the 13th International Conference on Environmental Degradation of Materials in Nuclear Systems – Water Reactors. Whistler, British Columbia, Canada. 19 p.

Hänninen, H., Brederholm, A., Saukkonen, S., Gripenberg, H., Toivonen, A., Ehrnstén, U., and Aaltonen, P. (2008) Hot Cracking and Environment-Assisted Cracking Susceptibility of Dissimilar Metal Welds. VTT Research Notes 2399. VTT Technical Research Centre of Finland, Espoo, Finland. 177 p.

Hänninen, H., Toivonen, A., Saukkonen, T., Brederholm, A., Aaltonen, P., and Ehrnstén, U. (2009) EAC Crack Initiation in Nickel-Based Dissimilar Metal Welds Using Doped Steam

Test. Proceedings of the 14th International Conference on Environmental Degradation of Materials in Nuclear Systems – Water Reactors. Virginia Beach, VA, USA. pp. 333–343.

Hänninen, H., Brederholm, A., Saukkonen, T., Ivanchenko, M., Toivonen, A., Karlsen, W., Ehrnstén, U., and Aaltonen, P. (2011) Environment-Assisted Cracking and Hot Cracking Susceptibility of Nickel-Base Alloy Weld Metal. VTT Research Notes 2582. VTT Technical Research Centre of Finland, Espoo, Finland. 155 p.

IAEA (2015) International Atomic Energy Agency (IAEA) Power Reactor Information System (PRIS). URL: https://www.iaea.org/pris/. Referred 30th September 2015.

Jiang, F., Zhao, K., and Sun, J. (2003) Evaluation of Interfacial Crack Growth in Bimaterial Metallic Joints Loaded by Symmetric Three-Point Bending. International Journal of Pressure Vessels and Piping. Vol. 80. pp. 129-137.

Joly, P., Yescas, M., and Keim, E. (2014) Fracture Toughness in the Ductile-Brittle Transition and Thermal Ageing Behavior of Decarburized Heat Affected Zone of Alloy 52 Dissimilar Metal Welds of Nuclear Components. Proceedings of the ASME-2014 Pressure Vessel and Piping Conference. July 20-24, Anaheim, California, USA.

Karlsen, W. and Pakarinen, J. (2009) TEM Investigation of Cracks in Dissimilar Metal Weld Inconel 182 Following Doped Steam Testing. Research Report VTT-R-05722-09. VTT Technical Research Centre of Finland, Espoo, Finland. 29 p.

Kim, Y.-J., Koçak, M., Ainsworth, R.A., and Zerbst, U. (2000) SINTAP Defect Assessment Procedure for Strength Mismatched Structures. Engineering Fracture Mechanics. Vol. 67. pp. 529-546.

Kuo, T., and Lee, H. (2002) Effects of Filler Metal Composition on Joining Properties of Alloy 690 Weldments. Materials Science and Engineering. Vol. 338. pp 202-212.

Laukkanen, A., Nevasmaa, P., Ehrnstén, U., and Rintamaa, R. (2001) Mapping of Characteristic Features of Bimetallic Welds from the Standpoint of Engineering Critical Analysis. Proceedings of the 16th International Conference on Structural Mechanics in Reactor Technology (SMiRT-16); Div. G, Fracture Mech. Washington DC, 12-17 August 2001. Ed.: Vernon C. Matzen, and C.C. David Tung. International Association for Structural Mechanics in Reactor Technology (IASMiRT), USA. Paper #1566. 8 p.

Laukkanen, A., Nevasmaa, P., Ehrnstén, U., and Rintamaa, R. (2007) Characteristics Relevant to Ductile Failure of Bimetallic Welds and Evaluation of Transferability of Fracture Properties. Nuclear Engineering and Design. Vol. 237. pp. 1-15.

Lee, H.T., and Jeng, S.L. (2001) Characteristics of Dissimilar Welding of Alloy 690 to 304L Stainless Steel. Science and Technology of Welding & Joining. Vol. 6. No. 4. pp. 225-234.

Lippold, J.C., and Kotecki, D.J. (2005) Welding Metallurgy and Weldability of Stainless Steels. John Wiley & Sons, Inc., Hoboken, New Jersey, USA. 376 p. ISBN: 978-0471-47379-4.

Moran, P.M., and Shih, C.F. (1998) Crack Growth and Cleavage in Mismatched Welds: a Micromechanics Study Using Cell Model. International Journal of Fracture. Vol. 92. pp. 153-174.

Morra, M., Othon, M., Willis, E., and McCracken, S. (2011) Characterization of Structures and Strains in 52-Type and 152 Welds. Alloy 690/52/152 PWSCC Research Collaboration Meeting. November 29 – December 2, Tampa, Florida, USA. pp. 1-183.

Nelson, J.W. and Lewis, W.J. (1967) Process for Narrow Gap Welding. United States Patent Office. Patent 3328556.

Nelson, T.W., Lippold, J.C., and Mills, M.J. (1999) Nature and Evolution of the Fusion Boundary in Ferritic-Austenitic Dissimilar Weld Metals, Part 1 – Nucleation and Growth. Welding Journal. Vol. 78. No. 10. pp. 329-337.

Nevasmaa, P., Laukkanen, A., and Ehrnstén, U. (2000) Fracture Resistance and Failure Characteristics of AISI 304/SA508 Bimetallic Weld in Ductile Regime. Proceedings of the 13th European Conference on Fracture – Fracture Mech.: Applications and Challenges (ECF 13). San Sebastian, Spain, 6-9 September 2000. ESIS / Eng. Mat. Advisory Services Ltd. Paper No. 1N.49. 8 p.

Naffakh, H., Shamanian, M., and Ashrafizadeh, F. (2009) Dissimilar Welding of AISI 310 Austenitic Stainless Steel to Nickel-based Alloy Inconel 657. Journal of Materials Processing Technology. Vol. 209. pp. 3628-3639.

Neves, J., and Loureiro, A. (2004) Fracture Toughness of Welds – Effect of Brittle Zones and Strength Mismatch. Journal of Materials Processing Technology. Vol. 153-154. pp. 537-543.

Seifert, H.-P., Ritter, S., Shoji, T., Peng, Q.J., Takeda, Y., and Lu, Z.P. (2008) Environmentally-Assisted Cracking Behaviour in the Transition Region of an Alloy182/SA 508 Cl.2 Dissimilar Metal Weld Joint in Simulated Boiling Water Reactor Normal Water Chemistry Environment. Journal of Nuclear Materials. Vol. 378. pp. 197-210.

Soares, B., De Abreu Mendonça Schvartzmanm M.M., and Reis da Costa Campos, W. (2007) Characterization of the Dissimilar Welding - Austenitic Stainless Steel with Nickel Alloy Filler Metal. International Nuclear Atlantic Conference. 6 p. ISBN 978-85-99141-02-1.

Wang, H.T., Wang, G.Z., Xuan, F.Z., and Tu, S.T. (2011) Numerical Investigation of Ductile Crack Growth Behavior in a Dissimilar Metal Welded Joint. Nuclear Engineering and Design. Vol. 241. pp. 3234-3243.

Wang, H.T., Wang, G.Z., Xuan, F.Z., and Tu, S.T. (2013) An Experimental Investigation of Local Fracture Resistance and Crack Growth Paths in a Dissimilar Metal Welded Joint. Materials and Design. Vol. 44. pp. 179-189.

Deriving η-factor for Welds

Sebastian Lindqvist
sebastian.lindqvist@vtt.fi

Abstract

Ageing nuclear power plants (NPP) require more accurate methods to assess the structural integrity of pipes. The accuracy of structural assessment methods of pipes can be increased by improving the accuracy of fracture toughness measurements of welds. In these measurements η-factor plays a crucial role. The η-factor is a parameter that relates the measured load-displacement data to the plastic strain energy. Currently, welds are assessed with η-factors developed for homogeneous specimens. Plastic η-factors developed specially for welds increase the accuracy of the fracture toughness measurements and the structural safety assessment methods. In this literature survey recently developed η-factors for similar metal welds are reviewed. The influence of different parameters, e.g. strength mismatch, on η-factor is considered.

1   Introduction

Integrity of pipes in nuclear power plants (NPP) is determined with leak-before-break (LBB) analysis. LBB is important for the design, safety and management of NPP piping. The LBB analysis requires knowledge of the weakest location in the pipe and the fracture toughness of this location.

The weakest location is normally in the weld region. Current safety standards consider the weakest locations to be in the HAZ and close to the fusion line. The reason for determining fracture toughness of HAZ is that brittle microstructures or zones with lower toughness are likely to occur close to the fusion line thereby obtaining lower resistance against crack extension (Donato et al. 2009). However, cracks can develop anywhere in the weldment, even in the weld metal.

The fracture toughness of the weakest location in a weld is determined with fracture toughness measurements (BS7448, ASTM 1290, ASTM 1820). In ASTM E1820 fracture resistance (J) of stationary cracks consists of an elastic component J_{el}, and a plastic component, J_{pl}, (equation (1)). Equation (1) is derived for cracked specimens under Mode I deformation. The other standards follow the same principles as ASTM E1820.

$$J = J_{el} + J_{pl} \tag{1}$$

where

$$J_{el} = \frac{K^2(1-v^2)}{E} \tag{2}$$

In equation (2) K is the elastic stress intensity factor for the cracked specimen, E is elastic modulus and **ν** is Poisson's ratio.

$$K = \frac{P}{\sqrt{BB_N W}} f\left(\frac{a}{w}\right) \qquad (3)$$

The plastic contribution to the strain energy is given in equation (4).

$$J_{pl} = \frac{\eta A_{pl}}{B_N b_0} \qquad (4)$$

In equation 4 A_{pl} is the plastic area under the load-displacement curve (figure 1), B_N is the net specimen thickness for a specimen with side grooves and b is the remaining ligament. Plastic η-factor is a dimensionless constant that relates the plastic contribution A_{pl} to J_{pl}. The factor is assumed to be a function of the a/W ratio and independent of loading (Cravero & Ruggieri 2007). A_{pl} can be defined in terms of load-load line displacement (LLD) data or load-crack mouth opening displacement (CMOD) data. Depending on the route the η-factor is either expressed as η_{LLD} or η_{CMOD} (Leonardo et al. 2013). The η values based on LLD have different character than η based on CMOD.
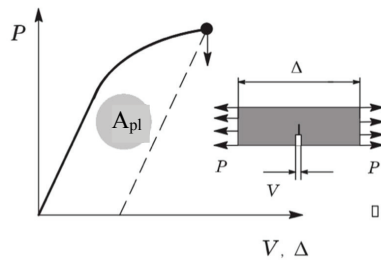
Figure 1. a) The plastic area under the load-displacement curve. (Leonardo et al. 2013)

ASTM E1820 and similar standards are developed for homogeneous specimens. The fracture toughness estimation equations in these fracture toughness standards are not necessary applicable to assess accurately fracture toughness of heterogeneous materials like welds. The problem of using the current fracture toughness standards results from the difference in deformation behaviour of homogeneous materials and welds. In homogeneous materials the plastic zone in front of the crack is symmetrical and of certain shape. In over- and undermatched welds the plastic zone can be discontinuous, unsymmetrical or forced into a smaller material volume (figure 2).
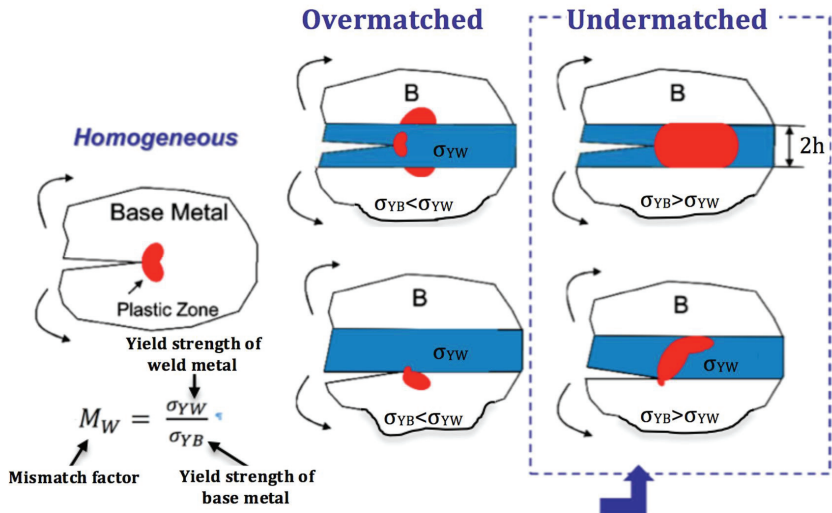
Figure 2. Heterogeneous fracture toughness specimens like welds have different regions (base metal, weld metal, HAZ) with varying material properties. The strength difference of the base metal and weld metal affects the measured fracture resistance. The ratio of the yield strength of the base metal, σ_{YB}, and the weld metal, σ_{YW}, is known as strength mismatch (M_W). The weld is said to be strength overmatched when $M_W > 1$ and strength undermatched when $M_W < 1$. (Koçak 2010)

For centerline cracked overmatched welds plastic deformation can occur in the base metal. In centreline cracked undermatched welds the plasticity is constrained to the weld. Unsymmetrical deformation zones are generated for cracks at the interface as seen in figure 2.

The deformation behaviour of over- and undermatched welds (figure 2) affects the measured CMOD in a way that is not characteristic for homogeneous materials. The measured CMOD can be suppressed or magnified by strength mismatch (M_w) condition in the heterogeneous specimen. This suppression or magnification of CMOD leads to under- or overestimations of the area under the load–displacement curve, A_{pl} (figure 1). If the current fracture toughness standards are used to calculate J_{pl} from the measured A_{pl}, then the results are inevitably inaccurate.

To calculate fracture toughness accurately from A_{pl} for a weld η-factors developed for heterogeneous specimens are required. Heterogeneous η-factors can be derived from finite element (FE) analyses. Plastic η-factors derived for heterogeneous welds show in which cases it is absolutely necessary to apply heterogeneous solutions and in which cases homogeneous η-factors give a good approximation of the fracture toughness. (Paredes & Ruggieri 2012)

Accurate η-factors derived for welds are a function of strength mismatch, M_w (Xuan et al. 2005). As the properties of the weld metal are close to base metal properties, η-factors developed for homogeneous specimens can be used. The η-factors for welds with relatively high M_w are expected to differ from the once derived for homogeneous specimens. Additionally, the η-factor can be affected by other parameters than M_w, like the weld width and configuration, crack location, strain hardening rate and the model used in FE calculations (Ruggieri 2012). To derive precise η-factors all of these parameters need to be taken into account. Precisely defined η-factors increase the accuracy of fracture toughness measurements of welds.

In this literature survey the main focus is on reviewing recently derived η-factors developed for similar metal welds where the weld metal has different properties than the base metal. The effect of different mechanical parameters, weld dimensions and finite element analysis routes on η-factor is considered.

2   Plastic η-factors for similar metal welds

In the following sections results on different investigations done for similar metal weld (SMW) centerline notched C(T), SE(T) and SE(B) specimens are reviewed. The test matrices and the dependence of the derived η-factors on strength mismatch, mechanical properties, weld width and FE analysis route are presented. Common for these analyses is that the material models used in FE method are assumed to consist of base metal and weld metal. The mechanical properties of HAZ are not taken into consideration (Savioli & Ruggieri 2013, Donato et al. 2009, Paredes & Ruggieri 2012). These results provide important information on the behaviour of the η-factor in welds.

2.1   Centerline cracked C(T) specimens

Savioli and Ruggieri (2013) derived η_{LLD} and η_{CMOD}-factors for weld centerline notched C(T) specimens (figure 3). Plastic η-factors were developed for strength evenmatched and 10, 20, 30 and 50 % strength overmatched welds. In these analysis the weld width, 2h, was 15 mm. To estimate the effect of weld width on the η-factor also calculations on 10 mm and 20 mm wide welds were done. The base plate material properties were varied between moderate, low and high hardening properties. The hardening coefficient (n) is 5 for high hardening material, 10 for moderate hardening material and 20 for low hardening material. The different material properties used for the weldment are shown in table 1. Both plane-strain and 3D FE analyses were done.
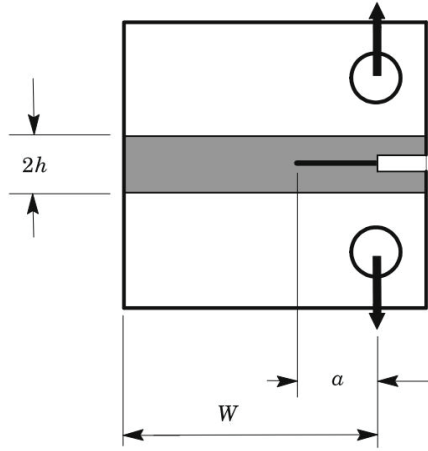
Figure 3. The model of the C(T) specimen that is used in the FE analyses. The model consists of the base metal and weld metal with the width 2h. (Savioli & Ruggieri 2013)

Table 1. The material matrix used in the analyses. The base metal hardening properties are varied and the weld metal properties are adjusted accordingly.

Mismatch level	Weld		Baseplate	
	σ_{ys} (MPa)	n	σ_{ys} (MPa)	n
10% overmatch	283	6.4	258	5
20% overmatch	309	6.9	258	5
30% overmatch	335	7.4	258	5
50% overmatch	386	8.4	258	5
Evenmatch	258	5	258	5

Mismatch level	Weld		Baseplate	
	σ_{ys} (MPa)	n	σ_{ys} (MPa)	n
10% overmatch	453	11.5	412	10
20% overmatch	494	12.8	412	10
30% overmatch	536	14.5	412	10
50% overmatch	618	17.4	412	10
Evenmatch	412	10	412	10

Mismatch level	Weld		Baseplate	
	σ_{ys} (MPa)	n	σ_{ys} (MPa)	n
10% overmatch	756	22.8	687	20
20% overmatch	824	25.5	687	20
30% overmatch	892	28.2	687	20
50% overmatch	1030	33.7	687	20
Evenmatch	687	20	687	20

The η_{LLD} and η_{CMOD}-factors derived from plane-strain analyses for the 15 mm wide weld with the base metal having moderate, high or low hardening properties are shown in figure 4. The η-factor is dependent on hardening properties of the base metal and mismatch level. The η-factor decreases with increasing strength mismatch. A decrease in the base metal hardening properties from 5 to 20, increases the sensitivity to strength mismatch. (Savioli & Ruggieri 2013)
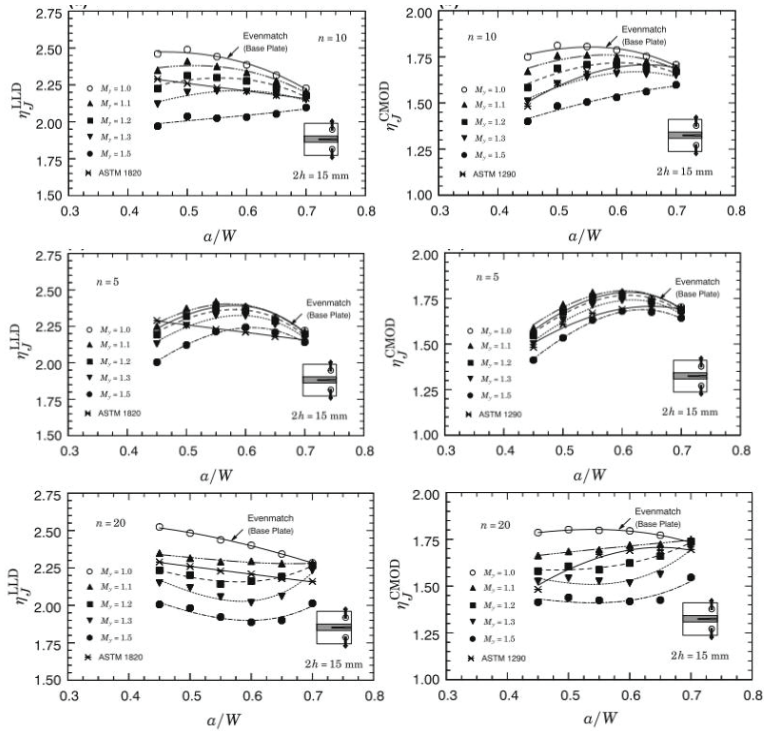
Figure 4. η_{LLD} and η_{CMOD} derived for SMW C(T) specimens with varying base metal hardening properties. The sensitivity of η-factor on strength mismatch is dependent of the base metal hardening properties. Regardless of the base metal properties the derived η-factors are not dependent on weld width in the range $0,1 \leq h/W \leq 0,2$. (Savioli & Ruggieri 2013)

In the analyses the plane-strain curves corresponding to the η-factors for the evenmatch (homogeneous) condition are larger than the homogeneous solutions given in ASTM E1820 for C(T) specimens. The difference between the two solution is in the range of 10–7 % for $0,45 \leq a/W \leq 0,6$. The ASTM formulations result into slightly conservative (lower) values of fracture toughness. A reason for the difference is that the η_{LLD} given by ASTM 1820 is formed from a limit load solution applicable to deeply cracked C(T) specimens. (Savioli & Ruggieri 2013)

Savioli and Ruggieri (2013) concluded also that the specimen thickness and the out-of-plane constraint have a big impact on the η-factor for centerline cracked C(T)

specimens. This is proved by comparing the 3D and plane-strain FE analyses. The 3D FE analyses yield different η-factors than the plane-strain analyses. Plastic η-factors derived from 3D analyses are in all conditions consistently lower than the corresponding plane-strain values.

In another investigation Koo et al. (2012) used 3D FE analyses to calculate η_{LLD}-factors for C(T) specimens. The analyses were done for both similar and dissimilar metal narrow gap welds. The results of the DMW analyses are presented later and the following paragraphs consider similar metal weld centreline notched C(T) specimens. Plastic η-factors were calculated for different strength mismatch conditions, weld widths (8 mm < 2h < 32 mm), and crack locations. The HAZ was taken into account in the 3D FE analyses and the HAZ width was fixed to 4 mm. The FE model was idealized as sandwich structure.

In contradiction to the previous analysis the HAZ is taken into account in the FE model. The mechanical properties of HAZ were measured with micro-Vickers hardness tester. The HAZ was 5–10% harder than the base metal, therefore, the yield strength of the HAZ was evaluated to be 10% higher than the yield strength of the base metal. The materials in the weldment were assumed to have the same elastic properties. (Koo et al. 2012)

The η-factors for similar metal weld centerline notched C(T) specimens were calculated for 20, 50 and 80 % strength overmatched welds and 10, 25, 40 % strength undermatched welds. In the FE analyses the base metal has high hardening properties and the weld width is 8 mm. (Koo et al. 2012)

The results of Koo do not agree with the previously presented η-factors of centreline cracked C(T) specimens. For an overmatched weld the derived η_{LLD}-factors are smaller than the corresponding ASTM E1820 solution. The η_{LLD}-factors derived for strength overmatched SMW C(T) specimen by Savioli were larger than the ASTM solutions. This contradiction is compared in figure 5.

(a)   (b)
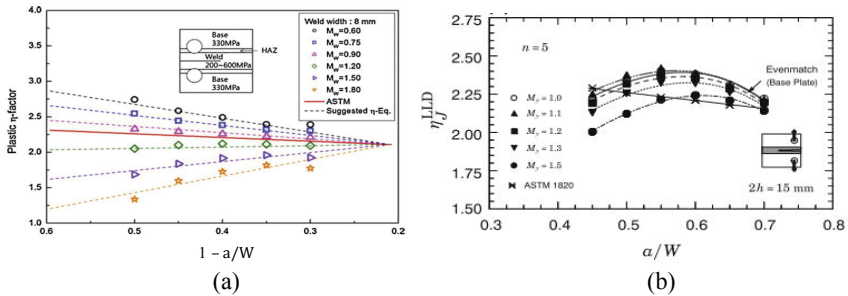
Figure 5. *Two different analyses done for SMW C(T) specimens. In both figures the homogeneous solution from ASTM E1820 is used as a reference. On the left side η-factors derived for strength overmatched welds are smaller than the ASTM E1820 values. On the right side η-factors derived for strength overmatched welds are larger than the ASTM E1820 values. The analyses on the left side were done with 3D models and on right side with plane-strain models.*

A reason for the difference in the magnitude of the η-factors is that the analyses of Savioli were based on the plane-strain model and Koo used the 3D model. Another possible reason for the difference is that the yield strength of the base metal in the analyses done by Koo (330 MPa) is larger than in the analyses done by Savioli (258 MPa). Thirdly, Savioli did not consider the effect of HAZ that can have a significant effect on η-factor.

The dependence of η-factor on strength mismatch and weld width can be evaluated with equation (5). The expression is applicable to centreline notched C(T) SMW specimens.

$$\eta = [3.43(\omega - 1.2)][(M_W - 1) + 0.522]\left[\frac{b}{W} - 0.21\right] + 2.11 \qquad (5)$$

where

$$\omega = \frac{W_{weld\,width}}{W_{specimen\,width}} \qquad (6)$$

2.2   Centerline cracked SE(T) specimens

Paredes and Ruggieri (2012) developed η_{LLD} and η_{CMOD}-factors for a wide range of crack sizes and different levels of weld strength mismatch, for weld centerline notched pin-loaded (H/W = 6) and clamped (H/W = 10) SE(T) specimens with weld groove width, 2h = 15 mm (figure 6). The strength mismatch varied between evenmatched, 10, 20, 30 and 50 % strength overmatch. The material properties are given in table 2. The base metal has moderate hardening properties. The effect of weld width on η-factor was also considered by varying 2h between 10 mm and 40 mm. Both plane-strain and 3D FE analysis were done.

Table 2. The material matrix used in the analyses. The base metal hardening properties do not vary.

Mismatch level	Weld		Baseplate	
	σ_{ys} (MPa)	n	σ_{ys} (MPa)	n
10% Overmatch	453	11.5	412	10
20% Overmatch	494	12.8	412	10
30% Overmatch	536	14.5	412	10
50% Overmatch	618	17.4	412	10
Evenmatch	412	10	412	10

Figure 6. The model of the SE(T) specimen that is used in the FE analyses. The model consists of the base metal and weld metal with the width 2h. (Paredes & Ruggieri 2012)

The effect of different parameters on η-factor is considered next. Figure 7 shows that the η-factor decreases with increasing mismatch level. The derived η-factors are relatively insensitive to the degree of strength mismatch in the range of 10–20% overmatch and crack size in the range $0,2 \leq a/W \leq 0,6$. Higher mismatch levels (30% and 50% overmatch) cause a 20 to 30 % deviation from the strength evenmatch condition.
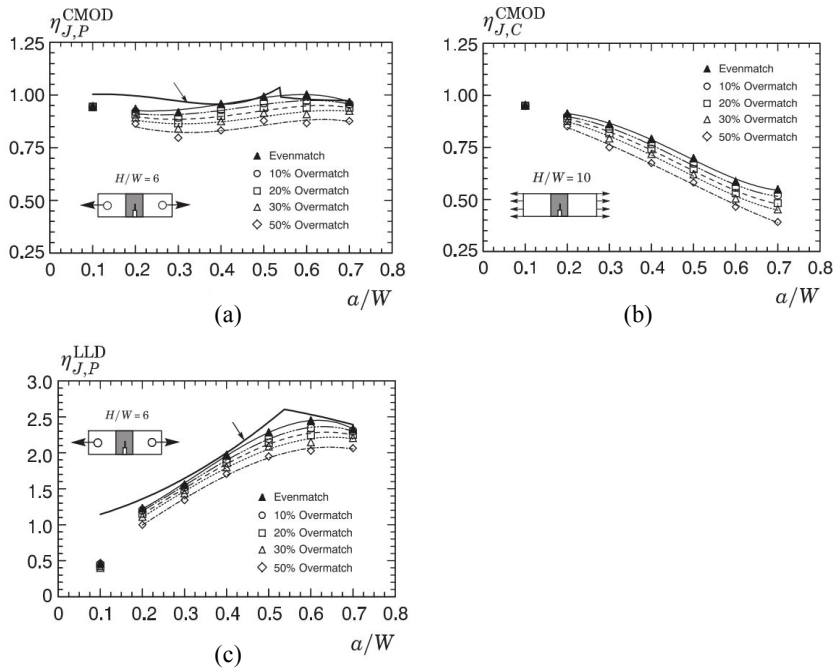
Figure 7. η-factors for clamped and pin-loaded SE(T) specimens. The results show the dependence of η-factor on strength mismatch. (Paredes & Ruggieri 2012)

Paredes and Ruggieri (2012) concluded also that the η-factor is not sensitive to weld width. The weld groove size in the range h/W = 0,1–0.40 does not affect η-factor remarkably for different levels of strength mismatch. A dependence between η-factor and weld width exists for deeply cracked specimens with strength mismatch above 30 %. The η-factors depend weakly on specimen thickness because the difference between the 3D and plane-strain analyses is small. (Paredes & Ruggieri 2012)

2.3   Centerline and HAZ cracked SE(B) specimens

Donato et al. (2009) analysed η_{CMOD}-factors for weld centerline and HAZ notched SE(B) specimens (W = 50 mm) (figure 8). They generated a large set of η-factors for different crack sizes and different levels of strength mismatch. The following strength mismatch conditions were considered: 20% undermatch, evenmatch and 20, 50 and 100% overmatch. The material properties used in the FE analyses are shown in table

3. The analyses were done for welds with groove width 5 mm and 20 mm ($0,1 \leq$ h/W $\leq 0,4$). The base metal has moderate hardening properties. The FE analysis was based on the plane-strain model.

Table 3. The material matrix used in the analyses. The base metal hardening properties do not vary.

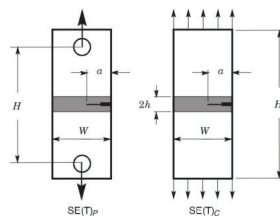| Mismatch level	Weld		Baseplate	
	σ_{ys} (MPa)	n	σ_{ys} (MPa)	n
20% Undermatch	330	7.3	412	10
20% Overmatch	494	12.8	412	10
50% Overmatch	618	17.4	412	10
100% Overmatch	824	25.5	412	10
Evenmatch	412	10	412	10
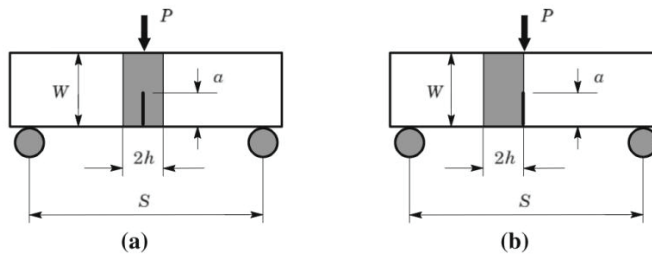
Figure 8. The model of the SE(B) specimen that is used in the FE analyses. The model consists of the base metal and weld metal with the width 2h. Two different crack locations are analysed. (Donato et al. 2009)

The η-factors developed for weld centerline cracked SE(B) specimens are not dependent of strength mismatch for strength mismatch under 20 **%** as shown in figure 9. For 2h = 10 mm (narrow groove) the ± 20 % mismatch level does not deviate remarkably from the evenmatch solution. At higher mismatch levels (50 and 100% overmatch) η-factor deviates with 10–15 % from the evenmatch weld. (Donato et al. 2009)
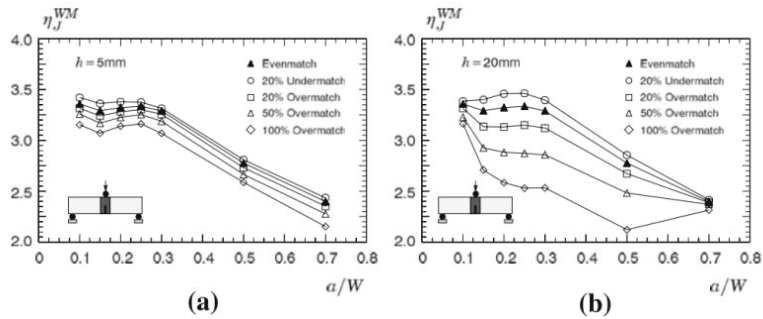
Figure 9. The η-factors decreases with increasing mismatch level. On left side weld width is 5 mm and on right side 20 mm. The sensitivity of η-factor on strength mismatch is larger for the wider weld. (Donato et al. 2009)

For the analyses with the wider groove (2h = 40 mm) the effect of strength mismatch on η-factor is more pronounced, especially for crack configurations in the range 0,15 ≤ a/W ≤ 0,5 and 50 % and 100 % strength mismatch levels. The difference between ± 20 % mismatch level and evenmatch weld is within 5 %. Therefore, the η-factor of the wider groove can be considered independent of weld width as long as the mismatch level in between ± 20 %.

For HAZ notch SE(B) specimens the mismatch level displays almost no effect on η-factor in the range 0,3 ≤ a/W ≤ 0,7 (figure 10). For shorter cracks (a/W ≤0,2–0,3), the effect of mismatch on η is larger, but the difference can still be considered negligible. In the FE models the HAZ is not concluded. The HAZ can have a significant effect on η-factor.
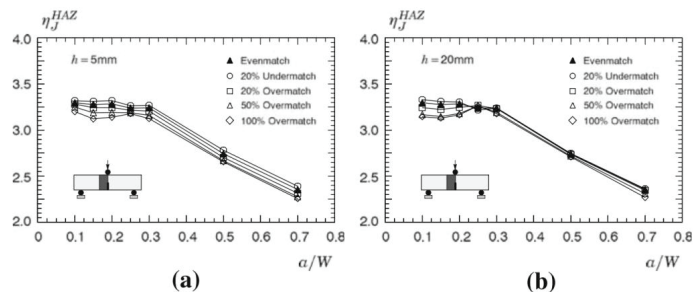
Figure 10. Cracks at the interface of weld metal and base metal. The η-factor is relatively constant for different strength mismatch levels. (Donato et al. 2009)

3   Discussion

3.1   Centerline cracked similar metal welds

The η-factors derived for centerline cracked similar metal weld SE(T), C(T) and SE(B) specimens are dependent on several factors. The η-factors are dependent on strength

mismatch, base metal strength and hardening, weld width and crack location. The FE analyses route influences also the results.

Centerline cracked SMWs C(T)
- The η-factor decreases with increasing strength mismatch.
- A decrease in the base metal hardening properties from 5 to 20, increases the sensitivity to strength mismatch.
- For moderate and high hardening base metals the η-factor is sensitive to strength mismatch, when the a/W ratio is below 0,6. Above a/W = 0,6 the sensitivity is negligible to mismatch levels smaller than 20 %. At a/W = 0,7 the strength mismatch does not affect the η-factor.
- For low hardening base metals the η-factor is highly sensitive to strength mismatch at all strength mismatch levels.
- The specimen thickness and the out-of-plane constraint have a big impact on the η-factor for centerline cracked C(T) specimens. This is proved by comparing the 3D and plane-strain FE analyses. The 3D FE analyses yield different η-factors than the plane-strain analyses. Plastic η-factors derived from 3D analyses are in all conditions consistently lower than the corresponding plane-strain values.

Centerline cracked SE(T) specimens
- the η-factor decreases with increasing mismatch level.
- The derived η-factors are relatively insensitive to the degree of strength mismatch in the range of 10–20% overmatch and crack size in the range $0,2 \leq$ a/W $\leq 0,6$.
- Higher mismatch levels (30% and 50% overmatch) cause a 20 to 30 % deviation from the strength evenmatch condition.
- η-factor is not sensitive to weld width. The weld groove size in the range h/W = 0,1–0.40 does not affect η-factor remarkably for different levels of strength mismatch.
- The η-factors depend weakly on specimen thickness because the difference between the 3D and plane-strain analyses is small.

Centerline cracked SE(B) specimens
- the η-factor decreases with increasing mismatch level.
- The η-factors developed for weld centerline cracked SE(B) specimens are not dependent of strength mismatch for strength mismatch under 20 **%** (weld width can be between 10-20mm)
- For the analyses with the wider groove (2h = 40 mm) the effect of strength mismatch on η-factor is more pronounced, especially for crack configurations in the range $0,15 \leq$ a/W $\leq 0,5$.

Interface cracked SE(B) specimens
- For HAZ notch SE(B) specimens the mismatch level displays no significant effect on η-factor in the range $0,3 \leq$ a/W $\leq 0,7$
- The HAZ property were not taken into account

The HAZs of the weld were not considered in the FE models used for the SMWs. According to Kim and Schwalbe (2001) this simplification is reasonable. They reported that HAZ properties are negligible compared to the properties of surrounding

materials, because HAZ width is very small compared to the weld width. Their assumption was concluded from yield load analyses of welds, but this does not mean HAZ properties would not affect deformation during fracture and thus the η-factor. Therefore the FE models can be improved by considering also the properties of the HAZ.

A challenge with the derived η-factors for SMWs is that η is dependent on several parameters. Zhou et al. (2014) solved this problem by calculating η for different parameters (hardening, weld width, a/W, plane stress and plane strain) for a certain strength mismatch (M_w) condition. This type of analyses produces a large scatter in the results. From this scattered data a best fit equation was derived together with upper and lower bound η-factor solutions dependent of a/W and M_w. With help of the upper and lower bound solutions the uncertainty of the measurement can be estimated.

The effect of plastic deformation on η-factor has not been extensively investigated. A deeper understanding of the shifts in the η-factor, due to different parameters (mismatch, weld width, plane-strain, 3D, strength, hardening), can be retrieved, by analysing the deformation zones from FE analyses. The weld width dependence of centreline cracked SMW SE(B) specimens may be explained with FE analysis from the deformation zones around the crack. Also the decrease in η-factor as strength mismatch increases can be explained by investigating the deformation zones.

3.2   Dissimilar metal welds

Dissimilar metal welds (DMWs) are important components of NPPs. Numerous flaws have been found in DMWs. DMWs in NPPs consist of at least three materials and therefore are more complicated to analyse than SMWs. However, most of investigations of η-factor for welds have focused on SMWs.

The η-factors derived for SMWs can not be directly related to NPP DMWs. NPP DMWs are strength undermatched on one side and the other side strength overmatched. Even if the SMW analyses can not be directly connected to DMWs, the analyses of SMW give information that can be applied to DMWs.

In the reported SMW analyses the effect of different parameters on η-factor was considered. The importance of knowing the effect of different parameters on η-factor grows for ageing NPP DMWs. The mechanical properties in an aging NPP can change and thus cause changes in the η-factor. In these situations knowledge of the effect of different parameters on η-factor helps to assess the significance of the changes. Generally, the most important parameter for η-factor is strength mismatch, but other parameters have an effect too.

In the SMW analyses of centreline cracked SE(B) specimens the η-factor is dependent on weld width. VVER DMWs are wider than narrow gap DMWs. Therefore, it can be expected that η-factors derived for VVER welds are more affected by strength mismatch than narrow gap welds.

The analyses of η-factors for DMWs should also focus on centerline cracks and not only on interface cracks. The SMW η-factor analyses prove that centerline cracks are

sensitive to strength mismatch. Strength mismatch above 20 % affects the η-factor of centreline cracks significantly.

The difference between plane-strain analyses and 3D analyses may be bigger in DMWs than in SMWs, because the FE models for DMWs are more complex. In DMWs the complexity is increased by the different properties of the base metals. In NPP DMWs the HAZ can have completely different properties compared to the base metal.

From NPP DMW structural safety assessment point of view, accurately defined η-factors increase the accuracy of the safety assessment. After the η-factors have been derived with accurate models, there is knowledge in which regions and conditions homogeneous solutions can be applied and in which regions and conditions more precise η-factors are needed.

This increased accuracy can become important for aged NPPs. The requirements for ageing DMW components increase. In these situations more accurate structural integrity analyses methods are needed. By estimating the fracture toughness accurately with validate η-factors, the accuracy of the structural integrity analyses methods (e.g. LBB) increase. The increased knowledge of η-factor gives also important information to design like reduction of conservatism in pipe thickness selection and weld material selection.

4 Conclusions

The plastic η-factors derived for similar metal welds are dependent on strength mismatch, hardening properties of the base metal, strength of the materials, weld width and crack location. Also the FE analyses route has an impact. The η-factors derived from plane-strain analyses can differ from the factors derived from 3D analyses.

Common features for SE(T), SE(B) and C(T) similar metal weld specimens with centerline cracks is that η-factor decreases with increasing strength mismatch and sensitivity of η-factor to mismatch is dependent on the a/W ratio. The η-factors are relatively insensitive to mismatch as long the weld strength mismatch is below 20 % and the a/W ratio is in a certain range. For SE(T) specimens the insensitivity to 20 % mismatch applies in a/W range $0,2 \leq a/W \leq 0,6$, for SE(B) in the range $0,1 \leq a/W \leq 0,7$, and for C(T) specimens a/W has to be larger than 0,6.

The η-factors can also be dependent on weld width. For SE(B) specimens the weld width $(0,1 < h/W < 0,2)$ plays an important role when the strength mismatch is above 30 %. Plastic η-factors calculated for C(T) specimens are not dependent on weld width in the range $0,1 < h/W < 0,2$. Weld width does not have a significantly effect on SE(T) specimens between $0,1 < h/W < 0,4$.

The effect of specimen thickness on η-factor can be investigated by conducting both plane-strain and 3D analyses. For SE(T) specimens thickness has a weak impact on η-factor, but for C(T) specimens thickness has a big impact on η-factor. The dependence of thickness on η-factor was not evaluated for SE(B) specimens.

C(T) specimens are also dependent on strain hardening properties of the base metal. As the base metal hardening properties increase from 5 to 20, the sensitivity to strength mismatch increases. For the other specimens base metal hardening properties were not varied in the analyses.

Accurately defined η-factors increase the accuracy of the safety assessment in NPPs. This can become relevant for ageing DMW components that require increased accuracy of the assessment methods. An accurate assessment method contains information of material regions and conditions in which homogeneous solutions can be applied, and of regions and conditions in which heterogeneous η-factors are needed. Additionally, knowledge of the dependence of η-factor on mechanical properties is important, because in ageing NPPs the mechanical properties can change. In an accurate safety assessment the changes are taken into account by deriving specific η-factors.

References

Cravero, S. & Ruggieri, C. 2007. Estimation procedure of J-resistance curves for SE(T) fracture specimens using unloading compliance. Engineering Fracture Mechanics. Vol. 74. pp. 2735–2757. Available at: http://linkinghub.elsevier.com/retrieve/pii/S0013794407000513 [Accessed August 29, 2013].

Donato, G.H.B., Magnabosco, R. & Ruggieri, C. 2009. Effects of weld strength mismatch on J and CTOD estimation procedure for SE(B) specimens. International Journal of Fracture. Vol. 159. pp. 1–20. Available at: http://link.springer.com/10.1007/s10704-009-9377-9 [Accessed August 29, 2013].

Kim, Y. & Schwalbe, K. 2001. Mismatch effect on plastic yield loads in idealised weldments II . Heat affected zone cracks. Vol. 68. pp. 183–199.

Kim, Y.-J. & Schwalbe, K.-H. 2001. Mismatch effect on plastic yield loads in idealised weldments: I. Weld centre cracks. Engineering Fracture Mechanics. Vol. 68. pp. 183–199.

Koçak, M. 2010. Structural Integrity of Welded Structures : Process - Property – Performance (3P) Relationship. 63rd Annual assembly and international conference of the international institute of welding. pp. 3–19.

Koo, J.-M., Huh, Y. & Seok, C.-S. 2012. Plastic η factor considering strength mismatch and crack location in narrow gap weldments. Nuclear Engineering and Design. Vol. 247. pp. 34–41. Available at: http://linkinghub.elsevier.com/retrieve/pii/S0029549312000945 [Accessed July 12, 2013].

Leonardo, M.L.S., Sarzosa, D.F.B. & Ruggieri, C. 2013. Effects of specimen geometry and loading mode on crack growth resistance curves of a high-strength pipeline girth weld. International Journal of Pressure Vessels and Piping. pp. 1–14. Available at:

http://linkinghub.elsevier.com/retrieve/pii/S0308016113001087 [Accessed August 13, 2013].

Paredes, M. & Ruggieri, C. 2012. Further results in J and CTOD estimation procedures for SE(T) fracture specimens – Part II: Weld centerline cracks. Engineering Fracture Mechanics. Vol. 89. pp. 24–39. Available at: http://www.sciencedirect.com/science/article/pii/S0013794412001269 [Accessed June 26, 2014].

Ruggieri, C. 2012. Further results in J and CTOD estimation procedures for SE(T) fracture specimens – Part I: Homogeneous materials. Engineering Fracture Mechanics. Vol. 79. pp. 245–265. Available at: http://www.sciencedirect.com/science/article/pii/S0013794411004115 [Accessed June 26, 2014].

Savioli, R.G. & Ruggieri, C. 2013. J and CTOD estimation formulas for C(T) fracture specimens including effects of weld strength overmatch. International Journal of Fracture. Vol. 179. pp. 109–127.

Xuan, F.Z., Tu, S.T. & Wang, Z. 2005. A modification of ASTM E 1457 C* estimation equation for compact tension specimen with a mismatched cross-weld. Engineering Fracture Mechanics. Vol. 72. pp. 2602–2614.

Zhou, H., Biglari, F., Davies, C.M., Mehmanparast, A. & Nikbin, K.M. 2014. Evaluation of fracture mechanics parameters for a range of weldment geometries with different mismatch ratios. Engineering Fracture Mechanics. Vol. 124-125. pp. 30–51. Available at: http://dx.doi.org/10.1016/j.engfracmech.2014.03.006.

Advances in the Ultrasonic Inspection of Dissimilar Metal Welds

Esa Leskelä
VTT Technical Research Centre of Finland Ltd
esa.leskela@vtt.fi

Abstract

In-service inspection (ISI) using non-destructive testing (NDT) is required to ensure the safe and sustainable operation of nuclear power plants. The reliability of ISI consists of technical and human factors. Complex components containing dissimilar metal welds (DMWs) are challenging for ultrasonic testing. Thus, thorough planning and verification of testing procedures is required. Continuous development and improvement in ultrasonic testing techniques together with better understanding of the material properties aids to improve the reliability of detection and sizing of defects in DMWs.

Phased array ultrasonic testing (PAUT) has been gaining increased acceptance in replacing conventional ultrasonic testing (UT) or radiographic examination in the ISI of DMWs. There are several variables in the PAUT techniques which have to be taken into account when developing a procedure. Modelling and simulation has become a commonly used cost-effective tool to aid that process. Some of the emerging UT techniques are still under development and more data is needed for the evaluation of the reliability and performance of the techniques. Research studies like round robin testing programs are useful for producing data which can also be utilized for simulation and modelling verification.

Keywords: dissimilar metal welds, in-service inspection, ultrasonic testing, phased array ultrasonic testing

1   Introduction

In-service inspections carried out by non-destructive testing (NDT) are required to ensure safe and sustainable operation of a nuclear power plants (NPP). NDT aids to evaluate the suitability of an NPP component for operation. In-service inspections should be able to detect degradation like cracking and wall thinning before the degradation affects the component's integrity and functional requirements [1].

Dissimilar metal welds (DMWs) containing Ni-based alloys 600, 182 and 82 are found susceptible to stress corrosion cracking (SCC), often referred to as primary water stress corrosion cracking (PWSCC) and interdendritic stress corrosion cracking (IDSCC) [1, 2]. PWSCC degradation has resulted in breaches of the pressure boundary and caused leakage in several DMWs. Thus, reliable detection and sizing of defects in DMWs using NDT is essential for the safe operation of the NPPs [3].

The reliability of ultrasonic testing can be expressed as the degree of a procedure to achieve the detection and characterisation targets of the defects [2]. Both technical and human factors have an influence on the reliability of ultrasonic examination of DMWs.

Complex geometries, boundaries, large grain size, and anisotropic weld metal together with tight and branching service-induced cracks make the ultrasonic testing (UT) of DMWs challenging. Still, UT has its advantages especially in the detection and sizing of inside surface breaking cracks. Those benefits include e.g. access from the outside surface, good performance in detecting planar flaws, possibility for height sizing and avoidance of radiation [4].

Ultrasonic techniques are constantly under development together with evolving material technology [3]. Continuous research work is needed to evaluate the performance and reliability of commercial and emerging ultrasonic testing procedures. An example of this work are the round robin testing (RRT) programs PINC and PARENT which the U.S. NRC has established during the past ten years [1, 5, 6, 7].

2 The main challenges of ultrasonic testing of dissimilar metal welds

2.1 Geometry

The main physical challenges of the UT of DMWs and associated Ni-based alloys are the boundaries, changes in wall thickness and pipe diameter, bevels or counter bores, different material types, and the use of buttering layer [4]. An example of a typical nozzle configuration of pressurized water reactor (PWR) steam generator (SG) is shown in Figure 1.
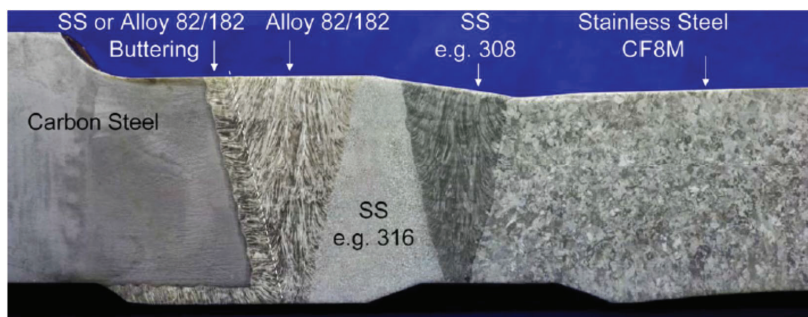
Figure 1. An example of a standard PWR SG nozzle DMW configuration illustrating UT challenges like geometry, grain growth and orientation, inside diameter / outside diameter (ID/OD) contour and metallurgical interfaces [8].

The geometrical discontinuities make the interpretation of ultrasonic data complicated and may cause misinterpretation. Strong geometric signals caused by sharp counter bores close to the HAZ or thickness transitions close to the weld root can mask low amplitude signals especially from a shallow crack [4]. Weld root or counter bore signal from the inside surface can prevent the identification of an isolated flaw corner response. On the other hand, continuous weld root signal can serve as a reference point assisting the data analysis [8, 9].

2.2 Material

The highly anisotropic austenitic weld metal affects the propagation of the ultrasonic waves. Large columnar grain structures of a DMW cause high attenuation and sound redirection [4]. The columnar crystals built during welding grow in a particular direction, which depends on the joint type, heat flow, gravity force, etc. The acoustic properties of such materials are directionally dependent. This limits the reliability of conventional UT and standard phased array ultrasonic testing (PAUT) which work under assumption of constant sound velocity and linear sound propagation [10]. Ultrasonic waves suffer from velocity variation, beam skewing, redirection, scattering and distortion in austenitic material which makes the detection and sizing of defects challenging [8, 11].

2.3 Access

Due to the coarse microstructure of the weld metal, access to both sides of the weld is required in the UT of DMWs. Ultrasound is not able to consistently penetrate through the austenitic weld metal in order to detect or size defects on the far side [12]. The access limitations and other challenging conditions may result in incomplete examination coverage, false calls, failure to identify service-induced defects and poor examination quality. Joint configuration does not always allow 100 % coverage of the inspection volume or is not consistent with the design configuration. DMWs in nozzles are typically much wider than stainless steel (SS) welds. This causes challenges especially when a defect is located on the opposite (far) side of the weld. Physical access to the area to be examined can be limited. Especially encoded examinations with scanning devices usually require more space than manual examinations [4]. Scan access can often be remarkably improved by grinding the weld OD surface flat [13]. In new plants where narrow gap welds are used, a smaller inspection volume is required [14].

2.4 Human factor

Human errors can be a result of environmental factors like physical environment, time pressure and examination time. Physical environment includes heat, humidity, radiation dose, contamination, and physical access. Proper planning and preparation minimize the stay time and physical access. Effective pre-job briefs of complex inspection are needed [15]. NDT, especially UT, is very skill-depended. Therefore a qualification or performance demonstration process is needed to ensure the high level of examinations [13].

3 Ultrasonic testing of dissimilar metal welds

3.1 General

Ultrasonic testing is more reliable in detecting planar defects such as cracks and lack of fusion than volumetric defects like pores and slag inclusions. Planar defects are typically found during service because cracking is a dominant service degradation process. UT is based on the interaction of acoustic wave energy with discontinuities in the inspected material. Differences in density or acoustic impedance result in reflection or scattering of the wave. The interpretation of ultrasonic signals can be complicated due to mode conversions and because different flaws can cause similar signals [16].

3.2 Implementation of ultrasonic testing

The pulse-echo (PE) testing is carried out using a single probe whereas in the transmit-receive (TR) technique one transducer is used for transmitting and the other for receiving. Schematic principle of conventional UT with the PE method carried out on the OD surface is shown in Figure 2 [1]. The TR technique is typically used for noisy materials like DMWs [16]. The benefits of this technique are the absence of near-surface dead zone, elimination of ghost echoes caused by internal reflections in the wedge, a better sensitivity and a better signal-to-noise ratio (SNR) [17].
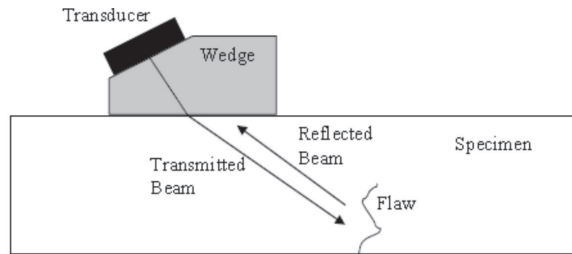
Figure 2. Schematic picture of conventional ultrasonic pulse-echo testing [1].

Most of the ultrasonic ISI techniques for DMW piping welds are based on inspection conducted on the OD of a pipe looking for inner surface breaking cracks [1]. Inspection from the OD surface can be performed by manual, mechanized or automated inspection. Inspection from the ID surface requires the use of a manipulator [18, 19]. Based on the PARENT blind testing results, better height sizing performance is observed for procedures that access test block ID versus test block OD [7].

Manual UT is carried out by the inspector who moves the probe on the scanning surface and visually monitors the screen of ultrasonic device online. Typically different angles and scanning directions are used in order to detect all possible differently oriented defects. In mechanised or automated UT the scanner enables the movement of the probe or a group of the probes over the scanning area and the data is recorded to be analysed offline providing a permanent record of the inspection [16].

3.3 Wave modes and frequency

Both shear wave (SW) and longitudinal (LW) modes are used in ultrasonic testing. SWs show a good SNR and an amplitude dynamic depending on defect depth in the base material and in the region nearby to the weld metal. The effect on amplitude dependence can be used for defect sizing. SWs are less suitable for defect assessment in the weld metal and buttering due to poor sound transmission through anisotropic, coarse-grained materials. When SWs are used for DMW examination, a low frequency is preferred due to less backscattering and noise [20].

LWs typically are better suited for ultrasound transmission through anisotropic, coarse-grained materials than SWs. The amplitude of LWs is not dependent on defect depth. In spite of that, LWs produce diffraction/bending effects at defect edges (tip echo) which are very usable for defect height sizing [20].

Mode conversions from LW to SW result in complicated interpretation of the signals [16]. However, mode conversions are commonly utilized in ISI. Creeping wave

technique is the most common mode conversion technique for detection and confirmation of ID surface breaking defects. The technique is based on a "creeper probe" which generates indirect creeping waves on the ID surface by mode conversion [21].

To reduce the impact of the microstructure, rather low (1.5 MHz) frequency TR probes with LWs together with SWs are used [12]. At lower frequencies, e.g. 0.8 or 1.0 MHz, the ultrasonic wavelengths in stainless steel are 7.1 and 5.7 mm, respectively. That in some cases causes a small defect to be smaller than the wavelength. Beam spot sizes at lower frequencies are also large. These two factors can prevent the reliable detection of small defects [9].

3.4 TOFD

The time-of-flight-diffraction (TOFD) is a technique where a setup of two LW probes is used for detection of crack tip signals in order to through-wall size the crack accurately. The principle of TOFD inspection is shown in Figure 3. The TOFD arrangement requires a large and relatively flat scanning surface. The amplitude of the diffracted signals can be low and the microstructure of austenitic material also generates noise. Therefore, coarse-grained materials with significant anisotropy like nickel-base alloys and cast iron will require additional validation and data-processing [4, 16, 22].
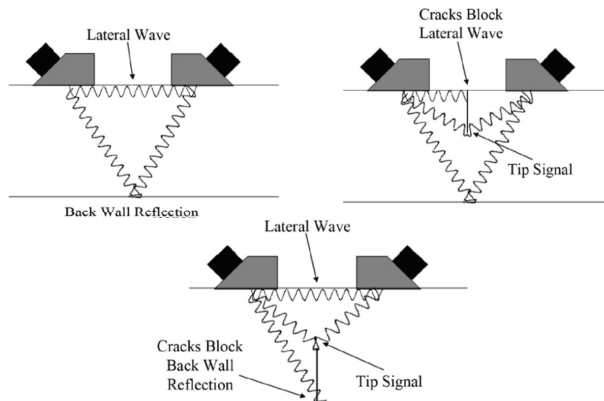
Figure 3. The principle of the TOFD technique [16].

3.5 Phased array ultrasonic testing

3.5.1 Principle of phased array ultrasonic testing

In the phased array ultrasonic testing (PAUT), an array of individual transducers transmits and receives ultrasound as directed by the electronics and software. Focal laws are used to control the firing of individual elements of a PA probe to allow for proper beam forming in the inspection object. The physical values and orientation of the probe and wedge as well as the desired values for angles etc. are entered into the software by the user. Software generates the needed delays for each element to produce the desired beam steering and focusing in the material [8, 17].

3.5.2   Benefits of phased array ultrasonic testing

Based on the results of PINC RRT, the use of conventional UT and PAUT together showed the most promise in the improvement of defect height sizing [1]. Conventional UT is an internationally standardized procedure. Inspectors and regulators have a lot of experience with the capabilities and limitations of conventional UT in the examination of NPP components. Conventional UT is often time-consuming because detailed inspection may require the use of many different probes typically generating an angle of 30, 45 and 60 degrees in the inspection object [1].

The use of the PAUT technique enables to replace several fixed-angle conventional UT probes with one probe. Focusing is possible at several depths as opposed to conventional UT where probe is focused only at one depth, if any [8, 17]. A range of SW and LW angles generated by PAUT makes it an ideal tool for detection and sizing of service-induced defects utilizing also mode conversion techniques like creeping wave and T-L-L (30-70-70) techniques [16, 21]. The versatility of PAUT technique can also be implemented to TOFD inspections where the use of dynamic depth focusing (DDF) can increase the SNR of diffracted signals and eliminate background noise [22].

To design the PAUT inspection, the beam can be simulated and ray-traced to visualize the sound field form. Simulation usually is performed under assumption of isotropic material which is not the true state for DMWs. However, simulation helps to estimate of the sound field parameters and transducer performance to design the array and develop the focal laws [8, 17].

3.5.3   Phased array data acquisition

The TR technique is commonly used in the PAUT of DMWs. An example of a TRL (transmit-receive longitudinal) matrix search unit is shown in Figure 4. The search unit consists of two PA probes mounted on a wedge which usually has a customized footprint to allow a good adaptation on the scanning surface [17].

Figure 4. TRL PA 32x2 matrix search unit [17].

The full advantage of a PAUT technique is achieved when data acquisition is done with small resolution in scanning direction, large mechanical increment in the index direction (across the weld), in combination with electronical linear and sectorial scanning. In linear scan, a group of arrays with fixed angle is moved electronically so that data provides many axial positions. Sectorial scan data represent multiple angles

in one axial position (Figure 5). Several scan lines can be combined in one merged data file. The use of matrix probe allows also beam skewing. [8, 9].
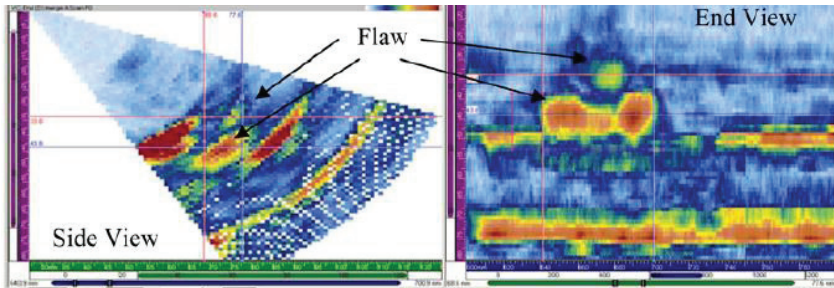
Figure 5. Example of sectorial scan PA data of a thermal fatigue (TF) flaw in a DMW [8].

3.5.4 Sampling phased array

The sampling phased array (SPA), also called full matrix capture (FMC), is a technique where A-scans for each individual element of a PA probe are acquired by all elements and then reconstructed by image reconstruction algorithm, e.g. total focusing method (TFM) [23]. The conventional PAUT system utilizes only a small portion of the overall data acquisition capability since the acoustic transmissions for specific incidence angles are time-phased and the received signals are then summarized. If the time-domain signals from the individual elements are acquired, the resulting data can then be summarized with arbitrary phase information to permit data processing of all possible incidence angles and physically available focus points from a single data set (Figure 6) [24].
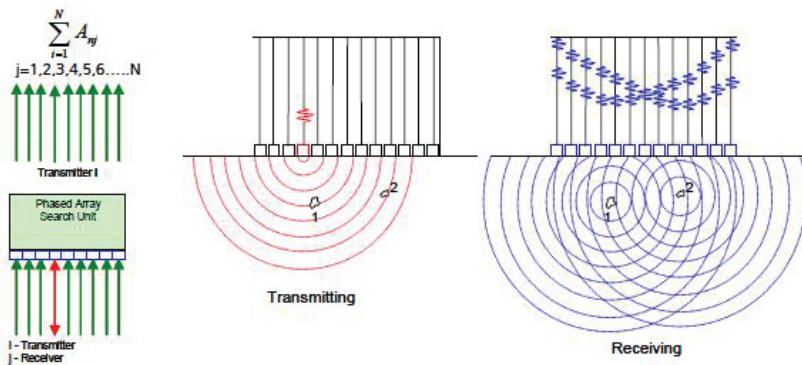
Figure 6. Data acquisition and processing for sampling phased array [24].

3.5.5 Adaptive phased array

Adaptive phased array technique allows for detailed inspections of samples with irregular surfaces. The system first measures the surface profile and then corrects the

delay laws used to focus the beam through the irregular surface. This enables scanning a variety of surface configurations unlike conventional UT or basic PAUT that require a custom probe and/or wedge for each surface profile [1].

3.5.6 Special ultrasonic testing techniques

There are several ultrasonic techniques which are not yet field-deployed and which require more investigation before possible qualification for DMW inspection. The techniques include e.g. the phased array asymmetric TOFD, laser ultrasound visualization and techniques based for on nonlinear acoustic phenomena such as higher harmonic UT and nonlinear resonant ultrasound spectroscopy. Several of these techniques were applied in PARENT open RRT and detailed description of them will be provided with PARENT Open Test Report [7].
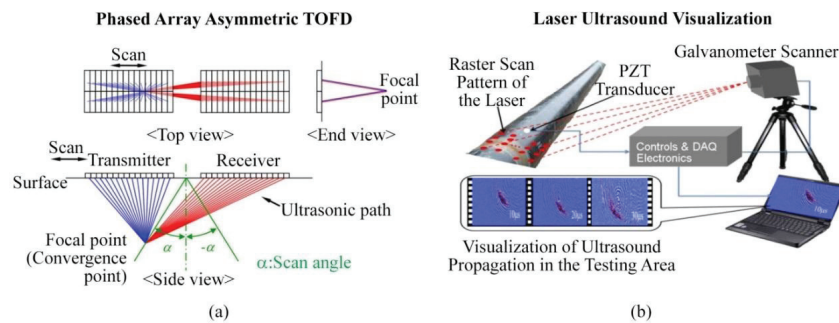
Figure 7. Illustration of the phased array asymmetric TOFD and laser ultrasound visualization techniques [7].

4 Modelling and simulation of ultrasonic examination of DMWs

Ultrasonic modelling and simulation have become widely used in inspection design and qualification. UT can be prepared before manufacturing of the components by using digital mock-ups. The changes in material and geometry can be evaluated beforehand as well as the sound beam propagation. The conditions such as radiation inside the NPP make it useful to apply ultrasonic simulation for demonstration of inspection capability and accessibility. Simulation can enhance the effectiveness of inspections and reduce training costs [25]. Interruptions in probe contact have a remarkable effect on the quality of examination and therefore it is very important to evaluate them in advance e.g. with the aid of simulation as shown in Figure 8 [15].
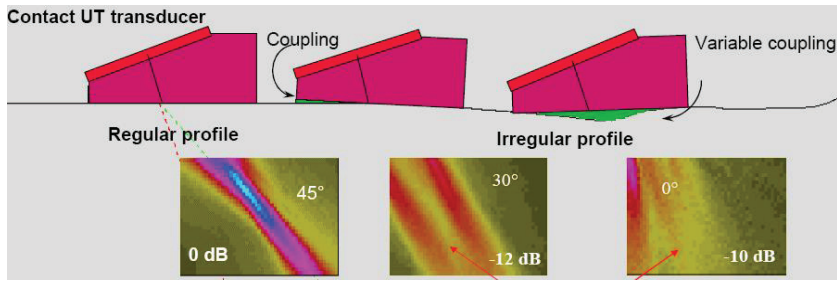
Figure 8. A modelling example of the effect of irregular scanning surface on probe contact. The scanning surface condition and shape is a key factor regarding the data quality and achievable examination coverage. [15].

Technical justification (TJ) minimizes the reliance on test pieces and allows generalizing specific test piece data effectively [20]. The use of modelling and simulation as a part of TJ is becoming more general [25]. Simulation can reduce the number of mock-ups and experimental trials since it helps to understand the influential parameters of an inspection of complex geometries. Modelling can help determining the "worst case" defects [26, 27].

Widely used CIVA platform developed by CEA LIST uses mathematical formulations which generally rely on semi-analytical models. Basic simulation using CIVA is generated assuming an isotropic material where the acoustic velocity in the material is constant for any angle of particular wave mode. This ideal case does not produce an exact representation of sound fields in real DMW components but provides a useful first-approximation for sound beam modelling. It also enables the estimation of sound field parameters and optimal array design together with focal law development [28]. Furthermore, CIVA enables the modelling and simulation of ultrasonic examination of DMW taking into account the backscattered noise for different inspection techniques [29].

One of the focus areas in the field of modelling and simulation is increasing development to address the problems of sound propagation in the inhomogeneous anisotropic austenitic materials [12]. There are several models which have been developed for sound propagation such as finite differences, finite elements or ray tracing models [30]. Figure 9 illustrates the difference in sound path modelling between isotropic, homogeneous and anisotropic, inhomogeneous materials [10].

Figure 9. Schematic comparison of sound paths for computation of propagation times in ferritic and austenitic steel [10].

The electron back scatter diffraction (EBSD) technique can be used to evaluate the texture (constituent crack morphology, boundaries and orientations) of the weld. When translating the weld map into the model it is important to identify closed regions with clear boundaries. The microstructural information is used for a model as shown in Figure 10 [31]. With the high resolution map, the behaviour of the sound field can be studied better and array ultrasonic concepts can be better tailored to the weld. Together with adapted delay laws (ADL) technique the inspection sensitivity can be improved by adapting the focal laws used for the inspection. The disadvantages of these methods are the costs which are a consequence of the time required and the high-level equipment [12].
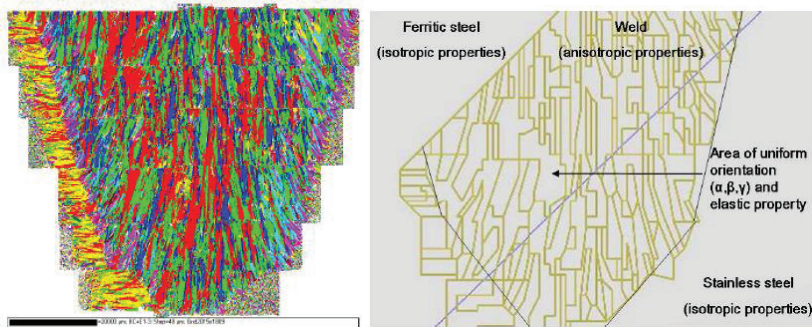
Figure 10. On the left: orientation map of a weld section; on the right: virtual map of a weld section [31].

5   Conclusions

The need to reduce inspection times, improve the pass rate of performance tests and to achieve improved inspection effectiveness has led to significant steps in ultrasonic technology. This has been achieved in cooperation with the manufacturers. The existence of qualified procedures and equipment has not stopped the efforts for continuous improvement. The developments in ultrasonic technology are expected to result in more effective and accurate evaluation of DMWs.

Emerging ultrasonic testing techniques require demonstration of conformity to codes, regulations and existing practices. Appropriate equipment and technology is available for conducting the evaluation of new emerging technologies by practical tests. Still, these techniques require more sophisticated and expensive equipment than the conventional UT or standard PAUT. Advanced techniques may also be time-consuming [13, 24].

The development of ultrasonic testing of dissimilar metal welds tries to address at least the following challenges: 1) to more accurately characterize large defects, 2) to enable inspections of difficult-to-access regions, and 3) to improve the detectability of small defects. Various research programs and round robin testing studies are still needed for this improvement. Modelling and simulation can help this task but this requires better understanding of the interaction between microstructure and ultrasound, in other words more appropriate data.

References

1. Cumblidge, S.E., et al., Results of the program for the inspection of nickel alloy components, NUREG/CR-7019; PNNL-18713. U.S. Nuclear Regulatory Commission, Washington, D.C., USA, 2010. 174 p + app. 377 p.

2. Anderson, M.T. and Sullivan, E.J. Managing PWSCC in butt welds by mitigation and inspection. NUREG/CR-7187; PNNL-23659. U.S. Nuclear Regulatory Commission, Washington, D.C., USA, 2014. 128 p + app. 109 p.

3. Prokofiev Iouri, Cumblidge, Stephen E. and Doctor, Steven R. Inspection of nickel alloy welds: Results from five-year international program. AIP Conference, San Diego, California, USA, 18–23 July 2010. 8 p.

4. EPRI. Guidelines for inspectability for new plant components. 1015139. EPRI, Palo Alto, CA, USA 2007. 57 p.

5. Braatz, B.G., Cumblidge, S.E., Doctor, S.R. and Prokofiev, I.G. Primary water stress corrosion cracks in nickel alloy dissimilar metal welds: Detection and sizing using established and emerging non-destructive examination techniques. IAEA-CN-194-025. International Atomic Energy Agency. 3. International Conference on Nuclear Power Plant Life Management (PLiM) for Long Term Operations (LTO), Salt Lake City, Utah, USA, 14–18 May 2012. 8 p

6. Braatz, B.G. & Heasler, P.G. PARENT quick blind round-robin test report. PNNL-22677. Pacific Northwest National Laboratory, Richland, Washington, USA, 2014.

7. Meyer, R.M., Komura, I., Kim, K., Zetterwall, T., Cumblidge, S.E. and Prokofiev, I. Overview of the program to assess the reliability of emerging nondestructive techniques open testing and study of flaw type effect on NDE response. PNNL-SA-112604. QNDE Review of Progress in Quantitative Nondestructive Evaluation. Minneapolis, Minnesota, USA, July 26–31, 2015. 11 p.

8. Diaz, A.A., Cinson, A.D., Crawford, S.L. and Anderson, M.T. An evaluation of ultrasonic phased array testing for reactor piping system components containing dissimilar metal welds. JCN N6398, Task 2A. Technical letter report. PNNL-19018. PNNL, Richland, WA, USA, November 2009

9. Crawford, S.L., Cinson, A.D., Prowant, M.S., Moran, T.L. and Anderson, M.T. Ultrasonic evaluation of two dissimilar metal weld overlay specimens. PNNL-21502. PNNL, Richland, WA, USA, June 2012.

10. Boller, C., Pudovikov, S. and Bulavinov, A. Quantitative ultrasonic testing of acoustically anisotropic materials with verification on austenitic and dissimilar metal joints. Fraunhofer Institute for Nondestructive Testing. Saarbrücken, Germany, 2012. ResearchGate: http://i3.rgstatic.net/publication/258569811_Quantitative_ultrasonic_testing_of_acoustically_anisotropic_materials_with_verification_on_austenitic_and_dissimilar_weld_joints/fulltexts/ef31752e21da77a35d.pdf/preview.png (accessed: 6.5.2014).

11. EPRI. Nondestructive evaluation: indication characterization, evaluation, and disposition guideline. 1025225. EPRI, Palo Alto, CA, USA, 2012.

12. Bartlett, A. et al. Phased array ultrasonic inspection of dissimilar metal joints. 25 January 2011. http://www.dissimilarweld.co.uk/publications/DIS-Gu-Rev.01.05.pdf, (accessed 29 August, 2013).

13. EPRI. Nondestructive evaluation: Historical view of nondestructive evaluation for stress corrosion cracking at nuclear power plants. 1021159. EPRI, Palo Alto, CA, USA, 2010.

14. Mouginot, R. and Hänninen, H. Microstructures of nickel-base alloy dissimilar metal welds. Aalto University publication series SCIENCE + TECHNOLOGY, 5/2013. Aalto University, Espoo, Finland, 2013. 178 p. ISBN 978-952-60-5065-2.

15. EPRI. Nondestructive evaluation: Guideline for conducting ultrasonic examinations of dissimilar metal welds, Revision 1. 3002000091. EPRI, Palo Alto, CA, USA 2013.

16. Moran, T.L., Ramuhalli, P., Pardini, A.F., Anderson, M.T. and Doctor, S.R. Replacement of radiography with ultrasonics for the nondestructive inspection of welds – evaluation of technical gaps – an interim report. PNNL-19086. Pacific Northwest National Laboratory, Richland, Washington, USA, April 2010.

17. Berlanger, J., Marois, D., Beaulieu-Charbonneau, L. and Maes, Guy. Improved solution for encoded phased array UT examination of dissimilar metal piping welds. 9th International Conference on NDE in Relation to Structural Integrity for Nuclear and Pressurized Components, May 22–24, 2012 - Seattle, Washington, USA. Pp. 737–746.

18. Depth-sizing uncertainties of inner diameter inspections of supplement 2 and 10 welds. U.S. Nuclear Regulatory Commission. Presented on a public meeting with industry regarding methods for sizing flaws that may be found during inner diameter in-service inspections of reactor inlet and outlet nozzle to safe end and safe end to pipe welds, March 16, 2012. ADAMS Accession No. ML12079A391

19. Kawanami, S., Kimura, T., Kurokawa, M., Nishida, J., Yamaguchi, T., Matsuura, T. and Tsuruta, T. Advanced phased array UT sizing technique on stress corrosion cracking in dissimilar metal welds of nozzles. 9th International Conference on NDE in Relation to Structural Integrity for Nuclear and Pressurized Components, May 22–24, 2012, Seattle, Washington, USA. Pp. 676–683.

20. Krüger, A and Rückelt, B. Technical justification in accordance with European ENIQ recommended practice no. 2 for the ultrasonic examination of dissimilar metal welds at surge line nozzles. 9th International Conference on NDE in Relation to Structural Integrity for Nuclear and Pressurized Components, May 22–24, 2012, Seattle, Washington, USA. Pp. 43–53.

21. Introduction to phased array ultrasonic technology applications. R/D Tech Corporation, Canada 2005

22. Nageswaran, C. and Bird, Colin R. Evaluation of the phased array transmit-receive longitudinal and time-of-flight diffraction techniques for inspection of a dissimilar weld. Insight Vol. 50, No 12, December 2008.

23. Han, Taeyoung et al. Phased array ultrasonic testing of dissimilar metal welds using geometric based referencing delay law technique. Smart Materials and Nondestructive Evaluation for Energy Systems 2015, San Diego, California, United States March 08, 2015, 10 p.

24. Bulavinov, A., Kröning, M. and Walte, F. Ultrasonic inspection of austenitic and dissimilar welds. 4th Pan American Conference for NDT - October 2007 - Buenos Aires, Argentina. 13 p.

25. Chen, H., Li, M., Liu, J and Li, Y. Application of ultrasonic simulation technology in technical justification. 17th World Conference on Nondestructive Testing, 25–28 Oct. 2008, Shanghai, China.

26. Foucher, F. and Dubois, P. Applications and recent evolutions of the CIVA simulation platform. 18th World Conference on Nondestructive Testing, 16–20 April 2012, Durban, South Africa. 10 p.

27. ENIQ Recommended Practice 6: The use of modelling in inspection qualification, 2nd Issue, ENIQ report No. 45, EUR 24914 EN, European Commission, 2011, 13 p.

28. Anderson, M.T., Diaz, A.A., Cinson, A.D., Crawford, S.L., Prowant, M. and Doctor, S.R. Final assessment of manual ultrasonic examinations applied to detect flaws in primary system dissimilar metal welds at North Anna Power Station. PNNL-22553. Pacific Northwest National Laboratory, Richland, Washington, USA, March 2014.

29. Mahaut, S., Chatillon, S., Leymarie, N, Jenson, F. and Calmon, P. Simulation tools for predicting non destructive testing of heterogeneous and anisotropic structures. International Congress on Ultrasonics, Vienna, April 9–13, 2007. 4 p.

30. Gardahaut, A., Lourme, H., Jenson, F., LIN, Shan and Nagai, M. ultrasonic wave propagation in dissimilar metal welds – application of a ray-based model and comparison with experimental results. 11th European Conference on Non-Destructive Testing (ECNDT 2014), October 6–10, 2014, Prague, Czech Republic.

31. Carpentier, C., Nageswaran, C. and Tse, Y.Y. Evaluation of a new approach for the inspection of austenitic dissimilar welds using ultrasonic phased array techniques. 10th European Conference on Non-Destructive Testing, Moscow 2010, June 7–11. 11 p.

Creep-fatigue design of GEN IV high temperature reactor plants

Pohja Rami[1]
[1]VTT Technical Research Centre of Finland Ltd

Abstract

The service conditions expected for the GEN IV reactors pose significant challenges to structural materials selection and qualification efforts. The components will undergo varied service conditions which include exposure to high temperatures and high neutron doses compared to the service conditions in today's commercial reactors. A considerable damage mechanism for materials used in GEN IV components is predicted to be creep-fatigue (CF) damage, which arises due to startup and shutdown or power transients during normal operation. Design codes, such as RCC-MRx and ASME III NH, for GEN IV nuclear reactors use interaction diagram based method for CF assessment. In the interaction diagram the fatigue damage is expressed as the ratio of design cycles over the allowable amount of cycles in service and the creep damage as the ratio of time in service over the design life. When standard laboratory CF tests with relatively large strain ranges and short hold or creep periods are assessed using the design code CF assessment procedures, the design codes seem to provide sufficient level of conservatism for safe design. But does the sufficient level of conservatism still remain with parameters relevant to power plant conditions? Can this type of test results and assessment and modelling methods emerging from them be extrapolated to GEN IV relevant conditions, where the stress and strain levels are lower, hold periods are significantly longer and lifetimes of components are expected to be about 60 years or more? Are there enough data and information on the long-term microstructural evolution and its effect on the creep and cyclic properties of e.g. P91 steel?

Keywords: GEN IV reactors, design codes, creep-fatigue

1. Introduction

The 2010-2012 implementation plan of the European Sustainable Nuclear Industrial Initiative
(ESNII), in the frame of the Sustainable Nuclear Energy Technology Platform (SNETP), established the road map for the start of construction of the European GEN IV prototypes [1]. Although significant differences exist among the various reactor concepts under consideration in Europe, the operational conditions envisaged for those systems are quite demanding and include exposure to higher temperatures, higher neutron doses and more aggressive environments compared to the service conditions of the most commercial reactors operating today. The service conditions expected for the GEN IV reactors pose significant challenges to structural and cladding materials selection and qualification efforts. The demonstrators and prototype Gen-IV reactors to be designed and constructed in the next decades will probably rely on materials that exist commercially today.

The modified 9Cr–1Mo (P91) steel and the austenitic stainless steel of the 316 type are candidate materials for several components of the GEN IV nuclear reactors. The ferritic-martensitic P91 steel has a good combination of mechanical properties, high thermal conductivity, low thermal expansion coefficient and good resistance to stress corrosion cracking in water–steam systems compared to austenitic stainless steels. Additionally, the 9-12% Cr steels, such as P91, are also considered to be creep resistant. The austenitic stainless steel 316 exhibits good intergranular corrosion

resistance, good structural stability and relatively good weldability. Several pan-European research projects have been carried out and are ongoing in order to assess the suitability of the aforementioned materials for GEN IV structural components.

Several GEN IV reactor structural components are expected to be subjected to cyclic thermal and mechanical stresses as a result of temperature gradients and changes in pressure. During the steady state operation creep deformation may occur under high temperature and pressure. The startups and shutdowns or power transients during normal operation may introduce fatigue damage to the components. The failure mechanisms under such loading conditions are complex interactions of creep and fatigue damage [2]. Figure 1 below gives an overview of the locations of the key damage modes expected in Sodium-Cooled Fast Reactor (SFR) type Generation IV nuclear prototype reactor (ASTRID) [3].
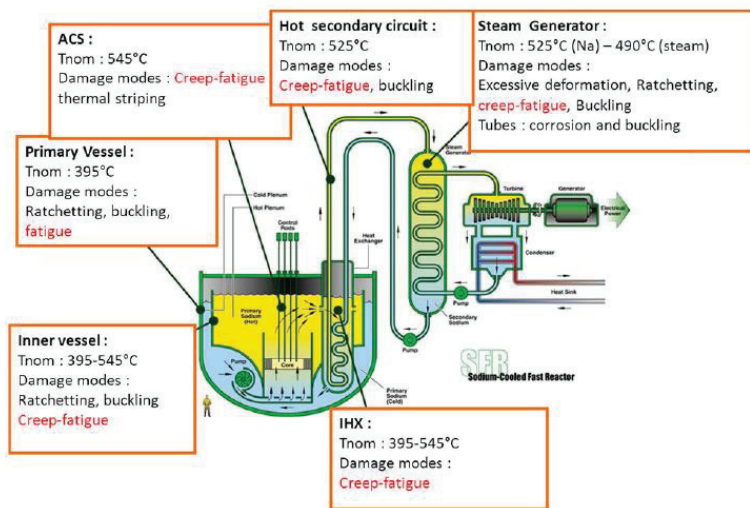
Figure 1. Main damage modes and their expected locations in SFR type GEN IV prototype reactor (ASTRID) [3].

2. Creep-fatigue (CF) assessment methods in design codes

Design codes, such as RCC-MRx [4], ASME III NH [5] and R5 [6] for GEN IV nuclear reactors use interaction diagram based method for creep-fatigue (CF) assessment. In the interaction diagram the fatigue damage is expressed as the ratio of design cycles over the allowable amount of cycles in service and the creep damage as the ratio of time in service over the design life. The design codes differ mainly from each other in the way how the creep damage is assessed. In ASME III NH and RCC-MRx, the calculations of creep damage are carried out using a time-fraction approach. The RCC-MRx procedure differs from the ASME III NH procedure, because ASME III NH uses monotonic stress-stain curves for determining peak stress and isochronous creep curves for relaxation. The R5 procedure is based on a ductility-exhaustion

methodology and is currently the only code following this technique. The code procedures use the results of creep tests to determine the creep damage accumulation models, which are subsequently applied to predict damage in creep-fatigue cycling and in particular strain-controlled dwells that arise during steady operation within a thermal cycle. For time-fraction approaches, the rupture strength of the material is used to calculate creep damage, while in the ductility-exhaustion approach the creep ductility is used to calculate creep damage.

2.1 The interaction diagram

The interaction diagram methodologies are based on summation of fatigue and creep damage
as presented in Eq. (1):

$$\sum_{n=0}^{N_{CF}} (d_c + d_f)_n = D_c + D_f \le D \tag{1}$$

where n is the cycle number at a given strain range, d_c the creep damage accumulated during that cycle, d_f the corresponding fatigue damage of that cycle, N_{CF} is the total number of cycles to failure, D_c the total creep damage at N_{CF}, D_f the total fatigue damage at N_{CF} and D the combined damage causing creep-fatigue failure. It has been shown that D depends for most methodologies on the way the creep damage is handled, and it is material dependent and below unity. In the nuclear design code RCC-MRx, a bi-linear interaction locus has been set at (0.3/0.3) for P91 steel. For design this means that the combined fatigue and creep damage that a component experiences during its service life should not exceed the (0.3/0.3) line, otherwise a failure may occur. It also assumes that rigorous safety factors are used for the calculated allowable d_f and d_c.

An important aspect to remember when dealing with the interaction diagram is that if the ordinate axis (creep damage) is defined with the different variants of the time fraction or ductility exhaustion rules the optimal locus point is not necessarily the same. For instance in the ASME III NH code the locus point for P91 steel is set at (0.1/0.01), seemingly allowing for very little creep damage. The calculation of the creep damage in this code is based on different criteria and models and it should not be directly used with other methods. The interaction diagram for P91 as defined by RCC-MRx, ASME III NH and R5 is presented in Figure 2 with the creep fraction defined as t/t_r and the fatigue fraction as N_f/N_{f0}. In the different design rules the N_{f0} (low cycle fatigue (LCF) cycles to failure from testing) is replaced by an allowable number of cycles for design.
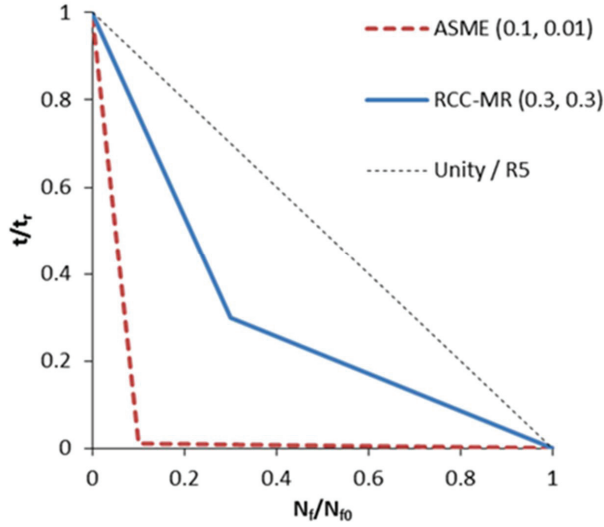
Figure 2. Interaction diagram for P91 steel as defined by RCC-MRx, ASME III NH and R5 [4], [5], [6].

2.1.1 The calculation procedure for creep and fatigue damage

Both in ASME III NH and RCC-MRx the fatigue damage is calculated utilizing design fatigue curves. The fatigue damage D_f is calculated by the Eq. (2):

$$D_f = \sum_i \frac{n_i}{N_{di}} \qquad (2)$$

where n_i is the number of applied repetitions of cycle type (i) and N_{di} is number of design allowable cycles for cycle type (i) determined from the design fatigue curves provided in the codes.

In RCC-MRx the creep damage D_C is calculated by the Eq. (3). T_{dk} is calculated by entering an equivalent stress Sr_j divided by 0.9 to the design creep rupture curve as in Eq. (4).

$$D_C = \sum_k \frac{\Delta t_k}{T_{dk}} \qquad (3)$$

$$\sigma_j = \frac{Sr_j}{0.9} \qquad (4)$$

Stress relaxation behavior is estimated by the creep strain law and the strain hardening rule presented in Eqs. (5), (6) and (7). The initial stress $\overline{\sigma_k}$ is calculated utilizing the

stress-strain curves provided in the code. If symmetrization effects are to be taken into account, $\Delta\overline{\sigma^*}$ is replaced by $K_s\Delta\overline{\sigma^*}$.

$$S(T,t) = \overline{\sigma_k} + \int_0^t \dot{\sigma_c}dt \tag{5}$$

$$\overline{\sigma_k} = K_s\Delta\overline{\sigma^*} \tag{6}$$

$$\dot{\sigma_c} = -E\dot{\varepsilon_c}/C_r \tag{7}$$

where C_r is elastic follow-up parameter and triaxiality coefficient which is taken to be equal to 3 except when the designer justifies a smaller value, $\dot{\varepsilon_c}$ is creep strain rate, E is elastic modulus and K_s is the symmetrization factor. In the ASME III NH procedure the creep damage and stress relaxation is calculated slightly differently and with different safety factors, leading to more conservative creep fractions.

The creep-fatigue assessment procedures and safety margins of design codes were evaluated in EURATOM FP7 MATTER project with emphasis on the RCC-MRx code and P91 steel. Creep-fatigue laboratory tests with strain range of 0.5-1.2%, temperature range of 550-600°C and hold periods up to 1800 seconds were performed for P91 and 316 steel in the project [7], [8], [9]. The test results were evaluated using both the time-fraction approach without safety factors and also the RCC-MRx procedure with safety factors for the same data points [10], [11], [12], [13]. Using the evaluation procedure of RCC-MRx the total creep fractions of the evaluated data were from one to three orders of magnitude above the (0.3/0.3) interaction locus due to strict allowable stress values provided in RCC-MRx, as shown in Figure 3. From design point of view this means that there is a safety margin of one to three orders of magnitude for the creep fractions. Accordingly, using the RCC-MRx procedure, the total fatigue fractions exceeded the (0.3/0.3) interaction locus by one order of magnitude, resulting to a safety margin of one order of magnitude for the fatigue fractions. For the time fraction approach without any safety factors, the data points resided near the (0.3/0.3) interaction locus, for both P91 and 316 steels, which justifies the use of safety factors of RCC-MRx procedure for design purposes.
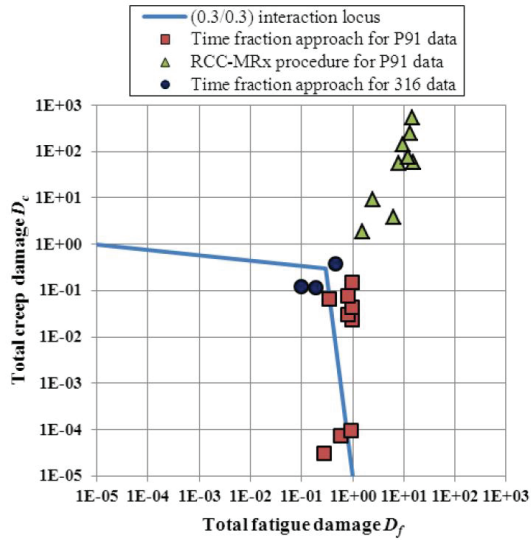
Figure 3. The creep-fatigue test results with hold periods for P91 and 316 steel evaluated with the RCC-MRx procedure and time fraction approach [11].

The design codes provide an alternative way to evaluate the CF test results, where the stress relaxation is not taken into account and the creep fraction is calculated using only the peak stress. From design point of view this conservative approach leads to larger safety margins for expected creep-fatigue loads of components. Figure 4 shows a creep-fatigue assessment using the RCC-MRx standard procedure and the alternative way (without stress relaxation) for CF tests performed in MATTER project for P91 steel. The data points in green colour in the plot are evaluated by taking the stress relaxation during the hold period into account using the RCC-MRx relaxation assessment procedure based on the creep strain rules. The data points in red colour in the plot are the same data points assessed using the peak stress at the beginning of the hold period without taking the stress relaxation into account. Figure 4 indicates that the stress relaxation has strong impact on the creep component in the RCC-MRx assessment procedure based on the interaction diagram. If the stress relaxation is not taken into account the creep fractions can increase by two orders of magnitude.
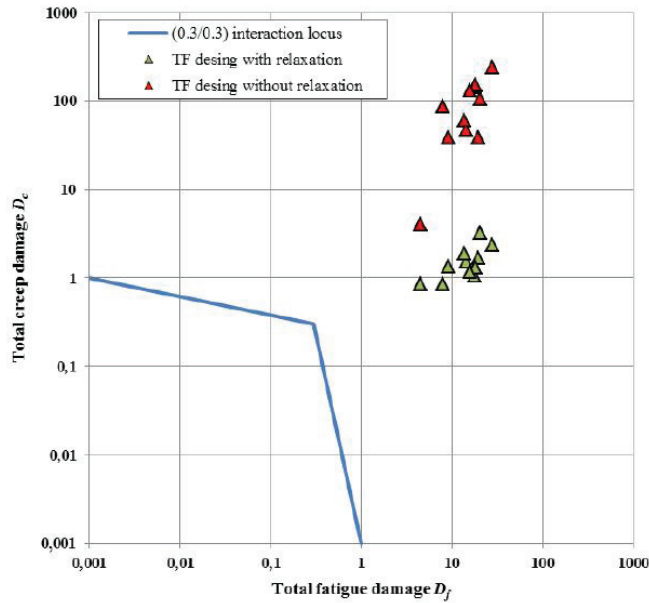
Figure 4. A creep-fatigue assessment using the RCC-MRx standard procedure and the alternative way (without stress relaxation) for CF tests performed in MATTER project for P91 steel [2].

The evaluation of creep-fatigue assessment procedures and safety margins of nuclear codes reveals that the interaction diagram models differ mainly in the definition of the accumulated creep damage. Especially the relaxation behaviour and calculation of the creep damage fraction related to rupture time, creep ductility exhaustion or energy based methods have very strong impact on the estimated cycles to failure in creep-fatigue. The interaction diagram models are at the time the only type of models currently applied in design codes. A creep-fatigue interaction diagram based evaluation according to RCC-MRx, ASME III NH and DDS [14] code with data obtained from various organizations such as Japan Atomic Energy Agency (JAEA), Electric Power Research Institute (EPRI), Oak Ridge National Laboratory (ORNL), Central Research Institute of Power Industry in Japan (CRIEPI), National Institute of Material Science in Japan (NIMS), and The University of Tokyo is shown in Figure 5. The data set includes CF data for P91 steel with different thermal aging history and testing environment, for which a more detailed description is given in [15]. In this assessment, both creep and fatigue fractions resided well above the interaction diagram locus provided by nuclear codes, as shown in Figure 5 [15]. Similar results were obtained when CF tests performed in MATTER project were evaluated, as shown in Figure 3 and Figure 4.
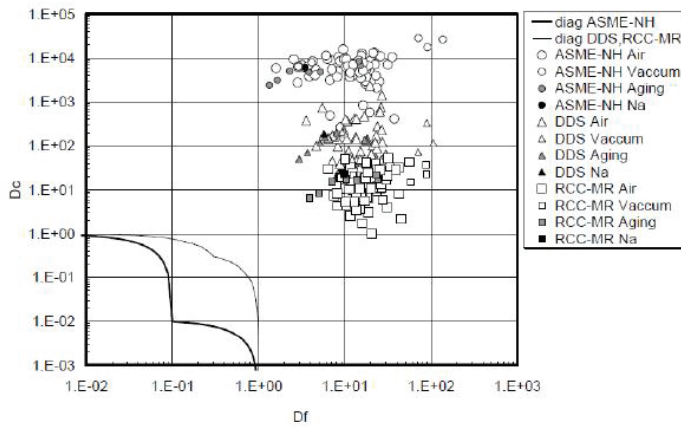
Figure 5. Creep-fatigue evaluation of experimental data for P91 steel by RCC-MRx, ASME III NH and DDS code procedures [15].

3. Discussion

When assessing CF tests with relatively large strain ranges and short hold or creep periods, the nuclear code creep-fatigue assessment procedures, although differ considerably from each other in the definition of the accumulated creep damage, seem to provide sufficient level of conservatism for safe design. However, the sufficient level of conservatism may not remain with parameters relevant to power plant conditions. The test results from short tests and assessment and modelling methods emerging from them may not be reliably extrapolated to GEN IV relevant conditions, where the stress and strain levels are lower, hold periods are significantly longer and lifetimes of components are expected to be about 60 years. There may not be enough data and information on the long-term microstructural evolution and its effect on the creep and cyclic properties of P91 steel to reliably predict the long-term behaviour. It has been suggested that although short-term creep tests for P91 steel indicate a linear relationship between the logarithms of the applied stress and the time to rupture, there is, in fact, a sigmoidal inflection at long lifetimes [16]. Kimura et al. [16] and Abe et al. [17] discuss an increase in the slope of the stress versus time to fracture with decreasing stress due to a loss of long-term creep strength.

Several studies have indicated that the P91 steel exhibits creep resistence deteriotation as a function of stress cycles [2], [13], [18], [19], [20], [21]. The stress applied during the holding period of a CF tests constantly decreases with the number of cycles, because the P91 steel exhibits a strong work softening effect, which is in [22] and [23] suggested to be caused by the coarsening of laths and subgrains and by the decrease of dislocation density. Therefore, for the CF tests carried out at low strain levels, the duration of the hold at a given creep strain (for tests in which the holding periods are stopped once a given creep strain is reached) starts to decrease from one cycle to the next. At the same time, the stress required to achieve the desired strain for the start of the creep period decreases from cycle to the next. This result suggests that the creep

resistance of P91 steel is severely deteriorated after cycling. Indeed, the stress applied at the end of the test can be more than 100 MPa lower than the stress applied at the first cycle to achieve equal strain, whereas the hold duration remains almost equal or even decreases (e.g. for 0.4% creep strain during the hold period of the test).

Figure 6 clearly illustrates this creep resistance deterioration. The creep rates measured at the end of the first holding period of CF tests can be compared with the actual minimum creep rates measured in conventional creep tests. Therefore, both the CF tests and the conventional creep tests enable assessment of the creep behaviour of the as-received material. The effect of cycling on the minimum creep rate is thus illustrated by comparing these results to the creep rates measured at the end of the holding period at $N_{50}/2$, with N_{50} being the number of cycles necessary to obtain a decrease of 50% of the applied stress. This term is conventionally used as a measure of the fatigue lifetime. These results clearly show that after cycling the minimum creep rate is several hundreds times faster than in the as-received condition. However, the creep resistance deterioration effect has not been taken into account in the nuclear design codes. The codes, such as RCC-MRx and ASME III NH, provide creep strain rules, which do not take the cyclic history of the assessed component into account.
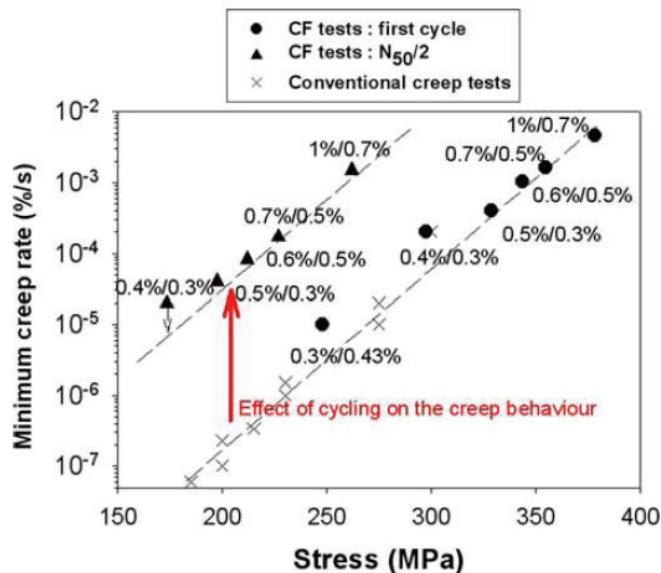
Figure 6. Comparison between the minimum creep rates measured at the first cycles of CF tests, at $N_{50}/2$ of the same CF tests, and in conventional creep tests. The dashed lines schematize the relationship between the minimum creep rate and the applied stress. Each point corresponding to a CF test is identified by the values $\Delta\varepsilon_{fat}/\varepsilon_{creep}$ [18].

Due to the lack of comprehensive understanding of the long-term creep-fatigue behaviour of P91 steel, it is stated in the Tome 6 of the RCC-MRx 2012 edition that

the code rules for interaction between fatigue and creep are not satisfactory defined from the point of view of safe design for P91 steel. This originates from test results which have recently become available, which indicate that the behaviour of such steels with cyclic strain softening makes it a non-conservative option to apply the alternative rule for progressive deformation when determining the effective primary stress according to code sections RB 3261.1111 to 1117 and RB 3262.1111 to 1117. It is stated that there is a need to redefine a method and/or a criterion for an alternative rule justifying the absence of progressive deformation and, in general terms, extend the knowledge of cyclic behaviour of such steels at elevated temperatures. Whilst awaiting the results of research and analysis on this subject so as to prevent the use of progressive deformation rules for this steel, it has been decided to incorporate the corresponding material properties and assessment rules, including cyclic curves, fatigue curves, creep strain rules and creep-fatigue interaction diagram, earlier stated in appendix: A3.18AS – cyclic behaviour and creep, in the probationary phase rules of the code [4].

It is noteworthy that the American Society of Mechanical Engineers (ASME) has taken different approach on P91 steel regarding to the ASME III NH code. The subgroup committee of ASME ETD published a code case N-812 (on 1st Jan 2013) to loosen overconservatism for P91 steel, which allows to use the creep-fatigue damage envelope with intersection point of (0.3/0.3) under certain circumstances [24]. Two conditions, however, should be applied in order to use this code case:

1. The elastic analysis procedure of ASME-NH should be followed.

2. The isochronous curves in ASME-NH should be used when evaluating the creep damage.

Previously the intersection point has been (0.1/0.01) for P91 steel in ASME III NH under any given circumstances. Figure 7 shows the CF interaction diagram for RCC-MRx and ASME III NH, including the ASME code case N-812.
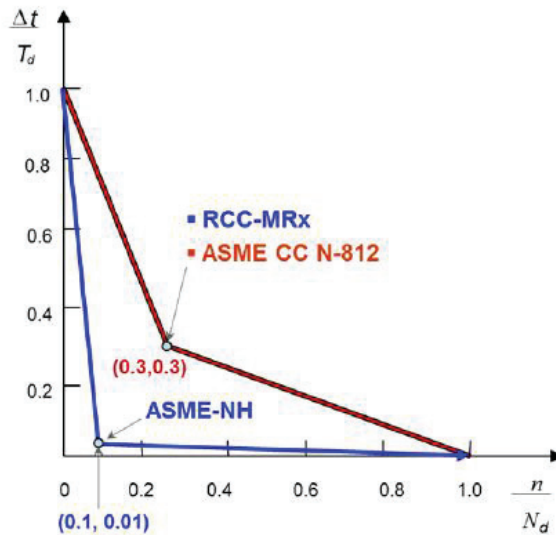
Figure 7. The creep-fatigue damage envelope in elevated temperature design codes (RCC-MRx and ASME III NH), including ASME code case N-812 [4], [5], [24].

As mentioned before, the design codes, such as RCC-MRx, ASME III NH and R5 for GEN IV nuclear reactors use interaction diagram based method for creep-fatigue (CF) assessment. However, for creep-fatigue assessment using interaction diagram based methods, the majority of currently available data for assessment and validation is situated in the regime of relatively large strain ranges and short hold periods. According to [22], [25] and [26], the damage propagates in this regime mainly by necking and is not really affected by creep damage (cavitation) in the grain boundaries. Thus, the extrapolation to long-term type of creep damage is thus somewhat questionable with the present available data. To properly validate the interaction diagram based methods, test data with long hold periods (in stress and strain control) is required. The tensile properties of softened material from both low-cycle fatigue (LCF) and CF tests at different locations in the softening curve also need to be thoroughly determined to further investigate the high creep strain rates measured in CF tests with stress-controlled hold times. The long to very long hold time tests may also improve the understanding of the long-term microstructural evolution in cyclic service.

4. Conclusions

The nuclear code CF assessment methods have been evaluated with emphasis on the RCC-MRx code and P91 steel using literature data and creep-fatigue data produced in the MATTER project. The following conclusions can be drawn:

(1) The design codes, such as RCC-MRx, ASME III NH and R5 for GEN IV nuclear reactors use interaction diagram based method for creep-fatigue (CF) assessment.

In this approach the creep and fatigue damage is handled separately and the total damage is defined as a summation of creep and fatigue fractions.

(2) The design codes differ mainly from each other in the way how the creep damage is assessed. However, none of the codes takes neither the specific material properties of P91 steel, such as the creep resistance deterioration as a function of stress cycles, nor the expected cyclic history of the component, properly into account.

(3) When assessing CF tests with relatively large strain ranges and short hold or creep periods, the nuclear code creep-fatigue assessment procedures seem to provide sufficient level of conservatism for safe design. However, the ability of the codes to correctly assess the CF behaviour of P91 steel under conditions relevant to power plant environments, where the stress and strain levels are lower and hold periods are significantly longer, has not been properly proven.

(4) To properly validate the nuclear code CF assessment methods in relevant conditions and to improve the understanding of the CF behaviour of P91 steel, CF test data with long hold periods (in stress and strain control) and with low stress and strain levels is required.

Acknowledgements

References

[1] R. Pohja et al., *Creep-fatigue interaction rules for P91,* European Comission Community Research Report, MATTER, Project no: 269706 – FP7-Fission-2010, 2014.

[2] R. Pohja, S. Holmström ja H.-Y. Lee, *Recommendation for Creep and Creep-Fatigue Assessment of P91 Components,* European Comission Community Research Report, MATTER, Project no: 269706 – FP7-Fission-2010, 2015.

[3] O. Gelineau, *Progress Report on design codes and rules with respect to the material property requirements for SFR and ASTRID,* European Comission Community Research Report, MATTER, Project no: 269706 – FP7-Fission-2010, 2011.

[4] *Design and Construction Rules for Mechanical Components of Nuclear Installations,* RCC-MRx, AFCEN, Paris, 2012.

[5] *ASME boiler and pressure vessel code,* Section III, Div. 1, Sub-Section NH, ASME, New York, 2007.

[6] *R5 - Assessment procedure for the high temperature response of structures,* Gloucester, UK, British Energy, 2003.

[7] R. Pohja, A. Nurmela, P. Moilanen and S. Holmström, *Multifunctional high precision pneumatic loading system (HIPS) for creep-fatigue testing,* Procedia Engineering, vol. 55, no. 1, pp. 573-577, 2013.

[8] S. Holmström, R. Pohja, A. Nurmela, P. Moilanen and P. Auerkari, *Creep and Creep-fatigue Behaviour of 316 Stainless Steel,* Procedia Engineering, vol. 55, no. 1, pp. 160-164, 2013.

[9] R. Pohja, A. Nurmela, P. Moilanen and S. Holmström, *Creep-fatigue properties of grade 91 steel,* in Proceedings of the 7th International Conference On Advances In Materials Technology For Fossil Power Plants, Waikoloa, Hawaii, USA, 2014.

[10] S. Holmström, R. Pohja and W. Payten, *Creep-fatigue interaction models for grade 91 steel,* Materials Performance and Characterization, vol. 3, no. 2, 26 p., 2014.

[11] R. Pohja and S. Holmström, *A comparison of creep-fatigue assessment and modelling methods,* in Proceedings of the 22nd International Conference on Nuclear Engineering, ICONE 22, Praque, Czech Republic, 2014.

[12] S. Holmström and P. Auerkari, *A robust model for creep-fatigue life assessment,* Materials Science & Engineering A, vol. 559, no. 1, pp. 333-335, 2013.

[13] S. Holmström, R. Pohja and C. Cristalli, *Creep-Fatigue Modelling for Design Rules: Case P91 Steel,* Prepared to be submitted to: International Journal of Pressure Vessels and Piping, 2015.

[14] *DDS - Demonstration fast breeder reactor elevated temperature structural design guideline,* The Japan Atomic Power Company, 1999.

[15] T. Asayama ja Y. Tachibana, *Collect Available Creep-Fatigue Data and Study Existing Creep-Fatigue Evaluation Procedures for Grade 91 and Hastelloy XR, DOE/ASME Generation IV Materials Project,* A report on Task 5 submitted to ASME ST-LLC, Revision 3 Final Report, JAEA, 2007.

[16] K. Kimura et al., *Inherent creep strength and long term creep strength properties of ferritic steels,* Materials Science and Engineering A, vol. 234-236, pp. 1079-1082, 1997.

[17] F. Abe et al., *Alloy design of creep resistant 9Cr steel using a dispersion of nano-sized carbonitrides,* International Journal of Pressure Vessels and Piping, vol. 84, no. 1-2 pp. 3-12, 2007.

[18] B. Fournier et al., *Creep-fatigue-oxidation interactions in a 9Cr-1Mo martensitic steel. Part I: Effect of tensile holding period on fatigue lifetime,* International Journal of Fatigue, vol. 30, no. 4, pp. 649-662, 2008.

[19] B. Fournier et al., *Creep-fatigue-oxidation interactions in a 9Cr-1Mo martensitic steel. Part II: Effect of compressive holding period on fatigue lifetime,* International Journal of Fatigue, vol. 30, no. 4, pp. 663-676, 2008.

[20] B. Fournier et al., *Creep-fatigue-oxidation interactions in a 9Cr-1Mo martensitic steel. Part III: Lifetime prediction,* vol. 30, International Journal of Fatigue, vol. 30, no. 10, pp. 1797-1812, 2008, pp. 1797-1812.

[21] Y. Takahashi, *Prediction of deformation and failure of modified 9Cr–1Mo steel under creep-fatigue interaction,* Materials at High Temperatures, vol. 29, no. 4, pp. 280-292, 2012.

[22] B. Fournier et al., *Comparison of variuos 9-12Cr steels under fatigue and creep-fatigue loadings at high temperature,* vol. 528, Materials Science and Engineering A, vol. 528, pp. 6034-6945, 2011, pp. 6034-6945.

[23] A. Saad et al., *Cyclic softening behaviour of a P91 steel under low cycle fatigue at high temperature,* Procedia Engineering, Vol. 10, pp. 1103-1108, 2011.

[24] *ASME Boiler & Pressure Vessel Code,* Code Cases: Nuclear Components - Supplement 7, 2013.

[25] E. Haney et al., *Macroscopic results of long-term creep on a modified 9Cr–1Mo steel (T91),* Materials Science and Engineering A, vol. 510-511, pp. 99-103, 2009.

[26] V. Gaffard et al., *Creep failure model of a tempered martensitic stainless steel integrating multiple deformation and damage mechanisms,* International Journal of Fracture, vol. 133, pp.139–166, 2005.

Material Concepts of Light Water Small Modular Reactors

Ville Rantanen
ville.rantanen@fortum.com
Fortum, Nuclear and Thermal Power

Abstract

Majority of nuclear power plants in commercial electricity production have a rather high power output. Most new units being built at the moment are well in the 1000-1600 MW_e range. At the same time the trend in power generation is shifting towards distributed energy systems, flexible production and smart grids. In addition concerns related to high capital costs of large power reactors and the need for electricity production in remote locations have made small power plants attractive.

Small Modular Reactors (SMRs) offer a viable alternative to big conventional nuclear reactors and SMRs fulfill many of the needs and aspirations related to flexibility and manageable capital investments. SMRs are also designed to be especially safe and many SMR designs include numerous passive safety features.

Many SMR concepts are still in the early design stages and studies about design-specific material concepts are scarce. This study is focused on material concepts of near-term pressurized light water SMR designs and is especially focused on RPV materials and steam generator tubes. As an example the NuScale reactor design is introduced.

1 Introduction

The term SMR is commonly used as an acronym for Small Modular Reactor. The term "small" refers to less or equal electric power of 300 MW and "modular" means that a single reactor can be grouped with other modules to form a larger power plant. Other definition and the one which International Atomic Energy Agency uses is Small and Medium-sized Reactor. According to IAEA small reactors have less or equal electric power of 300 MW and the medium-sized reactors are in the 300-700 MW electricity region. [1] [2]

There are also mentions of very small reactors (vSMR) and it has been proposed that vSMRs would include units under about 15 MW of electric power. [3]

Starting from the 1950s the size of nuclear reactor units has grown from around 60 MW_e to more than 1600 MW_e. Bigger unit size has been believed to provide economies of scale, especially in operating costs. At the same time smaller power reactors (up to 190 MW thermal) for naval use and for neutron sources have been built by the hundreds worldwide. Thus there is wide expertise in the engineering of both large and small power units. [3]

Nuclear reactor design trends have changed and evolved over the years. Reactor designs may be divided into four general Generations, which are [4]:

- Generation I (1950-1970)
  First prototypes of different designs and approaches including water and gas cooled reactors.

- Generation II (1970-1995)
  Commercial nuclear power plants, emphasis on power generation, Light Water Reactors and Heavy Water Reactors.

- Generation III/III+ (1995-2030)
  Improvement from Generation II reactors, mainly in safety, efficiency and economics.

- Generation IV (2030-)
  New reactor designs, utilizing thermal neutrons or fast neutrons.

2 Small modular reactor concepts

2.1 History

The concept of SMRs dates back to 1950s and 1960s. IAEA has presented the idea of small and medium power reactors in 1961 [5]. The U.S. Air Force did extensive R&D on various types of small reactors from the 1940s to 1960s with no significant results in achieving a militarily useful nuclear powered aircraft and did not see it achievable even in the foreseeable future. The U.S. Navy had better success with nuclear powered aircraft carriers and submarines. Especially the long refueling time was an undeniable advantage and technically there were no real alternatives to nuclear power generation in naval applications. This also meant that the economics of the reactors was not an issue. [6]

In the US Bechtel, Combustion Engineering, General Electric and Westinghouse all have designed reactors for the U.S Navy. These reactors are labeled with two alphabets and a number, such as S4W, in which the first alphabet tells the ship type and the latter the contracted designer. The number represents a consecutive generation number. In Russia compact reactors as KLT-3 and KLT-4 and integral reactors as ABV-6, ABV-6Y and ABV-6M were designed. In France there were the CAP series of integral reactors, such as K-48 and K-150. The output power of these reactors is relatively small. [2]

The main differences between naval reactors and civil reactors are that naval reactors operate under stressful conditions due to movement of the vessel and also the fact that especially in submarines reactors are designed mainly to provide a burst of energy every now and then for accelerating the vessel. Thus both the design and use of naval reactors differ from civil land-based reactors. [6]

U.S. Army´s Army Nuclear Power Program produced small reactors which are most comparable to small reactors now under development. These reactors were placed in isolated areas as Antarctica and remote Army bases. Such reactors are somewhat replaceable with diesel generators and the Army canceled the program in 1976. [6]

From the 1950s there were 17 civilian small reactors commissioned in the US. In 1986 the last small reactor in the US was connected to the grid. None of them are in operation today. These small reactors were essentially seen as prototypes and stepping-stones to larger reactors as the economies of scale was believed to prevail. The reactor size in the US and around the world increased and reached the 800-1300 MW level by the mid-1970s. [6]

Keeping this history of small and also large nuclear reactors in mind it can be said that the current SMR designs are mainly rooted from two origins: marine-based power reactors (such as mPower derived from Otto Hahn marine reactor) and land-based electricity generation reactors (such as Westinghouse SMR from AP1000). The design objectives of SMRs in many case are smaller power grade, smaller configuration size, smaller generation cost and smaller operational risk. [2]

2.2 Today

Today there are numerous different SMR concepts originating from around the world. Some of the concepts are on early stages of design, some are developed for near-term deployment, some are under construction and a few designs are already under operation.

Modern SMRs can roughly be divided to Generation III/III+ designs and Generation IV designs. A more detailed classification would also take into account the neutron spectrum and coolant which the designs utilize, as in Figure 1.
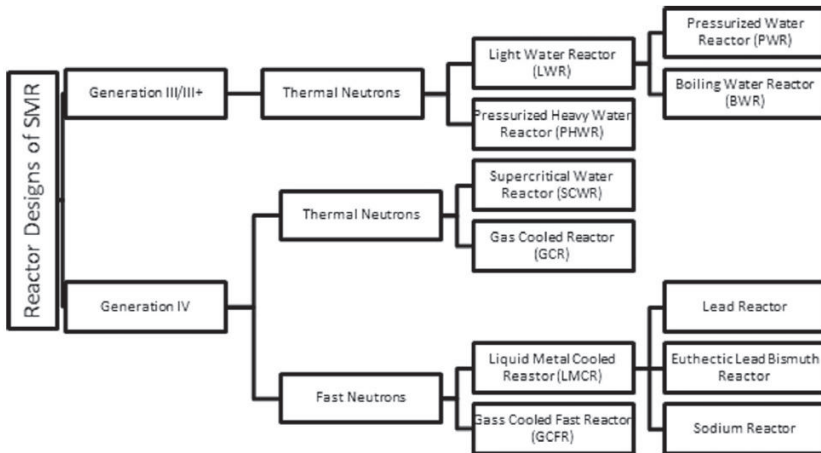
Figure 1. Classification of SMR designs. [4]

LWRs are the most common nuclear designs in the world. There are around 437 reactors in operation and of them 357 are LWRs. Of these LWRs 273 are PWRs. This means that of nuclear reactors the most experience has been gathered with PWR technology. Most of the LWR SMR designs are PWRs and at least Argentina, Brazil, China, France, Republic of Korea, Russian Federation and United States of America are pursuing this technology. [4] Of all SMR designs LWR SMRs are seen to include a relatively low technological risk. [3]

The SMR designs which represent Generation IV of nuclear energy are unlikely to be deployed in the next 15 years. Generation IV reactors may bring new opportunities especially regarding the usage and recycling of nuclear fuel. Generation III/III+ SMR designs are considerably more likely to be deployed in the near future even into

commercial use. In many cases substantial research and development efforts are required.

According to IAEA there are about 45 SMR designs under development and half of them are targeted to be deployed over the next ten years. The first three SMRs with advanced technologies are expected to become operational over the next four years are KLT-40S in Russia, HTR-PM in China, and CAREM in Argentina. [7]

In general the modern small modular reactors for power generation are expected to have greater simplicity of design, economy of series production largely in factories, short construction times, and reduced siting costs. Most designs include high level of passive or inherent safety features. Some designs are also designed to be placed below ground level which gives an increased resistance to impact-related threats. [3]

When focusing on PWR SMRs there are around 12 relevant designs and the basic properties of these designs are presented in Tables 1 and 2.

Table 1. Basic information of some PWR SMR designs. [4]

Design name	CAREM	FBNR	CNP-300	FLEXBLUE	IMR	SMART
Origin country	Argentina	Brazil	China	France	Japan	Korea
Electric power (MW$_e$)	25	40	325	160	350	100
Reactor pressure (MPa)	12.25	16	15.2	15.5	15.51	15
Core outlet temperature (°C)	326	326	302	310	345	323
Design life (years)	60	-	40	60	60	60
Fuel type	UO2	TRISO or CERMET	UO2	UO2	UO2	UO2
Enrichment (%)	1.8, 3.4	5-9	2.4-3	5	4.8	4.8
Refuelling period (months)	14	36-84	18	36	26	36
Circulation in RPV	Natural	Forced	Forced	Forced	Forced	Forced
Status of design	Under construction [3]	Conceptual design [1]	Operating [3]	Conceptual design [1]	Design in earlier stages, conceptual design completed [1] [3]	Near-term deployment, licensed/certified [1] [3]

There exists also other SMR designs such as VBER-300 (OKBM, Russia), SMR-160 (Holtec, USA), ACP100 (CNNC&Guodian, China), CAP150 (SNERDI, China), ACPR100 (CGN, China), ABV-6M, RITM-200, VVER-300 (Gidropress, Russia), SHELF, ELENA, CAP-100 and so on. Some of these are closer to deployment and some are a bit further away in different design stages. More information of different designs can be found from for example IAEA:s "Advances in Small Modular Reactor Technology Developments, 2014"-publication.

Table 2. Basic information of some PWR SMR designs. [4]

Design name	KLT40-S	UNITHERM	IRIS	mPower	NuScale	Westinghouse SMR
Origin country	Russia	Russia	International	USA	USA	USA
Electric power (MW$_e$)	35	6,5	335	150	45	225
Reactor pressure (MPa)	12.7	16.5	15.5	14.1	8.72	15.5
Core outlet temperature (°C)	316	325	330	320	329	310
Design life (years)	40	25	60	60	60	60
Fuel type	UO2	CERMET	UO2/MOX	UO2	UO2	UO2
Enrichment	< 20	19.75	4.95	< 5	4.95	< 5
Refuelling period (months)	28	240	48	48	24	24
Circulation in RPV	Forced	Natural	Forced	Forced	Natural	Forced
Status of design	Under construction, commercial start planned 2016-2017 [3]	Conceptual design [1]	Under development, basic design [8]	Near-term deployment, basic design [1] [3]	Near-term deployment, basic design [1] [3]	Near-term deployment, preliminary design completed [3]

Electricity generation is the main purpose of the reactor in many cases, but also other uses have been found. Some examples are water desalination, district heating, high temperature process heat for process industry. Some of the SMR concepts are designed to be able to perform daily load follow. For example Westinghouse SMR is able to load follow from 100 % to 20 % at a rate of 5 % change per minute [9].

Many of the LWR SMR designs boast with improved safety features such as an iPWR (integral pressurized water reactor) design, increased relative coolant inventory, increased relative heat surface area, increased passive cooling capability, smaller radionuclide inventory and under-ground construction. An iPWR means that the primary cooling system is integrated, i.e. the core, steam generators, the whole primary circuit coolant and control/absorber rods are located inside the reactor pressure vessel [10]. In an iPWR the maximum size of a pipe penetrating the reactor vessel is 5-7 cm in diameter, while in a large conventional PWR pipes connecting the reactor vessel to the external steam generator are 80-90 cm in diameter. [2]

The high level of integration in iPWRs also poses challenges to SMR development. The structure inside the RPV becomes more complicated as all primary system equipment are integrated into one single vessel. Components inside the RPV will be more prone to affect other components in the same small space. Also the radiation from reactor core will be more intensive and therefore the need for high quality welds, tube materials and the water chemistry control of the secondary system will be essential. The difficulties in equipment manufacture will likely turn to the assembling and commissioning from forging processing of big components. Maintenance of such a compact and complex structure may also prove to be challenging. [2]

3 Material concepts of light water SMRs

Structural materials are often the limiting factor for the realization of new or groundbreaking machines and plants. Practicable innovations in structural materials happen seldom and the implementation of such usually takes a long time. For example in GEN IV roadmap in 2002 some structural materials challenges and opportunities for advanced reactors were seen to be oxide dispersion strengthened (ODS) steels, advanced martensites, refractory alloys, aluminides, SiC based ceramics and layers for corrosion protection. Today only the advanced martensites have managed to become a part of current or future power plants under design or construction. This slow rate of development is mainly due to the fact that the transfer of a laboratory batch of novel material into a structural component requires very complex and multidisciplinary interactions between many different actors and disciplines. [11]

In technical progress of large machines the structural materials are often the limiting obstacle. Reasons are usually related to inadequate properties (toughness, strength, creep, corrosion resistance etc.), missing production technologies, missing forming or joining techniques or high costs. [11]

Structural materials in a nuclear power plant must be able to operate under demanding exposure condition. The main challenges for structural materials of nuclear reactors are temperature, radiation and corrosive media.

The operating temperatures in current water cooled Generation II and III/III+ nuclear reactors remain below 350 °C and in general these temperatures do no cause significant challenges to structural materials used. When the operating temperature of metallic materials under load increases the behavior of metals becomes time-dependent. In other words metals will undergo creep when subjected to constant load at elevated temperatures. This creep means a time dependent change in length. Creep has mainly an effect in conventional power plants and in Generation IV nuclear power plants, where temperatures of up to 1000 °C are considered. A usual rule of thumb is that at homologous temperatures (T/T_m, where T_m is the melting temperature in K) of more than 0,35 thermal creep becomes of engineering significance. This, for example, means that with austenitic stainless steel (melting temperature around 1375 °C) creep becomes an issue in temperatures over 300 °C. [11]

In core and close-to-core components in nuclear plants are exposed to radiation. Energetic particles (neutron, ions, electrons) interact with the atoms of solid materials and produce different effects (irradiation damage) in materials, mainly formation of point defects such as interstitial atoms and vacancies, defect clusters such as dislocation loops and stacking fault tetrahedral, and cavities (voids and gas-filled bubbles). These phenomena are, in brief, manifested by hardening, embrittlement, segregation, swelling and radiation creep of components. [11]

Also low activation of materials is appreciated. Neutron radiation activates materials and it would be beneficial if this activation would be as low as possible. Low activation means low radioactivity and this means improved safety of operation hands-on maintenance and also easier decommissioning of components.

The corrosive medium in PWRs is the primary or secondary side water, depending on the component and location of the component. All metallic materials experience some type of corrosion phenomena in certain environment. Materials selection in nuclear power plants is partially guided by corrosion, especially the attempt to minimize the harmful corrosion phenomena in operation conditions. Also water chemistry and water

chemistry control play an important role in mitigating corrosion. Some corrosion types to be taken into account are flow-assisted corrosion (FAC), stress corrosion cracking (SCC), irradiation-assisted stress corrosion cracking (IASCC), environment assisted cracking (EAC), general corrosion, microbiologically influenced corrosion, crevice corrosion, pitting corrosion, intergranular corrosion and galvanic corrosion.

The relatively low operating temperature of LWR PWRs helps in material selection. On the other hand the operating pressure is high, but it is usually compensated with bigger wall thicknesses of components.

Table 3. Comparison of some design details between NuScale and large reactor designs. [4] [12] [13] [14] [15]

Design name	Westinghouse AP1000	Areva EPR	Gidropress VVER-1200 (V-392M)	NuScale
Origin country	USA	France	Russia	USA
Electric power (MW$_e$)	1100	1650	1082	45
Reactor pressure (MPa)	15.5	15.5	16.2	8.72
Core outlet temperature (°C)	324.7	330	328.9	329
Design life (years)	60	60	60	60
Fuel type	UO2	UO2 and MOX	UO2	UO2
Enrichment	4.8	4.95	4.79	4.95
Refuelling period (months)	18	24	12	24
Circulation in RPV	Forced (4 pumps)	Forced (4 pumps)	Forced (4 pumps)	Natural
Status of design	Under construction	Under construction	Under construction	Near-term deployment [3]
SG	Delta-125, U-tube, vertical	U-tubes with axial economizer	PGV-1000MPK	Once-through, helical-coil, superheating, feedwater inside tubes, iPWR [2]

For the current generation of nuclear light water reactors the performance of structural materials is well established due to 50 years of operation experience and continuous improvement, optimization and research of the technical solutions. In recent years especially issues related to the long-time performance of materials and components under service conditions has been a major interest. [11]

Current LWR power plants mainly utilize low alloy steels, austenitic stainless steel and superalloys as structural parts and zirconium based alloys as fuel cladding. These material choices have been done to fulfill the strength and toughness requirements for

the pressure boundaries, liquid corrosion resistance and neutronics. Also the aspect of costs has had an effect on materials selection. [11]

Many LWR SMRs have quite similar operating conditions (pressure, temperature etc.) than the current large nuclear power plants. A comparison between NuScale and some new large reactor designs is presented in Table 3 below.

As can be seen from Table 1 and Table 2 the reactor pressure and core outlet temperature of LWR SMRs are around 12-17 MPa and 300-345 °C. The majority of SMR concepts are using UO2 fuel enriched to about 5 %. These values are more or less equal in modern large reactor designs (Table 3). All this means that these SMR LWR designs do not significantly differ from conventional nuclear power plant designs. Thus it is probable that materials selection and manufacturing techniques used in SMRs will mainly be similar to conventional Gen III/III+ nuclear power plants.

A general depiction of most common materials used in conventional PWR NPPs is presented in Figure 2 below. A reasonable guess would be that many of the materials below will also be used in LWR SMRs.

Figure 2. Materials used in PWRs. [16]

As can be seen from Figure 2 the primary circuit of a PWR includes many components such as the reactor pressure vessel, core internals, control rod mechanisms, fuel, primary piping, pressurizer, steam generator and coolant pump. In this paper the RPV materials and the structure and materials of steam generator are discussed in more detail.

3.1 RPV

Reactor pressure vessels of LWRs are made from low alloy carbon steels and they usually have primarily a tempered bainitic microstructure. Some typical RPV steels by ASME are A302, A533B, A508 (508 Class 3 is similar to RCC-M 16MND5 and DIN

20MnMoNi55). Modern RPVs are usually manufactured in the form of ring forgings which are welded together. The size of the forgings is large which presents manufacturability challenges. One example of the difficulties related to manufacturing large vessels and forgings is the situation in Belgium in Doel 3 and Tihange 2, where hydrogen-induced flaws have been discovered in the RPVs [17]. There have been studies which suggest that mechanical properties of the RPV material would be more strongly influenced by radiation than previously expected [17]. [11]

Especially RPVs but also other vessels that contain primary circuit water and pressure act as a barrier to the outside and therefore must fulfill stringent safety measures. Major demands for pressure vessels are [11]:

- High strength in all operating temperatures
- High fracture toughness and low ductile to brittle transition temperature
- High resistance to corrosion
- Homogeneous microstructure and mechanical properties
- Good resistance to thermal and radiation embrittlement
- Good weldability and non-destructive inspectability

Many RPV designs avoid welds in the belt line. Belt line is the area of the vessel where there is highest radiation exposure and thus highest tendency for radiation embrittlement. The inside of RPVs are cladded with austenitic stainless steel cladding. The alloy steel provides strength and stainless steel provides corrosion resistance. The cladding is usually approximately 10 mm thick. [11]

Material inhomogeneity and microstructure of vessels may affect mechanical properties, make ultrasonic inspection more difficult and even hide existing flaws.

Some main dimensions of a few current large NPP designs and NuScale are given in Table 4.

Table 4. Information of some large nuclear reactors and NuScale RPV design.

	EPR [14]	**AP1000** [13]	**AES-2006** [15]	**NuScale** [18]
Base material	16MND5	Carbon steel	15H2NMFA	
Inner diameter of cylindrical shell [mm]	4870	4038.6	4232	~2743.2
Wall thickness of cylindrical shell [mm]	250	203	197.5	
Design pressure [MPa]	17.6	17.2	17.64	~12.7 (Operating pressure)
Total height, inside [mm]	13083	12056		~19812 (Overall height)
Transport weight [t]	520		330	

The diameter of rector pressure vessel in SMRs is smaller than in larger nuclear reactors thus making SMR RPVs easier to manufacture. Handling of smaller forgings is easier, material homogeneity is improved and also the number of vendors capable of manufacturing said forgings should be bigger. All this makes also factory manufacturing and batch production more plausible.

One possible advancement in RPV materials would be to change to more corrosion resistant materials such as 3Cr-3WV-steel. 3Cr-3WV-type steel is more corrosion resistant as the common RPV steels and by using said steel a RPV could be made without cladding. The higher chromium means also that the steel is more resistant to hydrogen embrittlement. This 3CR-3WV steel should also be more resistant to irradiation embrittlement than the current LWR RPV steels and this would allow to build a smaller-diameter RPV. Introdictuon of this kind of a new RPV material would need comprehensive fabrication and irradiation studies and also inclusion to design codes. [11]

3.2 Steam generator

In nuclear reactors steam generators convert heat into steam and the steam is used to drive a steam turbine.

There are basically two kinds of steam generators used in nuclear power plants. Large reactors mostly use recirculating steam generators (RSG). In SMR designs the main type is once-through steam generator (OTSG). In an OTSG the flow in the secondary system is forced by circulating water by feed-water pumps. OTSG generates superheated steam which enhances the heat efficiency and removes the need for moisture separators thus simplifying the system. For example mPower and NuScale designs produce superheated steam. [2]

One type of OTSG is helical-tube OTSG. By the helical structure heat exchange surface can be increased in certain space volume. Helical geometry also causes secondary flow in pipes prompting heat exchange. Helical-coil OTSG has first been equipped on nuclear icebreaker Lenin in 1958. A major issue of a helical-coil OTSG is the non-uniformity of the convective heat transfer. If there is excessive temperature deviation inside the steam generator it may cause damage to heat transfer tubes. Two advanced gas-cooled reactors at Heysham UK operate under low power conditions in order to protect the tubes. [2]

Table 5. Steam generator properties of a few modern large reactor designs.

	EPR [14]	**AP 1000** [13]	**AES-2006** [15]
Type	U-tube with axial economizer	Delta-125, U-tube, vertical	PGV-1000MPK
Number of SGs	4	2	4
Total tube outside area [m²]	7960	11477	6105
Number of heat exchanger tubes	5980	10025	10978
Tube outside diameter [mm]	19	17.5	16
Transport weight of one SG [t]	520	663.7	330
Tube material	Inconel 690	Inconel 690-TT	08H18N10T

Nuclear reactors of western design usually utilize steam generator tubes made from nickel-based superalloys as 600MA, 600TT, 690TT or nickel-iron based as Incoloy 800 [11]. The degradation mechanism for the tubes is generally Environment Assisted

Cracking (EAC) [11]. The Russian 08H18N10T tube material is pretty much equivalent with AISI 321, which is a titanium stabilized austenitic stainless steel [19].

There are some major differences in Western and Russian steam generator designs. The steam generators in Russian VVER-based designs as the AES-2006 are horizontal, as in Western designs they are vertical. In PWRs the tube sheet and collector are made from low alloy steel and cladding, whereas in VVERs from 10GN2MFA, 08H18N10T and cladding. The steam generator vessel itself is low alloy steel in PWRs and 10GN2MFA or 22K in VVERs. The tube grid is made from 08H18N10T in VVERs and from carbon or stainless steel in PWRs. This comparison shows that there are many viable options to steam generator design and materials. [19]

As the SMR designs vary, also the structure of steam generators vary. For example in NuScale the feedwater flows inside the steam generator tubes as opposed to Westinghouse SMR where the primary coolant flows inside the tubes. [2]

3.3   Fuel and core design

A common goal of SMR designs is higher burnup and longer lifecycles of fuel compared to conventional large nuclear power plants. With higher burnup the uranium resources can be utilized more fully and longer refueling intervals decrease proliferation risks, lower radiation doses and provide a possibility for unattended operation in remote areas. [2]

A common approach in SMR fuel development is to rely to simplification of design and ease of licensing. Reactor fuel development is time consuming and costly and different challenges come from clad oxidation, water chemistry, assembly strengthening, fission gas release, burnable poison and manufacturing. Consequently many SMR designs utilize existing fuel designs with good operating experience. [2]

The design of SMR reactor cores focuses on the core dimensions, on the optimized core loading, on effective fuel cycle, and on the safety limits. The diameter of the reactor core is related to the radial size of the reactor pressure vessel which itself is limited if the pressure vessel is to be shipped by rail car. The length of the control rods, control rod drives and the reactor internals depends on the height of the core. The fuel and core design is an iterative process between assembly design and the core management. [2]

Reactor internals in LWR environment are usually made from austenitic steels because of the superior corrosion resistance they possess. The 304/316 group is the most used. Austenitic stainless steels suffer from void swelling. [11]

3.4   General

Generally many of the specific SMR materials issues are uncertain due to the preliminary state of their engineering designs at this time. Possible modifications in the water chemistry of SMRs compared to what has been utilized in existing LWRs is one example of a major factor influencing materials selection and materials performance. [16]

Manufacturing processes made possible by the factory assembly may provide advantages in material performance compared to standard fabrication techniques. New advanced manufacturing techniques such as additive manufacturing could provide reduced fabrication costs or make possible completely new designs in for example

specialized pump or valve components. With additive manufacturing it is important to compare the microstructure and performance of the materials to conventional solutions as wrought materials. [16]

Many SMR designs include the use of integral containment. Integral containment means that the steam generator of a PWR is located within the RPV. In some designs the primary water flows across the outside of the tubes. This implies to a reversed situation in primary and secondary sides steam generator tubes compared to conventional steam generators used in PWRs currently in use. [16]

The use of integral containment eliminates the possibility of a large-pipe LOCA (Loss Of Coolant Accident). However, the inversion of primary and secondary sides of a tubed steam generator may bring also new challenges. Stress corrosion cracking is still a possible phenomenon and the limited accessibility of steam generators for routine inspection may cause problems unless steam generator reliability can be improved. [16]

4 NuScale

In 2013 NuScale Power was selected as the winner of the second round of the U.S. Department of Energy five-year cost-sharing program to develop nuclear small modular reactor technology. Thus NuScale is one of the most promising SMR concepts and it is seen as one of the designs to be deployed in the near term [20].

4.1 Background of the concept

The design of NuScale is based on the MASLWR (multi-application small light water reactor). MASLWR started as a collaborative research program proposed by Oregon State University (OSU), Idaho National Engineering and Environment Laboratory (INEEL) and Nexant (which was, at the time, a subsidiary to Bechtel). In 2007 NuScale Power Inc. was formed to commercialize the small nuclear power technology under development at OSU. At that time MASLWR was renamed to NuScale to reflect the development made to the original design at OSU. [20]

In 2008 NuScale started pre-application discussions with the U.S. Nuclear Regulatory Commission with the intention of submitting an application for design certification for the modular and scalable reactor technology. NuScale also entered into a strategic partnership with Kiewit Construction (annual revenue around 8 billion USD). A detailed NuScale plant cost study was conducted in 2009 and it determined that NuScale would be a highly competitive alternative to both nuclear and fossil plants. [20]

General Dynamics Electric Boat was selected as the firm to manufacture the major modular components, the integrated containment and reactor module. Electric Boat has delivered more than 100 nuclear submarines to the U.S. Navy thus having related manufacturing experience. The intention is to take advantage of standard systems and components assembled in the factory and automated forming, rolling, bending and welding processes to produce precise products with high repeatability. [20]

NuScale is to submit design certification application to the NRC in second half of 2016. The target for the design certification is 2020 and commercial operation is targeted in 2023. [1]

4.2 Basic Design

One NuScale reactor module produces a net electric power of over 45 MWe and NuScale reactor is designed to be made up of one to twelve independent reactor modules. Most suitable configurations are plants of 6 or 12 reactor modules which means plant output of around 270 or 540 MWe. NuScale modular design allows incremental refueling outages and system maintenance. [1]

The nuclear power module of NuScale is composed of a reactor core, a pressurizer and two steam generators integrated within the reactor pressure vessel. This design eliminates the external piping to connect the steam generators and pressurizer to the RPV. The RPV is housed in a compact steel containment vessel. The water provides a passive heat sink for long-term emergency cooling. The main structure of NuScale is shown in Figure 3. [18]

The reactor operates based on natural convection, the design does not include main circulation pumps. Safety features are fully passive. Each reactor module includes a high pressure containment vessel immersed underwater. The pool in which reactor modules lie is below-grade. The primary system and containment are prefabricated at the factory and then transported to the plant site. Thus construction schedule is approximated to be 36 months. The modular design of NuScale allows new modules to be added or existing refueled independently while the other modules continue to operate. [1]
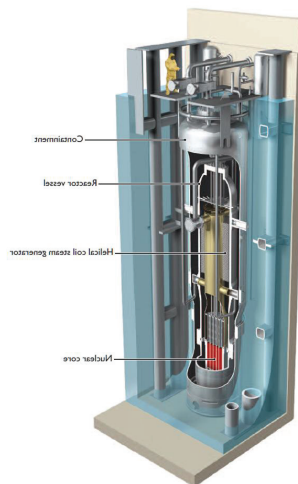

Figure 3. Overview of the NuScale power module. [20]

4.3 Specific design features

The reactor pressure vessel is placed within an additional pressure vessel made of high-strength stainless steel. This complex is placed underwater in a below-grade pool shared with all modules. This solution provides post-accident passive containment cooling and decay heat removal for an unlimited period of time. There is a vacuum between the containment vessel and the RPV to minimize heat loss and provide thermal insulation. [1]

The integral reactor vessel design of NuScale includes the nuclear core, steam generator and pressurizer within a single vessel. The approximate dimensions of the pressure vessel are 17,4 m (45 feet) in length and 2,9 m (9,6 feet) in diameter. The containment vessel is 18,3 m (60 feet) long and 4,6 m (15 feet) in diameter [20]. [1]

NuScale design incorporates two independent helical-coil steam generators that are located in the space between the upper riser and the RPV shell. The feedwater enters the feed plenums, flows up through the inside of SG tubes and is then directed to the turbine plant. The reactor coolant flows through the riser, is then turned by the pressurizer baffle plate and flows down over the shell of the helical steam generator tube bundle. [1]
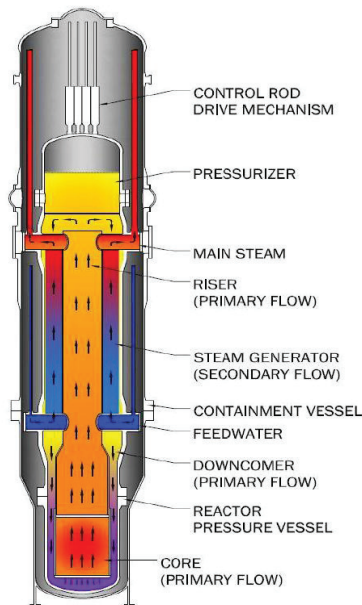

Figure 4. NuScale power module. [18]

The fuel used will be UO_2 enriched to less than 4,95 % U^{235}. The fuel assembly will be 17x17 and the active height if the fuel is 2,0 m. The core will be made up from 37 fuel assemblies and 16 control rod assemblies. [18]

4.4   Helical-coil steam generators

Each NuScale power module include two once-through helical-coil steam generators. The steam generators consist of tubes connected to feed and steam plenums with tubesheets. Preheated feedwater enters the lower feed plenum through nozzles on the RPV. Feedwater flows through the interior of the steam generator tubes and the heat is transferred from the reactor coolant to feedwater. The feedwater heats up, changes phase and exits the steam generator as superheated steam. [18]

Usually in PWRs the reactor coolant flows inside the steam generator tubes and the feedwater flows outside the tubes. As mentioned, in NuScale design feedwater flows

inside steam generator tubes. This means that the inner surface of the NuScale tubes is colder than the outer surface. This might cause cracks to initiate and grow from the outer surface. If so, the non-destructive inspection of steam generator tubes might become more challenging. Conventional steam generator tubes are inspected from the inside using an eddy current probe and also the cracks are usually on the inner surface. Steam generator tubes are quite thin so the cracks propagating from the outer surface may still be detected with an eddy current technique used inside the tubes.

The accumulating irradiation damage might be bigger in NuScale than in conventional larger power plants. Also the effects of radiation on steam generator might be bigger than in conventional large reactors. On the other hand the amount of active fuel in the core and the core diameter is smaller in NuScale than in conventional reactors.

4.5 The structure of the steam generator

There are two types of documents publicly available concerning NuScale steam generators, the one being general documents and brochures about the design of the plant and the other being US patents discussing helical coil steam generators. The latter are more detailed but also they leave many details open.

The US Patent 8,752,510 B2 from 2014 describes the structure of a general helical coil steam generator. By coiling the heat transfer tubes it is possible to increase the surface area of the tubes for a given axial cylinder in order to maximize the heat transfer from the primary coolant to the secondary coolant. [21]
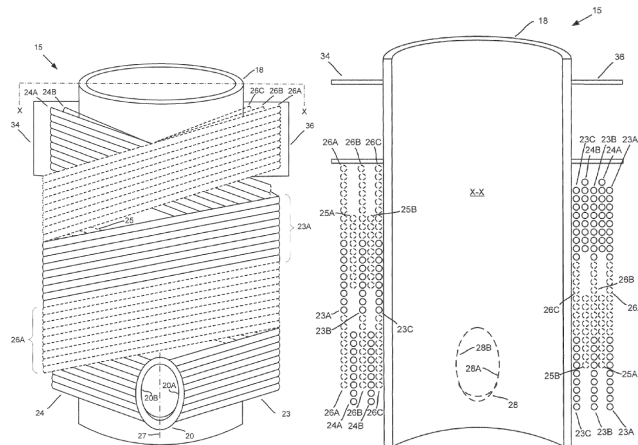

Figure 5. In the left: an illustration of an heat transfer system comprising a plurality of heat transfer tubes. In the right: cross-section taken through the heat transfer system in the left. 15 = The heat transfer system, 18 = Thermal housing, 20 = Lower integral tubesheet/plenum, 23 = First set of heat transfer tubes, 24 = Second tube set [21]

There are two sets of heat transfer tubes, of which first rotates clock-wise around the thermal housing and the second counter-clockwise. It is also possible that there are more than two tube bundles. The tube bundles are independent thus allowing to continue operation even in the case of failure in one steam generator bundle. The number of rotations about the central axis, the paths of the tubes and the helical angle of the tubes may vary in order to minimize the variation in the lengths of the tubes as

the location of the tubes transitions from inside columns to outside columns. The similar lengths of the tubes helps to achieve constant pressure drop and equal fluid flow. [21]

The number of revolutions of the coils is between 3¼ and 4¾. It is also possible that there is fewer or more revolutions of the coils in other embodiments. [21]

The patent also covers the manufacturing steps to produce a steam generator. Connecting the tubes to a tube sheet is the major issue. Steam generator tubes are typically friction or pressure-fit to the tube sheet by roll-expanding a portion of the tubes within the tube sheet using a mechanical, pneumatic or hydraulic device to provide a leak tight joint. [21]

5 Summary

Of all SMR designs most promising and closest to deployment are light water SMRs. In many aspects the LWR SMRs resemble quite much the operating LWR fleet of larger reactors. Thus most of the material issues of LWR SMRs are expected to be comparable to those faced by Generation II and III reactors. There exists a wide operational expertise of light water reactors in electricity production and naval applications.

The high level of integration in integrated PWRs also poses challenges to SMR development. The structure inside the RPV becomes more complicated as all primary system equipment are integrated into one single vessel. Components inside the RPV will be more prone to affect other components in the same small space. Also the radiation from reactor core will be more intensive and therefore the need for high quality welds, tube materials and the water chemistry control of the secondary system will be essential. The difficulties in equipment manufacture will likely turn to the assembling and commissioning from forging processing of big components. Maintenance of such a compact and complex structure may also prove to be challenging. The smaller size and different geometries of components of LWR SMRs compared to big nuclear reactors may also bring new challenges with manufacturing techniques.

The technological risk of LWR SMRs is seen to be low compared to Gen IV SMRs or other advanced SMR designs. There still is a certain gap in between the designs and technologies of SMRs and commercializing these technologies. In many cases substantial research and development efforts are required.

6 Bibliography

[1] IAEA, Advances in Small Modular Reactor Technology Developments. A Supplement to: IAEA Advanced Reactors Information System (ARIS), Vienna, Austria: International Atomic Energy Agency, 2014.

[2] Z. Liu and J. Fan, "Technology Readiness Assessment of Small Modular Reactor (SMR) designs," *Progress in Nuclear Energy,* vol. 70, pp. 20-28, 2014.

[3] World Nuclear Association, "Small Nuclear Power Reactors (Updated May 2015)," 2015. [Online]. Available: http://www.world-nuclear.org/info/Nuclear-

Fuel-Cycle/Power-Reactors/Small-Nuclear-Power-Reactors/. [Accessed 21 5 2015].

[4] M. K. Rowinski, T. J. White and J. Zhao, "Small and Medium Sized Reactors (SMR): A Review of Technology," *Renewable and Sustainable Energy Reviews, volume 44,* pp. 643-656, 2015.

[5] IAEA, "Prospects for small and medium power reactors," *International Atomic Energy Agency Bulletin,* pp. 3-8, January, Vol. 3-1 1961.

[6] M. V. Ramana, "The Forgotten History of Small Nuclear Reactors," IEEE Spectrum, 27 Apr 2015. [Online]. Available: http://spectrum.ieee.org/energy/nuclear/the-forgotten-history-of-small-nuclear-reactors. [Accessed 6 8 2015].

[7] L. Kollar, "Small Modular Reactors Offer Option for Near-Term Nuclear Power Deployment (IAEA Department of Nuclear Energy)," 16 September 2015. [Online]. Available: https://www.iaea.org/newscenter/news/small-modular-reactors-offer-option-near-term-nuclear-power-deployment. [Accessed 18 September 2015].

[8] M. H. Subki, "Status of Global SMR Development and," in *6th INPRO Dialogue Forum on Global Nuclear Energy Sustainability:*, Vienna, Austria, 2013.

[9] Westinghouse, "The Westinghouse Small Modular Reactor," Westinghouse Electric Company LLC, 2013.

[10] R. Mazzi, "CAREM: An Innovative Integrated PWR," in *18th International Conference on Structural Mechanics in Reactor Technology (SMiRT 18)*, Beijing, China, 2005.

[11] H. Wolfgang, Materials for Nuclear Plants, From Safe Design to Residual Life Assessments, London: Springer, 2013.

[12] "AP1000 Nuclear Power Plant," Westinghouse Electric Company LLC, 2015. [Online]. Available: http://www.westinghousenuclear.com/New-Plants/AP1000-PWR. [Accessed 7 September 2015].

[13] IAEA, "Status report 81 - Advanced Passive PWR (AP 1000)," IAEA ARIS, 2011.

[14] IAEA, "Status report 78 - The Evolutionary Power Reactor (EPR)," IAEA ARIS, 2011.

[15] IAEA, "Status report 107 - VVER-1200 (V-392M)," IAEA ARES, 2011.

[16] S. J. Zinkle and G. S. Was, "Materials challenges in nuclear energy," *Acta Materialia,* vol. 61, pp. 735-758, 2013.

[17] FANC, Federal Agency for Nuclear Control, "Doel 3 and Tihange 2 reactor pressure vessels, Final Evaluation Report," 2013.

[18] NuScale Power, LLC, "NuScale Plant Design Overview, Revision 0," NuScale Power, LLC, Corvallis, Oregon, 2014, November 7.

[19] K. L. Murty, Materials Ageing and Degradation in Light Water Reactors: Mechanisms and Management, Elsevier, 2013.

[20] J. N. Reyes and P. Lorenzini, "NuScale Power: A modular, scalable approach to commercial nuclear power," *Nuclear News,* no. June, pp. 97-104, 2010.

[21] Williams D. K., Fassett D. P., Webb B. J., Bees W. J. and Kruskamp A. S., "Helical coil steam generator". U.S.A Patent US 8,752,510 B2, 17 June 2014.

[22] NuScale Power, LLC, "NuScale Power," 2015. [Online]. Available: http://www.nuscalepower.com. [Accessed 26 5 2015].

[23] Allen T., Busby J., Meyer M. and Petti D., "Materials challenges for nuclear systems," *Materialstoday,* vol. 13, no. 12, pp. 14-23, December 2010.

[24] M. M. Morra, "Process Parameters Affecting Inhomogeneity of Material Microstructure," Strålsäkerhetsmyndigheten (SSM, Swedish Radiation Safety Authority), Report number: 2012:70 ISSN: 2000-0456, 2012.

Review on Critical Properties of Copper Overpack Material in Nuclear Waste Package

Vesa P Lindroos*
Aalto University School of Chemical Technology, Department of Material Science,
Laboratory of Hydrometallurgy and Corrosion
*Corresponding author, vesa.lindroos@aalto.fi

Abstract

The design requirements for nuclear waste repository vessels are based on approximated long-term physical and chemical environmental conditions. Besides the design requirements, the actual definition of failure of the copper overpack in repository environment has not been determined. The definition of failure is critical in establishing the consensus about mechanisms affecting the integrity of the repository vessel during long-term exposure. Furthermore, the prevailing equilibrium conditions determine the actual possibility of failure, that is, commonly proposed copper corrosion through hydrogen evolution would quickly reach equilibrium state in compacted bentonite clay, thus inhibiting further damage.

1. Introduction

It has been suggested that Finnish and Swedish concepts for spent nuclear fuel management may be considered the most advanced in the world [1,2]. The geological environment in Canada, Finland and Sweden consists of crystalline bedrock. Among others, in these aforementioned countries, the repositories are located under sea surface and are therefore saturated with ground water [2].

The repository plans feature engineered barrier systems (EBS). The EBSs are included in multiple barrier system (MBS), which in Finland and Sweden among other countries, there is a primary spent fuel package surrounded by corrosion resistant overpack and the bore hole has a backfill of compacted bentonite clay around the capsule [1,2] and finally, natural barrier, such as granite bedrock. The primary package and overpack designs around the world feature several candidate alloys and metals, which are shown in table 1. [1]

Table 1. Planned materials in spent nuclear fuel management (Adapted from [1])

Metallic material	Country
Carbon steel, low alloy steel, cast iron	Argentina, Belgium, Canada, Finland, France, Germany, Japan, Sweden, Switzerland, USA
Copper, Cu alloys	Argentina, Canada, Finland, Sweden, Japan, USA
Stainless Steel	Belgium, France, USA
Titanium	Canada, Germany, Japan, USA
Nickel Alloys	Argentina, Germany, France, USA

In Finnish and Swedish management plans, Cu has been selected as material for the corrosion resistant overpack due to its thermal and mechanical properties, as well as its properties in reducing environments [1]. The backfilled compacted bentonite clay restricts gas and mass transfer to and from the near proximity of the overpack surface [3]. After the initially dissolved oxygen in ground water has been consumed after approximately 200 years, the near-field environmental conditions on the overpack surface become anoxic. Traditionally, Cu has been considered immune to corrosion in anoxic conditions.

The planned overpack material selections is defined by two conceptual approaches: corrosion tolerance and corrosion resistance. Corrosion resistance as design approach in selection of materials is the rationale in case of Cu, Cu alloys and materials such as stainless steel, Ni alloys and Ti. The aforementioned materials are either considered corrosion resistant due to corrosion resistant protective passive films on the material surface or due to established understanding of thermodynamical immunity in reducing environments, especially regarding Cu [2]. However, during the 1980's [4] and later on in the 2000's [5] there has been quite controversial research proposing that water itself is an oxidant to Cu.

The environmental conditions are closely related to the conceptual approaches in design through materials selection. In oxidizing environments, Cu is considered to be in the region of corrosion tolerance before the residual oxygen from the surrounding ground water has been consumed. However, the two different conceptual design approaches of corrosion tolerance and corrosion resistance pose an challenging scaling problem. Even though the life time predictions are not specific to spent nuclear fuel management, the timescale of 100,000 years brings very special challenges to scaling the corrosion rates [6].

The controversial suggestion challenging the immunity of Cu in anoxic water have flamed scientific discussion about its effect on integrity of the spent nuclear fuel management plans. However, lost in the scientific debate is the consideration of relevant scale of phenomena and what constitutes as a container failure [6,7].

2. Environmental Conditions and Corrosion of Copper

The environmental conditions are restricted by the EBSs. The near-field conditions are affected significantly by the interaction of bentonite clay backfill, surrounding crystalline bedrock and the ambivalent ground water system [2]. The backfill affects the flow rates of elements, ground water, gas and possible reaction products by limiting penetration, thus determining water chemistry [2,6,7]. The key environmental near-field conditions in the spent fuel repositories are dependent on several factors. These significant factors, among others, include amount of dissolved oxygen, ground water pH, temperature and pressure. Temperature is a result of high-level waste (HLW) with high enough activity to generate significant quantities of heat through radioactive decay and long-lived radionuclides. The peak temperatures may well exceed 100 °C. [2]

Radionuclides have an additional effect on repository environmental conditions. Water in contact with the capsule will be exposed to gamma radiation leading to radiolysis of water [8]. Through gamma radiation absorption to water, oxidizing and reducing species such as H_2O_2, $HO\cdot$, $H\cdot$, H_2 and e^-_{aq} are produced [8-9]. Two of the produced species, H_2O_2 and hydroxyl radical ($HO\cdot$) have thermodynamic capability

to initiate corrosion of Cu [9]. This sort of radiation induced corrosion is expected in the initial phase of repository [9]. It is estimated that the Cu surface will receive total dose of maximum 100 kGy during the first 100 years of the repository [9].

The ground water in Finland poses additional challenges in terms of corrosion resistance. As the repositories in Finland and Sweden are saturated with ground water and since the repository ground water in Finland and Sweden are relatively saline and contain several other electrolytes, special attention must be paid to assess the effect of these electrolytes on corrosion of Cu. While some of the electrolytes are considered to hinder corrosion of Cu, others are considered to promote it. The Finnish ground water contains significant amount of chlorides that are suggested to have a role in corrosion of Cu [7,10]. The combination of high concentration of chlorides and low pH promote general dissolution of Cu, but on the other hand, formation of cuprous-chloro complexes, such as $CuCl^{2-}$ stabilize oxidation of Cu(I) and in combination with high temperatures, inhibits pitting corrosion and stress corrosion cracking (SCC) [2,6,7,11].

Based on the anoxic water samples from Olkiluoto, the theoretical pH of the anoxic groundwater is around pH 8 [10]. Furthermore, it has been considered highly unlikely that acidic conditions would develop in saturated repositories as the initial dissolved oxygen is consumed [7]. While Cu is thermodynamically unstable in low pH and with high chloride concentrations, proposed low probability of acidic conditions contradict Cu dissolution.

In addition to chlorides, the sulphides of the ground water have an effect on the Cu dissolution. After the consumption of the initial dissolved oxygen, the overpack is exposed to sulphide-containing environment for a large portion of its designed lifetime [3]. Unlike with chlorides, sulphates do not form stable complexes with Cu(I) and thus potentially lead to dissolution of Cu as Cu^{2+} [12]. Through proposed mechanism [3] of Cu and HS^-, the formed Cu_2S is highly insoluble and that reduces the activity of Cu^+ and furthermore, the Cu/Cu^+ equilibrium potential [2]. Additionally, it has been proposed that in sulphide containing ground water H_2O or HS^- becomes oxidant of Cu [2]. Additionally, it has been suggested that in most probable mechanism with low concentration of HS^- the cathodic reaction involves interfacial reduction of HS^- [3]. However, it has been pointed out as an important notion that even in the bulk solutions, the rate of the anodic process for the HS^- concentration is limited by the rate of sulphide transfer to surface [3].

The initial dissolved oxygen in the ground water has been suggested to have two roles in corrosion of Cu. The first one is the interfacial cathodic reaction, in which O_2 is reduced to OH^- and the second one is to contribute to oxidation of Cu(I) to Cu(II) [7]. Additionally, it must pointed out that OH^- as a reaction product promotes local alkalinity [2]. These reactions, among others, are shown in Fig. 1.
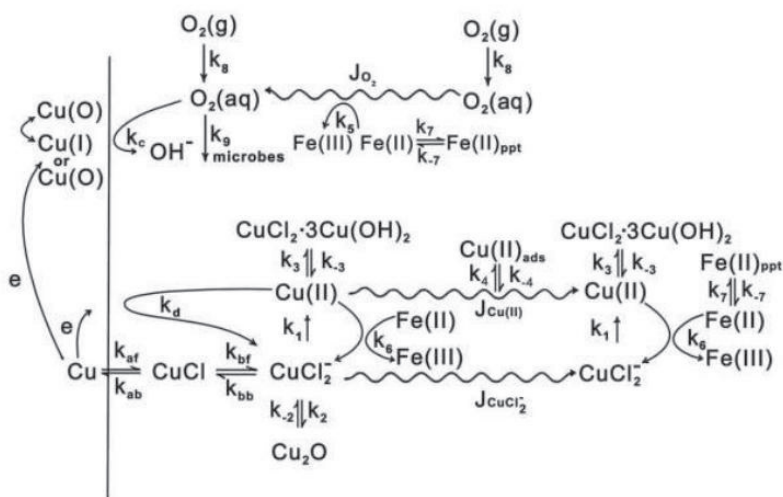
Figure 1. Suggested reaction scheme in saline ground water with dissolved oxygen [7]

The corrosion of Cu in aqueous solutions with dissolved oxygen includes anodic dissolution of Cu with chlorides as adsorbed intermediate product $CuCl_{ad}$ to produce $CuCl^{2-}$ complex. This exact reaction is the first of the aforementioned reactions linked to the reduction of O_2 on Cu surface to produce OH^-. [2,7]

Pitting corrosion is not considered to be expected in anoxic stage of the repository [2]. Pitting corrosion propagation is dependent on sufficiently fast mass transport to the pit and out of it in order to avoid formation of protective corrosion product film, that might lead to death of the pit propagation [2]. Furthermore, the near-field environment in the repository is not expected to lead to pitting corrosion, but mere roughening of the surface after the initial dissolved oxygen has been consumed, as noted in synthetic ground water after 2 years of exposure [2]. However, it has also been suggested that pitting corrosion by the effect of sulphate and nitrate is possible [13]. Sulphates and nitrates have been stated to be mainly responsible for initiation of pitting corrosion on Cu surface [13]. Furthermore, it was reported that pitting corrosion rate did not decrease in anoxic water but in fact increased by approximately factor of 40, so it was concluded that oxygen is not required for considerable corrosion rate through sulphides [13]. On the other hand, also crevice corrosion is considered unlikely due to weak hydrolysis of Cu(I) in the the presence of chlorides and furthermore, the dissolution of Cu(II) requires presence of oxygen [2].

During the anoxic stage of the repository, sulphides have been identified as an aggressive agent that potentially contributes to SCC. However, the limited mass transfer to near-field environment also limits flux of HS^- resulting in concentration too low to support SCC. SCC may occur in environments containing among others ammonium, nitrite and acetate solutions, which may be produced by microbial activity. In addition to aforementioned solutions, the microbial activity may contribute to HS^- concentration through sulphate-reducing bacteria. However, it had

been pointed out that strong evidence suggests compacted bentonite buffer to suppress microbial activity, even though there is no clear understanding on the mechanism. [2]

3. Corrosion of Copper in Anoxic Water

The traditional understanding on thermodynamical immunity of Cu in anoxic environments has been challenged [4,5] by proposing water itself being an oxidant to Cu. This proposed phenomenon has affected considerations of structural integrity of spent nuclear fuel management repositories in Finland and in Sweden. However, the studies suggesting corrosion of Cu have been broadly criticized. While several studies with closed containers and pressure gauge experiments [5,14-15] have been conducted, the most relevant critique is focused on the experimental methods and tightness of the containers and used apparatuses. Furthermore, the effect of pre-existing oxidized layers and initial deaeration of the test solutions have been considered to affect the suggested reactions [7].

It has been pointed out that understanding on Cu immunity in anoxic environment is based on an assumption of hydroxide-free oxide (Cu_2O) having an equilibrium with partial pressure of hydrogen [5]. Additionally, the established consensus regarding immunity of Cu is based on traditional Pourbaix diagrams [5]. However, it has been argued that even though the proposed Cu corrosion is contradicting traditional understanding of Cu thermodynamics, the suggested corrosion of Cu through hydrogen evolving reaction involving Cu surface reaction with hydroxyl ions should not be considered neglected since the thermodynamic databases are not complete [16].

The corrosion of Cu is suggested to occur with hydrogen evolving reaction. The possibility of hydrogen evolution has been researched with pressure gauge apparatuses for better characterization of increased pressure. The difficulty of repeating the experiments and differing results has been the main source of critique [11]. Regardless of these aforementioned difficulties, there has been significant, proven hydrogen evolution [5,14-15]. In these experiments, the presence of $H_2(g)$ was observed with various methods: pressure increase above Pd-foil acting as a selective barrier [5,14-15], mass spectrometry of gas, water and glass vessel [11], and finally, hydrogen thermal desorption (TDS) of the Pd-foil [12]. These experiments showed a clear difference between Cu samples and Pt references by a factor of 25 to 30 with higher pressure with Cu [14]. The parallel experiments with similar equipment showed smaller pressure with Pt reference samples by factor of 50, regardless of similar difficulties in tightness as in the other experiments [15]. Additionally, TDS has been used to detect outgassing of hydrogen from Cu [17].

While there is evidence of $H_2(g)$ in the experiments, there is no clear understanding of the mechanisms leading to gas evolution. The most controversial suggested mechanism is a previously unknown hydrogen-containing corrosion product H_xCuO_y, which is proposed to form with a following overall reaction (1) [5]:

$$Cu \ + \ y\,H_2O \ \rightarrow \ H_xCuO_y \ + \ (2y-x)\,H_{ads} \tag{1}$$
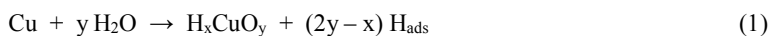
To support the proposed mechanism, a modified Pourbaix diagram was presented for $Cu - H_2O$ system [5]. The modified diagram was based on experimental data and interpretations made of the pressure gauge apparatus experiments. The modified
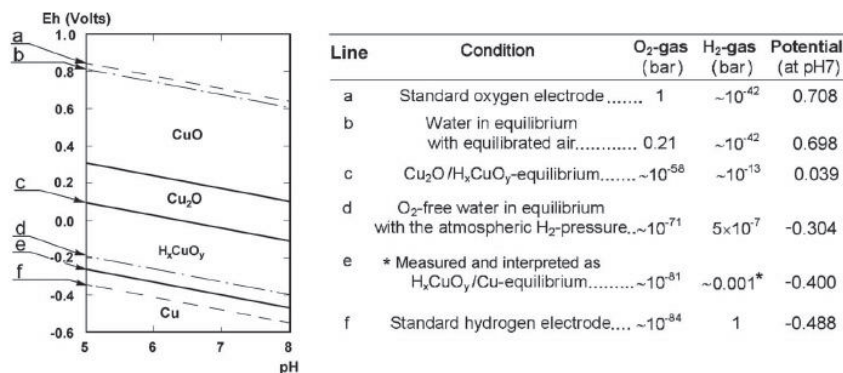
diagram is show in Fig. 2.

Line	Condition	O_2-gas (bar)	H_2-gas (bar)	Potential (at pH7)
a	Standard oxygen electrode....... 1		$\sim 10^{-42}$	0.708
b	Water in equilibrium with equilibrated air........... 0.21		$\sim 10^{-42}$	0.698
c	Cu_2O / H_xCuO_y-equilibrium.......	$\sim 10^{-58}$	$\sim 10^{-13}$	0.039
d	O_2-free water in equilibrium with the atmospheric H_2-pressure..	$\sim 10^{-71}$	5×10^{-7}	-0.304
e	* Measured and interpreted as H_xCuO_y/Cu-equilibrium..........	$\sim 10^{-81}$	$\sim 0.001^*$	-0.400
f	Standard hydrogen electrode....	$\sim 10^{-84}$	1	-0.488

Figure 2. Modified Pourbaix diagram for unknown species H_xCuO_y [5]

The formation of the unknown species H_xCuO_y follows proposed equilibrium line (e) just above SHE (f) and was suggested to be explained by corrosion of Cu in anoxic water with slow $H_2(g)$ evolution [5]. This slow $H_2(g)$ evolution is considered to indicate corrosion of Cu with an additional notion that $H_2(g)$ bubbles could not be seen at standard atmosphere [5]. Based on the proposed modified Pourbaix diagram, it was suggested that Cu is indeed not thermodynamically immune to corrosion in pure anoxic water [5]. However, it has been pointed out that Cu would only corrode in anoxic water when partial pressure of $H_2(g)$ would be under 1 mbar [7] and that $H_2(g)$ breakthrough pressure In compacted bentonite clay is between 7 and 10 MPa, so the equilibrium partial pressure would be quickly reached [3].

The modified Pourbaix diagram and suggestion of unknown hydrogen-containing corrosion product has been criticized vastly. To asses the feasibility of unknown species, thermodynamic calculations were conducted for Eq. 1 with cofactor values x=y=1 and x=y=2, respectively [18]. With cofactor values x=y=2, the corrosion product $Cu(OH)_2$ was deemed thermodynamically unfavorable and it was pointed out that magnitude of $H_2(g)$ evolution was calculated to be too high to be related with Cu oxidation by water itself [18]. Cofactor values x=y=1 would produce CuOH as corrosion product. It was pointed out that chemical potential data for CuOH is scarcely available, but the calculations showed that reported [5] $H_2(g)$ evolution would be very unlikely to be resulted from oxidation of Cu by water [18]. However, it has been argued that generally little known fact of stability of hydrogen-free reaction would mean that a hydrogen-containing corrosion product CuOH would be favored over hydrogen-free products CuO and Cu_2O in Cu – H_2O system [19].

In addition to proposed reaction mechanism producing unknown species from Cu (Eq. 1), another route was presented to produce $Cu(OH)_2$ with Cu_2O and H_2O as reactants [18]. To accommodate the magnitude of evolved $H_2(g)$, it was proposed that initial surface film Cu_2O would be result of residual oxygen in the test solution leading to at least 0.21 μm thickness of the film, which was deemed feasible [18]. While these calculations [18] contradict the modified Pourbaix diagram, additional

thermodynamic simulations and ab initio molecular dynamics simulations were presented to show agreement with experimental data and that there indeed is a stable CuOH corrosion product [20]. Regardless of energically favorable simulation results, it was pointed out that the actual results are contradicting previous calculations and thus Cu_2O being more favorable than the previously unknown non-stoichiometric corrosion product [21].

On the other hand, it has been proposed that $CuOH_{ad}$ could be formed in a reaction mechanism, where $CuOH_{ad}$ is to be considered as catalytic intermediate that transforms into Cu_2O in the potential region, where the latter is more stable [22]. However, it was pointed out that the aforementioned transition reaction might be slower in anoxic media, leading to significant stabilization of the intermediates over the Cu_2O [22]. Furthermore, there has been voltammetrically and ellipsometrically hypothesized adsorbated that contain oxygen in both, alkaline and neutral solutions [22]. Apart from the suggested reaction mechanism [22], yet another route for CuOH formation has been proposed. In alkaline solutions, it was found that CuOH would be a surface species resulting from cathodic reduction of Cu electrode [23]. However, even though the experiments have verified existence of $CuOH_{ad}$, the formation requires pre-oxidized surface [21].

While the general corrosion with traditional understanding and with new proposed reaction mechanisms remain debatable and the fact that there is no clear definite evidence that $H_2(g)$ evolution is directly related to corrosion [22], there is also a proposed view that there is OH transport via grain boundaries, even though dissociated O transport in bulk Cu is negligible. Since the grain boundaries have lower density as a result of atomic mismatch, grain boundaries are more suitable for diffusion, oxidation and corrosion. A simulation has showed that in all temperatures, OH diffuses rapidly dissociating in grain boundaries due to strong bonds between dissociated O and surrounding Cu atoms. This is suggested to possibly lead in formation of Cu oxides inside the grain boundaries and dissociated H to be transported by thermal motion. As a result, formed Cu oxides would consequently lead to formation of nano crystals and lattice expansion, thus contributing to elevated risk of cracking. [16]

Even though there have been several different experimental conditions thus making it impossible to draw conclusion, the reported radiation experiments have shown 30 higher pitting corrosion rates than experiments without radiation [8-9]. Furthermore, it has been suggested on thermodynamic basis that the Cu corrosion is driven by the radiolytic products such as H_2O_2 and $HO\cdot$ [9]. Gamma-radiation induced corrosion is reported to produce mainly Cu_2O with only small fractions of Cu(II) compounds in anoxic water and formation of the products is dependent on radiation dose [9].

4. Feasibility of Failure

The scientific debate on Cu corrosion in anoxic pure water has been going on since the 1980's. However, lost in the debate about the possibility of water itself being an oxidant to Cu is the feasibility and the effects of proposed water-induced corrosion in repository environmental conditions [7]. In the center of discussion about feasibility and effects of proposed Cu corrosion through $H_2(g)$ evolution and effect of the dissolved electrolytes in the repository conditions is the relevance of mass transfer and relevant corrosion rates in relation to design concept of corrosion allowance [7].

It has been pointed out that $H_2(g)$ transfer through compacted bentonite requires significant MPa scale breakthrough pressure and that the proposed equilibrium pressure [5] at mbar scale would be quickly reached [11] thus limiting the extent of Cu corrosion on the overpack surface. The critical factor in this consideration is the corrosion rate in terms of the corrosion allowance.

In addition to possibly limiting equilibrium pressures is the dissolved electrolytes that might have a role in Cu dissolution. While there is evidence of $H_2(g)$ evolution [5,14-15] in pure water, the debate remains with electrolyte-containing ground water and synthetic ground water, since ground water contains several corrosion suppressing electrolytes [11]. The ground water contains several ions, such as HS^- and Cl^- that might promote dissolution of Cu [2,7,10] , but at the same time, the ions form complexes and reaction products, such as highly insoluble Cu_2S and $CuCl^{2-}$ that stabilise and suppress the general dissolution of Cu [2,7,11]. This far there has been no evidence supporting a possibility of Cu dissolution in saline solutions, such as bentonite bore water or deep ground waters in repository environment, so the underlying issue about feasibility of Cu corrosion in the repository conditions remain, even if there was potential Cu corrosion phenomenon in pure water [6]. However, reportings [8-9] of gamma-radiation-induced radiolysis products in anoxic water propose feasibility of corrosion in the initial stages of the repository.

With all the discussion about possibility for corrosion of Cu, there has been only relatively little definition of what constitutes as overpack failure and furthermore, what are the relevant failure modes. It has been stated that in the strict sense, the definition of failure of the corrosion protective overpack is penetration through the repository capsule protective layer. However, the question remains, does the corrosion protection overpack still provide some useful containment function even after it has seized to function as an absolute barrier. Regardless of more philosophical considerations, the failure in Finnish and Swedish repositories constitutes as penetration through the corrosion protective overpack, unless there is an additional, sealed containment of the inner repository vessel. [6]

5. Discussion

As the spent nuclear fuel repository plans in Finland and Sweden feature two-stage sequential concepts of corrosion allowance and corrosion avoidance, there is a constant discussion about the integrity of the repository plans featuring a Cu overpack as a corrosion protective layer in anoxic environmental conditions. After the initial, dissolved oxygen is consumed from the ground water in saturated repository with mass transfer limiting compacted bentonite clay buffer after the first approximately 200 years, the Cu overpack is considered corrosion resistant.

The corrosion environment in the repository is considered to be stable and only varies from oxic contitions to anoxic conditions after the dissolved oxygen is consumed from the ground water. These conditions are still considered to be favorable for Cu-based corrosion shielding. Even though the ground water in the Olkiluoto area is relatively saline and contains other electrolytes, such as sulphides, these electrolytes are considered to hinder Cu corrosion, since the water chemistry is neutral in pH and acidic conditions are considered unlikely to develop. Furthermore, HLW induces significant amount of heat through high activity level and long-lasting half-life of radionuclides in the HLW. The repository conditions are close to 100 °C

due to the radiation induced heat, which itself leads inhibition of corrosion phenomena like SCC, even though the temperature decreases by time. Additionally, gamma-radiation it self has been reported to cause corrosion of Cu.

A previously undefined, hydrogen-containing corrosion product has been proposed to be formed in anoxic conditions. The corrosion phenomenon is argued to be observed through hydrogen gas evolution. This naturally has provoked discussion and scientific interest over the past 30 years, since it might have an effect on integrity if the spent nuclear fuel repository plans in Finland and in Sweden, since it would cause Cu overpack to degrade significantly faster than intended for repository lifetime. The reported findings of hydrogen gas evolution have been vastly criticized due to their contradicting nature against traditional understanding on Cu thermodynamics. To address the criticism concerning the thermodynamic feasibility, it has been argued that the thermodynamic databases are not yet complete.

However, the relevance of these findings and the feasibility of the proposed phenomenon remains under debate, since it has been suggested that thermodynamic equilibrium would be quickly reached due to limited mass transfer of hydrogen gas and thus limiting the possible corrosion damage on the Cu overpack. Furthermore, it has been noted that observed hydrogen gas evolution might not be directly linked to corrosion of Cu, but instead a result of other non-related factors. In addition to general feasibility of the hydrogen evolving corrosion phenomenon, it has been suggested that pre-formed oxide layers on the Cu surface could be considered to prevent corrosion.

Even though there is evidence of hydrogen evolution in pure water, the actual source of the observed hydrogen gas remains to be unknown. Furthermore, the debate remains whether or not the dissolved electrolytes in Olkiluoto ground water have an effect on the corrosion of the Cu and would it effectively compromise the structural integrity of th Cu overpack as corrosion resistant barrier. While some of the dissolved electrolytes are known to promote dissolution of Cu, they also form corrosion stabilizing products that are considered to hinder the actual corrosion. This far, there is no reported evidence showing a possibility for Cu dissolution in saline ground water. It can be concluded that even though corrosion of Cu could be possible in anoxic and low-oxygen environments, the feasibility for failure-inducing corrosion in the spent nuclear fuel repositories seems very unlikely.

References

1. RB Rebak, Materials in Nuclear Waste Disposition, JOM, vol 66, no. 3. 2014
2. MA Rodriguez, Anticipated Degradation Modes of Metallic Engineered Barriers for High-Level Nuclear Waste Repositories, JOM, Vol 66, no. 3, 2014.
3. F King, C Lilja, M Vähänen, Progress in the Understanding of the Long-term Corrosion Behaviour of Copper Canisters, Journal of Nuclear Materials, 438, p. 228-237. 2013.
4. G Hultquist, Hydrogen Evolution in Corrosion of Copper, Corr. Sci. 26 (1986) 173-176.
5. P Szakálos, G Hultquist, G Wikmark, Corrosion of Copper by Water, Electrochem. Solid-State Lett. 10 (11) C63-C67 (2007).
6. F King, Predicting the Lifetimes of Nuclear Waste Containers, JOM, Vol 66, no. 3. 2014
7. F King, Critical Review of the Literature on the Corrosion of Copper by Water,

SKB, Technical Report TR-10-69, 12/2010.

8. Å Björkbacka, S Hosseinpour, C Leygraf, M Jonsson, Radiation Induced Corrosion of Copper in Anoxic Aqueous Solution, Electrochem. Solid-State Lett. 15 (5) C5-C7 (2012).

9. Å Björkbacka, S Hosseinpour, M Johnson, C Leygraf, M Jonsson, Radiation Induced Corrosion of Copper for Spent Nuclear Fuel Storage, Radiation Pysics and Chemistry, vol. 92, p. 80-86. 2013.

10. U Vuorinen, K Ollila, M Snellman, Olkiluodon pohjavesikemia – suolainen ja murtovesi – suolaisen referenssiveden resepti (Ground water chemistry in Olkiluoto – saline and brackish water – recipe of saline reference water), Posiva, Working Report 97-25, 1997. (In Finnish)

11. F King, C Lilja, M Vähänen, Progress in the Understanding of the Long-term Corrosion Behaviour of Copper Canisters, Journal of Nuclear Materials, 438, p. 228-237. 2013.

12. F King, C Lilja, Localised Corrosion of Copper Canisters in Bentonite Bore Water, SKB, Technical Report TR-13-27, 12/2013.

13. S Eriksson, H-P Hermanson, Pitting Corrosion of Copper in Nuclear Waste Disposal Environments, SKI, Report 98:2, 1998.

14. R Becker, H-P Hermansson, Evolution of Hydrogen by Copper in Ultrapure Water without Dissolved Oxygen, SSM, Research Report 2011:34.

15. S Lehmusmies, A Pehkonen, O Forsén, T Saario, R Becker, M Granfors, Corrosion of Copper by Water under Oxygen-free Conditions, EUROCORR2012, Istanbul 9-13 Sept. 2012.

16. AB Belonoshko, A Rosengren, A Possible Mechanism of Copper Corrosion in Anoxic Water, Philosophical Magazine, vol. 92, No. 36, p. 4618-4627, 12/2012.

17. G Hultquist, Why Copper May Be Able to Corrode in Pure Water, Corr. Sci., 93, p. 327-329, 2015

18. MJ Apted, DG Bennett, T Saario, A Review of Evidence for Corrosion of Copper by Water, SSM, Research Report 2009:30, ISSN: 2000-0456, 2009.

19. G Hultquist, MJ Graham, O Kodra, S Moisa, R Liu, U Bexell, JL Smialek, Corrosion of Copper in Distilled Water without O_2 and the Detection of Produced Hydrogen, Corr. Sci., 95, p. 162-167, 2015.

20. G Hultquist, P Szakálos, MJ Graham, AB Belonoshko, GI Sproule, L Gråsjö, P Dorogokupets, B Danilov, T Aastrup, G Wikmark, G-K Chuah G, J-C Eriksson, A Rosengren, Water Corrodes Copper. Catal. Letters, vol 132, p. 311-316. 2009.

21. DW Shoesmith, Mechanism of Copper Corrosion in Aqueous Enviroments. Mechanisms of Copper Corrosion in Aqueous Environments, Written statements by the panel members. Kärnavfallsrådet, Report 2009:4e. 2009.

22. M Bojinov, I Betova, C Lilja, A Mechanism of Interaction of Copper with a Deoxygenated Neutral Aqueous Solution, Corr. Sci., vol. 52, p. 2917-2927. 2010.

23. S Härtinger, B Pettinger, K Doblhofer, Cathodic Formation of a Hydroxide Adsorbate on Copper (111) Electrodes in Alkaline Electrolyte, Journal of Electroanal. Chem., vol. 397, p 335-338, 1995.

The Engineering materials research group of Department of Engineering Design and Production of Aalto University arranged a postgraduate course on nuclear materials. The course consisted of three day long lecture session given in April 20-22, 2015. Lectures were given by professionals from nuclear power related research institutes (Aalto and VTT), nuclear industry and authority. The course also included a seminar session held October 8, 2015. The seminar session was targeted to postgraduate students, who prepared articles from their field of expertise. This proceeding is the collection of these seminar articles.

BUSINESS +
ECONOMY

ART +
DESIGN +
ARCHITECTURE

SCIENCE +
TECHNOLOGY

CROSSOVER

DOCTORAL
DISSERTATIONS